OPTIMAL DESIGN OF BOW PLATING FOR SHIPS OPERATING IN ICE

PETER W. BROWN

National Library of Canada
Acquisitions and Bibliographic Services Branch
395 Wellington Street
Ottawa, Ontario
K1A 0N4

Bibliothèque nationale du Canada
Direction des acquisitions et des services bibliographiques
395, rue Wellington
Ottawa (Ontario)
K1A 0N4

Your file Votre référence

Our file Notre référence

NOTICE

The quality of this microform is heavily dependent upon the quality of the original thesis submitted for microfilming. Every effort has been made to ensure the highest quality of reproduction possible.

If pages are missing, contact the university which granted the degree.

Some pages may have indistinct print especially if the original pages were typed with a poor typewriter ribbon or if the university sent us an inferior photocopy.

AVIS

La qualité de cette microforme dépend grandement de la qualité de la thèse soumise au microfilmage. Nous avons tout fait pour assurer une qualité supérieure de reproduction.

S'il manque des pages, veuillez communiquer avec l'université qui a conféré le grade.

La qualité d'impression de certaines pages peut laisser à désirer, surtout si les pages originales ont été dactylographiées à l'aide d'un ruban usé ou si l'université nous a fait parvenir une photocopie de qualité inférieure.

Canada

OPTIMAL DESIGN OF BOW PLATING FOR SHIPS OPERATING IN ICE

BY

© PETER W. BROWN, B.ENG.

A THESIS SUBMITTED TO THE SCHOOL OF GRADUATE STUDIES

IN PARTIAL FULFILMENT OF THE REQUIREMENTS FOR THE DEGREE OF

MASTER OF ENGINEERING

FACULTY OF ENGINEERING AND APPLIED SCIENCE

MEMORIAL UNIVERSITY OF NEWFOUNDLAND

SEPTEMBER, 1993

ST. JOHN'S NEWFOUNDLAND CANADA

ISBN 0-315-91603-6

To my parents,

Don and Peggy.

ABSTRACT

Extensive work has been carried out in recent years to ensure that ice-capable ships are both safe and economical. The present analysis provides a methodology which can be employed by the designer to calculate the optimum bow plating thickness for operation in ice. To this end, a local ice load model is re-evaluated using a probabilistic analysis of full scale data, probabilities of failure for plating are calculated and plate thickness is optimised.

Full scale data for the MV Canmar Kigoriak and USCGC Polar Sea were ranked; curves were fitted through the tail of each data set; and Type-I extreme probability distributions were derived for the three panel sizes. The Canmar Kigoriak data were then subdivided based on contact area and a simulation was performed to derive the load distributions on subregions of the instrumented panel. Finally, a local ice load model which accounts for annual number of impacts and exposure was confirmed.

To evaluate the strength of bow plating, three limit states (three-hinge collapse, permanent set and membrane collapse) were selected. Statistical distributions for each of the input parameters were established. The probability of failure was calculated, for each limit state using a range of plate thicknesses, frame spacings and annual numbers of impacts, using *First Order Reliability Method* software. The probability of failure was approximated as a plane for each limit state and frame spacing.

Plate thickness was optimised for minimum cost. Minimum safety levels for permanent set and membrane collapse were also specified. The objective function

considered costs due to construction, aesthetics, repair and replacement. Cost due to lost use of the ship and increased weight can also be specified. These costs were considered to be specific to the vessel under consideration and hence, were considered outside the scope of the present analysis. Optimum plate thicknesses are presented and compared with those specified by the *Proposals for the Revision of the Arctic Shipping Pollution Prevention Regulations.*

ACKNOWLEDGEMENTS

The author thanks his family for their continued support and encouragement. The author also extends his thanks to Dr. Ian J. Jordaan for his support and guidance throughout this project, to Dr. M.R. Haddara for his insight and help regarding structural optimisation and to Prof. D.A. Friis for his useful discussion of cost analysis. Thanks to Ms. Michelle Johnston for her assistance with critical zone modelling and to Mr. Mark Fuglem, Dr. G. George and Mr. Bin Zou for their assistance with probability modelling. The kind support of Mr. V.M. Santos-Pedro, Manager, Arctic Ship Safety, Canadian Coast Guard, is appreciated. Thanks to the members of the ASPPR Review Committee for their insight and expertise offered during the project, to the staff of the Memorial University Centre for Computer Aided Engineering for the considerable use of their facilities and to my colleagues in the graduate programme at Memorial University for their friendship. Finally, the author thanks the following for their support of the project: Newfoundland Offshore Career Development Awards Committee, Natural Sciences and Engineering Research Council, Faculty of Engineering and Applied Science, Memorial University and Society of Naval Architects and Marine Engineers, Arctic Division.

CONTENTS

LIST OF FIGURES

LIST OF TABLES

NOMENCLATURE

Chapter 1

F_{max} - the maximum bow force generated during a collision with a large ice floe

L - load

Pr[.] - the probability of [.]

R - capacity or resistance

Φ - risk or probability of failure

Chapter 2

C_f - cost of failure

C_g - generalised cost

C_i - initial cost

Φ - risk or probability of failure

Chapter 3

a - area

$a_{subscript}$ - slope of force plot - natural log plots

a_s - area of a subpanel

c - coverage

$c_{subscript}$ - y-intercept of force plot - natural log plots

$F_X(x)$ - cumulative distribution function

$F_Z(z)$ - extreme cumulative distribution function

i - rank of the item within the data set

j - number of fixed area subpanels

k - number of moving area subpanels

m - number of hits for a fixed annual number of impacts

$m_{subscript}$ - slope of force plot - common log plots

n - fixed annual number of impacts

n_i - number of items in data set

P - pressure

Pr[.] - probability of [.]

$p_e(j, k)$ - probability of coverage for given j and k values

p_e - probability of exceedance

p_{nc} - probability of non-exceedance

r - exposure parameter

x - x-axis data type, generally force or pressure

x_0 - x - intercept parameter - natural log plots

y - y-intercept of fixed area force plot - common log plots

α - slope of the pressure distribution

μ - number of hits for an expected annual number of impacts

ν - expected annual number of impacts

upper case letters - random quantities in probabilistic distributions

lower case letters - fixed quantities in probabilistic distributions

subscripts

j - fixed area

k - moving area

Chapter 4

A - annuity payment

a_0, a_1 and a_2 - coefficients of cost.

C - total cost

C_D - cost of damage

C_i - blending function coefficient

C_s - cost of steel

$C_{subscript}$ - individual costs

$E(.)$ - expected value of (.)

$F_X(x)$ - cumulative distribution function (CDF) of X

$f_X(x)$ - probability density function (PDF) of X

i - net interest rate

i_g - rate of inflation

i_i - interest rate

L - applied load

N - total number of panels being analyzed

N_p - total number of plates being analyzed

n - number of payments

n_p - number of panels making up a plate

n_f - annual number of panel failures

P - tensile load at plate edges

$(P/A, i, n)$ - present worth factor

P_U - ultimate tensile load at plate edges

P_V - present value of an annuity

Pr[.] - probability of [.]

q - uniform load

q_{3H} - three-hinge collapse load

q_p - load to cause permanent set

q_U - ultimate membrane collapse load

R - capacity or resistance

s - frame spacing

T - temperature

t - thickness

W_{max} - maximum deflection at midspan

w - weighting coefficient

$\dot{\varepsilon}$ - strain rate

ε_s - nominal membrane strain

θ - angle

ν - expected annual number of impacts

ν_p - plastic Poisson's ratio

ρ - density

σ_u - ultimate stress

$\sigma_u(T)$ - ultimate stress at temperature, T

$\sigma_u(0)$ - static ultimate stress

$\sigma_u(\dot{\varepsilon})$ - dynamic ultimate stress at strain rate,$\dot{\varepsilon}$

σ_y - yield stress

σ_{ys} - specified yield stress

$\sigma_y(0)$ - static yield stress

$\sigma_y(T)$ - yield stress at temperature, T

$\sigma_y(\dot{\varepsilon})$ - dynamic yield stress at strain rate, $\dot{\varepsilon}$

Φ - risk or probability of failure

$\Phi_{U \mid P}$ - probability of ultimate failure given that permanent set has not first occurred

subscripts

2t - twice thickness

3H - three-hinge collapse

A - aesthetics

C - construction

L - replacement or loss

P - permanent set

R - repair

s/10 - ten percent of spacing

U - ultimate or membrane collapse

Abbreviations and Acronyms

ASPEN - Arctic Shipping Probability Evaluation Network

ASPPR - Arctic Shipping Pollution Prevention Regulations

CAC - Canadian Arctic Class

CCGS - Canadian Coast Guard Ship

CDF - Cumulative Distribution Function

COV - Coefficient of Variation

CSA - Canadian Standards Association

FORM - First Order Reliability Method

MV - Motor Vessel

PDF - Probability Density Function

RMS - Royal Motor Ship

USCGC - United States Coast Guard Cutter

1 INTRODUCTION

1.1 COMPONENTS OF SHIP STRUCTURE AND ASSOCIATED LOADS

The complex nature of the structure of a ship and the associated response to applied loads make it desirable to divide the structure into three components. These are primary, secondary and tertiary (Paulling, 1988). The primary, or global, strength classification is concerned with the *hull girder*. For this classification, the hull is treated as a free-free beam. Loads affecting the hull girder are generally global impact loads. An example is the maximum bow force resulting from ice ramming, F_{max}, calculated for a ship when applying *Proposals for the Revision of the Arctic Shipping Pollution Prevention Regulations* (ASPPR Proposals; Melville Shipping Ltd., 1989).

The secondary, or semi-local, strength classification is concerned with the strength of a ship panel, generally taken between two bulkheads or deep web frames. This is a more localised load in which one considers a cross-stiffened plate. The designer is now concerned with the area of contact between the ice feature and the bow of the ship in the impact just mentioned.

The tertiary, or local, strength classification is concerned with the strength of the plating between two frames. This region of the ship is subjected to more localised loads, especially to critical zones that result from the ice failure mechanism (Jordaan et al., 1991). This is the region of interest for the present analysis.

1.2 OVERVIEW

One of the most serious obstacles facing ships operating in arctic and subarctic waters is ice. Damage may result from an arctic class vessel striking multiyear ice or ice island fragments or from a subarctic vessel striking an undetected growler or bergy bit. As was learned from the review and verification of the ASPPR Proposals (Carter et al., 1992), all Canadian Arctic Class (CAC) vessels can operate in areas where multiyear ice is present. Recent damages to vessels operating in the Canadian Arctic have been summarised by Keinonen et al. (1991). A similar report was prepared by Kujala (1991) for ships operating in the Baltic Sea. The potential threat of a ship hitting multiyear ice is a primary consideration behind safe design of arctic capable ships.

For subarctic vessels, it is estimated that 10,000 to 30,000 icebergs are calved from the Greenland ice cap each year with several hundred reaching the drilling sites on Canada's east coast (Grandy, 1991). The International Ice Patrol report that thirty-seven vessels between 1856 and 1973 experienced major ice damage (Scarborough, 1974). A well-known example is the RMS Titanic disaster of 1912 in which 1513 lives were lost. Therefore, one should ensure that a vessel operating in this region is designed for safe, economical operation.

As one might assume, not all vessels will have the same probability of striking an extreme ice feature or will experience the same number of impacts per year. An ice management vessel will generally experience more encounters with multiyear ice than will a transiting vessel. Similarly, an arctic vessel will be more likely to impact ice than will

a subarctic vessel. Hence, the design load is calculated as a function of the operating profile of the ship and the expected number of impacts for each type of ship will be estimated based on available information.

Optimisation of hull structures is sometimes limited by using design codes. Rules tend to be succinct and explanation of their basis is often lacking. Without this background, it may be difficult to appreciate the mechanisms that make the design safe, resulting in a design that may not be optimal. In addition, rules are generally based, at least partially, on a database of information that has been collected over the years and updated based on incidents of damage. This may result in the following complications.

1. Ship designs which fall outside the confines of the database may not be as safe as one would expect.
2. Databases of ice-capable ships are still small and are not as dependable as those available for typical sea-going ships.
3. Areas that are over-designed may not be improved upon (i.e., changes generally occur only after a failure).

Thus, a rationally-based design, using state-of-the-art structural theory, is expected to be more safe and efficient. A rationally-based structural design is considered to be:

> A design that is directly and entirely based on structural theory, analysis and optimisation, and achieves an optimum structure based on a designer-selected measure of merit (Hughes, 1988).

The objective of the present research is to provide background to the ASPPR Proposals (Melville Shipping Ltd., 1989). This includes revisiting and verifying the ice load model proposed by Jordaan et al. (1993; see also Maes and Hermans, 1991) for ships

operating in arctic and subarctic waters and to use these loads to optimize the hull plating using plastic design methods.

1.3 METHODOLOGY AND SCOPE

The methodology used to complete this analysis includes the following.

1. Completion of a probabilistic analysis of the ship-ice interaction using available full scale data.
2. Incorporation of the results of the probabilistic analysis into an algorithm to calculate the design pressure, load (L), for a given set of criteria.
3. Plating, resistance (R), is designed to meet an acceptable minimum probability of failure, $\Phi = Pr[L - R < 0]$. Φ must account for the variability of the load and resistance curves.
4. Optimisation of the structure for minimum cost.

The costs resulting from this analysis must be further evaluated considering the mission profile for the ship.

The final methodology is deterministic but is based on probabilistic methods. The use of a deterministic design format is seen as reasonable because it means that two similar vessels will have similar strength, i.e., "the master will be dealing with a *known entity*" (Carter et al., 1992).

Under item 1. above, the data for each vessel were separated into bins as a function of contact area. The data for each area were sorted and analyzed using

probabilistic methods. This results in a formula that allows the designer to calculate the expected maximum pressure. Also, the probability of a small load being spread over a larger area, as a function of location, was considered.

Under item 2. above, the algorithm proposed by Jordaan et al. (1993) is re-evaluated and verified. The designer calculates the design pressure as a function of loaded area and expected annual number of impacts (rams). The present research is concerned only with the analysis of local ice pressure.

Under item 3. above, the safety of a given design is calculated using *First Order Reliability Method* (FORM) software (Gollwitzer et al., 1988). The resistance of the structure is evaluated for three limit states:

a. three-hinge collapse;

b. permanent set; and

c. membrane collapse.

The FORM algorithm calculates the probability of failure for a given limit state and loading condition accounting for the uncertainty in the equation parameters. Frame spacing and span are included to define the size of the plate panel.

Under item 4. above, a minimum cost objective function is considered. The initial cost of construction and annual costs for aesthetics, repairs and replacement are considered. The annual costs are evaluated as a present value assuming a 20-year vessel life, 7% rate of inflation and 10% rate of investment. Supporting frames, designed to meet ASPPR Proposals (Melville Shipping Ltd., 1988), are only considered for initial cost purposes and are not evaluated during damage analysis.

2 PREVIOUS EXPERIENCE RELEVANT TO ARCTIC SHIPPING

2.1 FULL SCALE DATA

As part of its operations in the Beaufort Sea, the MV Canmar Kigoriak performed a series of full scale trials in August and October 1981 (Dome Petroleum Ltd., 1982). The authors instrumented two regions of the port shoulder of the Canmar Kigoriak with strain gauges and proceeded to ram the vessel into thick first-year ice floes (August) and multiyear ice floes (October) in order to determine the magnitude of ice loads experienced by the bow. The two regions, designated A1 and A2, are 1.25 m^2 and 6.0 m^2 respectively with A1 forward of A2. These two areas were in turn subdivided into subpanels determined by the location of the strain gauges. The loads were calculated by summing the shear differences between the gauges. These measurements also allowed the authors to estimate the area over which the load was applied. The maximum force and the area on which it was measured are presented in the report noted above.

Full scale trials were also performed aboard the USCGC Polar Sea between 1982 and 1984 (Daley et al., 1986). This vessel was instrumented with strain gauges on the port bow. The instrumented area measured 9.1 m^2 and was subdivided into 60 subpanels of 0.15 m^2. An assumption made by the authors was that the maximum pressure on an area composed of more than one subpanel occurred at the same time as the maximum pressure on a single subpanel. The maximum pressure-area curve, for each ram, was built

by adding the next highest contiguous subpanel pressure. This assumption is seen as reasonable for small areas (say < 5 subpanels) but is assumed to give lower than maximum pressures for larger areas; see Chapter 3 for further discussion. Hence, the Polar Sea data cannot be directly compared with that of the Canmar Kigoriak for large areas. The Polar Sea data presented is comparable with the Canmar Kigoriak for small areas.

2.2 ANALYSIS OF LOCAL PRESSURE

Before trying to establish a model, one must have some understanding of the phenomena being modeled. Glen and Blount (1984) reported on the nature of localised ice loads. The results of full scale tests performed using the CCGS Louis S. St. Laurent characterize localised pressure as a dynamic area of high pressure. These areas of high pressure were later termed critical zones (Jordaan et al., 1991). This area of high pressure is small and does not conform to any particular pattern. The peak pressure measured on the 8 mm transducers was 53 MPa although the mean peak pressure averaged 27 MPa. These results are consistent with more recent studies (Xiao and Jordaan, 1991; Frederking et al., 1990; for example).

Det norske Veritas Canada (Nessim et al., 1984) was commissioned by the Government of Canada to perform a state-of-the-art review of available methods for computing global and local loads produced by ice-structure interaction. The results of this review were that "available models were not yet fully satisfactory" and that engineering

solutions made use of empirical results and theoretical idealisations, both of which are conservative. The authors further recommended that probabilistic methods should be explored if consistent risk levels are to be applied to structures subjected to ice loads, that uncertainty should be incorporated into these models and that full scale data should be obtained in order to calibrate a proposed model. Since this time, much work has been done to improve ice load models.

An early example of a statistical analysis of local ice loads was that of the full scale trials of the Polar Sea, presented by Daley et al. (1984). Work by Daley and his coworkers eventually led to the formulation of the *Arctic Shipping Probability Evaluation Network* (ASPEN). ASPEN is a computer program designed to evaluate the risk to a ship operating in the Canadian Arctic and is summarised by Daley at al. (1991). This was an ambitious program designed to provide a quantitative evaluation of the ASPPR Proposals for which the authors should be commended. The ASPEN software would evaluate the mission profile of a vessel, derive the maximum impact load which could be expected by the vessel over its lifetime and produce a design which would resist this load to a specified reliability. It was stated in discussion with the ASPPR Subcommittee that ASPEN specified structural dimensions in excess of what was considered sufficient based on experience (Frederking et al., 1991). This could perhaps be improved upon by replacing the design equations used with limit state equations. It is the present reviewer's opinion that the program should be subdivided into stand-alone single-task modules thus allowing the system to be improved with greater ease.

The use of short data extremal techniques is discussed by Maes and Jordaan (1986). This type of evaluation is fostered by the need to develop a design load for a structure of which the lifespan is significantly longer than the period over which data has been collected. The method advocated uses rates of occurrence which are exchangeable random quantities as opposed to independent, identically distributed ones. This implies that the order of impacts and non-impacts is unimportant. Next, the authors considered the uncertainty regarding the conditional arrival rate. This allows one to account for scatter in the data, errors in the "best fit" line and allows one to deal with the fact that few data points in the extremal zone exist. This method allows for improved extremal values when insufficient data is available. This topic is further discussed by Jordaan (1987) to include an allowance for avoidance. Avoidance of a potential encounter by a mobile structure (i.e., a ship) involves manoeuvring around the floe. In the case of a fixed structure (i.e., a gravity based structure), ice management techniques are employed.

A detailed statistical analysis of the local pressures measured on board the Polar Sea, MV Arctic and Canmar Kigoriak was performed by Maes and Hermans (1991). The authors considered methods for combining and analyzing the data and investigated the assumptions regarding the distribution of the extreme values, sample size and independence of the data. The uncertainty of predictions is analyzed and the validity of using the test data to predict lifetime risk is examined. It was found that both the Polar Sea and Canmar Kigoriak data sets can be used for extreme analysis. It was also determined that good agreement between the two data sets existed, especially for small areas. The probability distributions were derived using the tail-weighted Gumbel least-

squares method for different area classes. Exposure was taken into account. A detailed analysis is performed accounting for both model and statistical uncertainty. Lastly, the annual extreme value distribution and expressions for the T-year return period are derived.

An analysis of local ice pressure using probabilistic techniques was performed by Jordaan et al. (1993). This evaluation produced an algorithm which would allow the designer to calculate a design bow pressure corresponding to the mission profile of the ship and to the area being considered for areas up to 6 m^2. This methodology was based on local pressure data from the Polar Sea and Canmar Kigoriak and involved extrapolation techniques using extremal statistics. There is good agreement between the Maes and Hermans (1991) analysis and the fitted curve.

Varsta (1984) developed a semi-empirical method to derive ice loads based on data collected aboard the IB Sisu. The methodology employed first required measurement of the design ice pressure, normal to the ship's hull. Next, the maximum expected ice pressure was calculated using the measured daily maxima measured during winter, 1979, taken to the extreme for the lifetime of the ship (i.e., the 25-year load). The author next derived the average pressure as a function of shell strength rigidity; an allowance was made for the decrease in design pressure with load length. Last, the design force was calculated as a function of load height and load length. Two problems the reviewer sees with this analysis are first, the choice of the lifetime of the ship as opposed to a more conservative (say the 100-year) load. Second, the formulation is derived to account for the shape of the bow. This is reasonable if the original data has been converted to an

axis which is not normal or if the formulation accounts for the shape of the test bow (i.e., the reviewer would assume that the data recorded during trials is normal to the hull).

An approach to maintain the safety of existing ice-capable ships was discussed by Køhler and Jørgensen (1985). The authors combined non-linear finite element analysis, the structural particulars of the vessel, the mass of the design ice floe and the crushing strength of ice, to determine the safe operating speed of the ship when operating in ice. The authors reported that the results of the analysis compare favourably with the damage history of the vessel in question. The authors further advocated that a safe design can be developed for a given speed. Expected problems with this method might include the time and expense required to setup a model of each vessel to be considered, ensuring that the critical mode of failure is considered, and estimating the parameters of the design ice feature. Experience with ships operating in ice (Daley et al., 1986; St. John et. al, 1984; Dome Petroleum Ltd., 1982; German and Sukselainen, 1984; for example) also shows that above a speed of about 4 knots, there is little evidence for dependence of either local pressure or global force on velocity.

Masterson and Frederking (1992) examined local contact pressures developed during an interaction between a ship structure and ice. The authors used data collected from the following sources.

1. Ship trials on board the Arctic, Canmar Kigoriak and the Polar Sea.
2. Indentor tests from Hobson's Choice Ice Island, Pond Inlet and flat jack tests.

3. Measurements made in the Beaufort Sea on the Moliqpak structure and in the North Atlantic on Hans Island.

By combining this data the authors were able to compare the effect of contact area on pressure for the range of 0.1 m^2 - 100 m^2. It was found by the authors that despite the range of conditions from which the data came, the overall picture was coherent and showed decreasing pressure with increasing area up to approximately 20 m^2 after which the curve levelled off. The present reviewer feels that this is a good comparison of the data. Subdividing the data into subsets of related type would be a useful extension. The present work suggests that a probabilistic analysis is also a useful extension.

2.3 ANALYSIS OF PLATING

Clarkson (1956) presented an approach aimed at designing rigidly clamped plates to withstand lateral pressure. This paper was one of the first to develop a methodology incorporating elastoplastic design of plates for use in ship design. The approach presented began with the acknowledgement that very few plates on a ship are actually flat. For plates deflected beyond 70% of thickness, plate strength primarily resulted from membrane stresses as opposed to bending stresses. This allowed *dished* plates to provide greater resistance than flat plates. Clarkson also noted that once a plate was plastically loaded, it would act elastically up to where it was last loaded. The author discussed the theory behind elastoplastic analysis of flat plates; two approximate methods, the corner yield method and the method of plastic hinges, were considered. Numerical examples

were completed to examine the accuracy of the corner yield and plastic hinge methods. Finally, design curves were presented and verified. The author did not consider any deformation beyond the centre hinge formation.

The study of steel plates loaded beyond the elastic limit was extended by Young (1959). The primary aim of this paper was to develop a design method for ship plating based on plastic analysis of plate bending. Membrane forces and plastic deformation in the centre region of the plate were accounted for, hence advancing the work by Clarkson (1956). The analysis was limited to long plates, aspect ratio ≥ 3:1, subjected to normal loading. This analysis resulted in the derivation of formulae to be used in the design of steel plates. One reviewer, Dr. J.B. Caldwell, did note that unlike the work of Clarkson, Young's work lacked a clearly defined unserviceability criterion.

Experimental results were presented by Hooke and Rawlings (1969) for clamped, rectangular plates subjected to uniform transverse pressure. Nineteen tests were performed accounting for width to thickness relationships from 50-160 and aspect ratios (width / length) of 1, ⅔, ½ and ⅓. All tests were conducted into the plastic region. It was found that experimental results exceeded theoretical predictions for every case. Some of this deviation was attributed to slightly less than perfect clamping. Reasonable agreement between experimental results with aspect ratio = ⅓, and Clarkson's approach was noted. It can be stated that these experiments lend support to the theories which preceded them.

More recently, work in this area has been presented by Hughes (1981 and 1983). Hughes (1981) presented an explicit formula for the design of welded plates subjected to uniform pressure. This analysis was based on an acceptable level of permanent set to be

specified by the designer. For convenience, design curves were also provided. This work was later expanded to include concentrated loads (Hughes, 1983). Two types of concentrated loads, multiple location and single location, were considered. It was found that multiple location loads could be treated as uniform loads. For single location loads, a mathematical relationship was developed; in addition, design curves were presented.

Analyses of full scale collision damage (Minorsky, 1959 and McDermott et al., 1974) has also been presented. The work by Minorsky was involved with collisions between two ships. While this type of collision lies outside the present analysis, it did lend support to the large amount of reserve strength built into a vessel. McDermott et al. also supported the use of plastic analysis to estimate the loads that resulted from tanker collisions. In their analysis, the authors made use of the *effective strength*, the mean of yield strength and ultimate strength, of the steel. Use of the effective strength is supported by Egge and Böckenhauer (1991) and Nessim et al. (1992).

2.4 SAFE DESIGN OF STRUCTURE

Kulak et al. (1990) define structural design as a balance between creative art and reasonably exact science. To this end, the structural designer must aim to:

1. provide a safe, reliable structure to perform its intended function; and
2. ensure that the structure is economical to build and maintain.

To ensure a safe, reliable structure, the designer checks that the performance of a structure is sufficient to resist the various limiting conditions at appropriate loads.

Two classes of limit states generally considered in steel construction are ultimate limit states and serviceability limit states (Kulak et al., 1990). Ultimate limit states are concerned with safety, i.e., load exceeding capacity, foundering, loss of stability, and excessive pollution. Serviceability limit states are concerned with unsatisfactory behaviour of the structure under normal operating conditions, for example, excessive permanent deformation and loss of structural support. The *Canadian Standards Association* (CSA) code S.471 for fixed offshore structures (Jordaan and Maes, 1991) suggest safety levels of 10^{-5} against Class 1 or ultimate failures and 10^{-3} against Class 2 or serviceability types of failure. In addition to damage caused by a single extreme load, the designer must also account for progressive damage caused by repeated loads (Moan and Amdahl, 1989). It is noted that progressive damage analysis lies outside the scope of the present analysis.

Mansour (1972) presented a probabilistic design model for the longitudinal strength of a ship. This method acknowledged the random nature of the variables involved with modelling the physical problem. This is believed to make the model more realistic. An acceptable risk based on economic criteria was selected for the analysis. The generalised cost function suggested is:

$$C_g = C_i + \Phi C_f \tag{2.1}$$

where C_g is the generalised cost; C_i is the initial cost of construction plus maintenance costs less the value of the ship when no longer in use; Φ is the probability of failure; and C_f is the total cost of construction or repair, revenue loss due to interruption of operation and other expenses derived from the failure. The probability of failure, Φ, is derived by

minimising C_g. One difficulty expressed by the author was obtaining an accurate value for C_f, especially when human lives are involved.

Considerable work has been completed with regard to evaluating the reliability of a structure (Galambos and Ravindra, 1978; Mansour et al., 1984; White and Ayyub, 1985; Ayyub and White, 1987; White and Ayyub, 1987; for example). White and Ayyub (1985) stated that new materials and improved fabrication techniques have made standard design techniques obsolete. This was supported by Mansour et al. (1984) who stated that ABS ships became less safe with increased size, however, they also concluded that methods used for offshore structures were not appropriate. Analysis of steel buildings (Galambos and Ravindra, 1978) and of ships (Mansour et al., 1984) made use of the load and resistance factor design (LRFD) method. The LRFD method did require calibration. Several methods of calibration were evaluated. The first-order second-moment (FOSM) method was found to be a useful method of calibration only when all variables were normally distributed (White and Ayyub, 1985). The mean-value first-order second-moment (MVFOSM) method, the advanced first-order second-moment (ASM) were found to overestimate the safety of the ship (Mansour et al., 1984). The exact Level-III method was found to give accurate results but was limited in scope, i.e., any changes in the distribution required major changes to the routine (White and Ayyub, 1985). Reliability-conditioned (RC) partial safety factors, proposed by Ayyub and White (1987) and extended to marine structures by White and Ayyub (1987), were thought to be the most efficient method of calibrating safety factors because they gave accurate results and could be easily applied to general types of problems. The LRFD method falls outside the scope

of the present analysis because calibration requires that the safety of existing vessels is known.

A method for assessing the life of a ship's structure is discussed by Ayyub et al. (1989). The authors first discuss potential failure modes grouping them as catastrophic, serviceability ending, serviceability limiting, non-limiting or nuisance. For illustration purposes, the authors chose ductile yielding of an individual plate panel and fatigue cracking of structural details, however, caution that in the case of a real analysis, all modes of failure and failure combinations must be explored. The authors next defined the end of structural life as an economic factor. Those defined for illustrative purposes are as follows.

1. The need to replace more than five panels in a specified area during one inspection period.
2. One fatigue failure of a critical detail at the end of an inspection period.

The authors assessed the structural strength of the vessel with regard to plate deformation and fatigue. It was found that for two year inspection intervals that there was a 28% chance that a vessel would sustain enough damage to constitute the *end of structural life* as defined after 15 years. It was further found that after 15 years, that there was only a 2% chance of a vessel reaching the *end of structural life* as a result of fatigue failure. A comparative assessment of patrol boat bottom plating is presented by Ayyub et al. (1990) using the two failure mode (deemed most likely) specified above. A number of improvements are recommended.

3 ANALYSIS OF LOCAL PRESSURE

3.1 OVERVIEW

Two very good sources of full scale data are available for performing an analysis of local ice loads. These are reports on the 1981 deployments of the Canmar Kigoriak (Dome Petroleum Ltd., 1982) and the 1983 deployment of the Polar Sea (Daley et al., 1986). In both cases, the bow of the ship was instrumented with strain gauges and measurements were made for repeated rams.

The data collected on board the Canmar Kigoriak were obtained during the August and October, 1981, deployments of the vessel in the Canadian Beaufort Sea. August rams were conducted primarily in heavy first year and second year ice while October rams were conducted in multiyear ice. In all, 397 rams were conducted. Measurements were made on two instrumented panels designated A1 (1.25 m^2) and A2 (6.0 m^2) located on the port shoulder of the ship. Both of these panels were subdivided into smaller areas termed *subpanels*. Force measurements and contact areas were estimated by summing shear differences between strain gauges. In the case of A1, the panel was divided into six equal subpanels of 0.208 m^2. In the case of A2, the panel was divided into three subpanels of 0.667 m^2 and twelve subpanels of 0.333 m^2. Schematic drawings of these areas are presented in Figure 3.1. The test data are found in Appendix A of Dome Petroleum Ltd. (1982). These data include the maximum force recorded during the ram and the area over which it was measured.

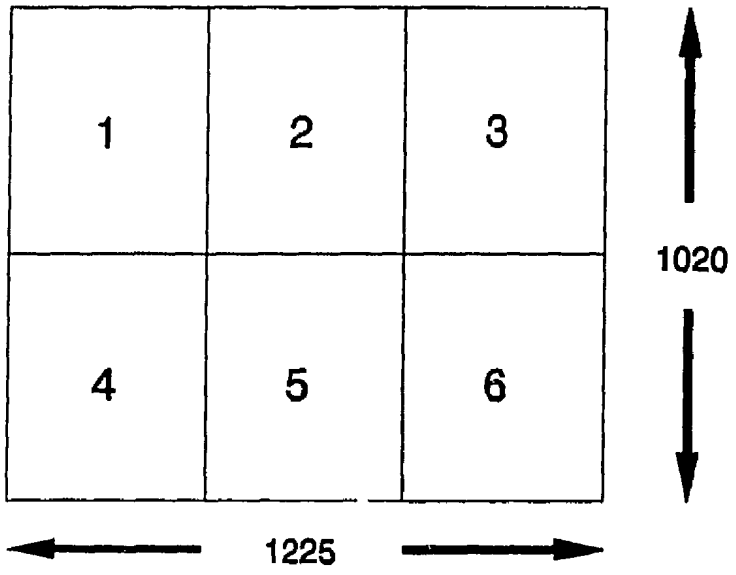

Figure 3.1(a): Schematic Diagram of the 1.25 m^2 Instrumented Panel (A1).

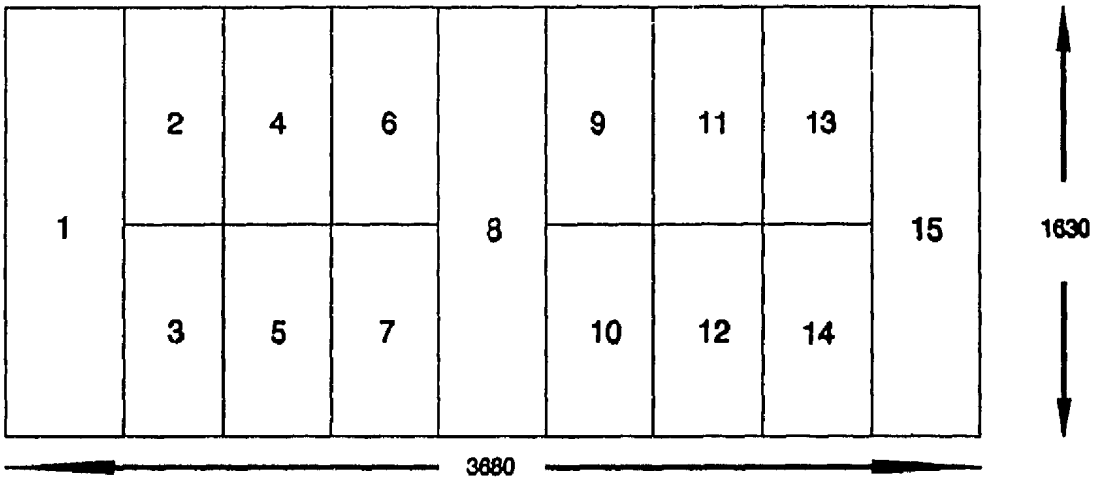

Figure 3.1 (b): Schematic Diagram of the 6.0 m^2 Instrumented Panel (A2).

Pressure measurements were performed on board the Polar Sea during an April, 1983 deployment of the vessel in the North Chukchi Sea. This data set consists of 513 impacts with heavy first year and multiyear ice features. The data were measured on an instrumented area of 9.1 m^2. This area was subdivided into 60 subpanels of 0.152 m^2. For each impact, the highest force measured on a single subpanel was recorded. These data are provided in Appendix A of Daley et al. (1986). The peak pressure on larger areas (see Figure 6, Daley et al., 1984) was calculated by averaging the peak force just mentioned with the next highest force on an adjacent subpanel at the same point in time, and so on. Discussion of the method employed and further analysis of the data is found in Section 3.5.

3.2 General Analysis of Ice Loads

Using the ice load data just mentioned for the Canmar Kigoriak and Polar Sea, the *fixed area* ice pressure was calculated as follows. The force data for each data set (i.e., A1 and A2 for the Canmar Kigoriak and the 1 subpanel data for the Polar Sea) were entered into a spreadsheet, sorted in ascending order and ranked from 1 to n_i. The fixed area pressure was calculated for each measurement by dividing the force by the reference area (for example, A1 = 1.25 m^2). The probability on non-exceedance, p_{ne}, was calculated for each point according to:

$$p_{ne} = F_X(x) = \frac{i}{n_t + 1} \tag{3.1}$$

where $F_X(x)$ is the cumulative density function, i is the rank of the data point and n_t is the number of data points in the set. It is noted that only impacts which produced a load on the instrumented panel (called *hits*) are considered. Ship rams which produced no load on the panel (i.e., *misses*) are accounted for in the exposure model. The Weibull plotting position (Equation (3.1)) is used for convenience. More elaborate plotting positions, which reduce bias, can be selected (Arnell et al., 1986). This does not affect the result significantly for large samples.

These data were plotted with respect to exceedance probability, $p_e = 1 - p_{ne}$, (see Figure 3.2). It can be seen in Figures 3.2(a-c) that these plots are generally exponential in the tail (i.e., the larger values produce a straight line when plotted on semi-log paper). The one exception to this, Figure 3.2(b), which presents a *levelling off* trend in the tail. This is the result of an anomaly within a particular subset of the data and is discussed in Section 3.3 (see also, Maes and Hermans, 1991). A curve of the form:

$$-\log(p_e) = m_j x + y_j \tag{3.2}$$

where m_j is the slope, x is the pressure and y_j is the y-intercept is fitted to the tail using least-squares regression. For each data set presented in Figure 3.2, the coefficients of form are given in Table 3.1. These curves are discussed further in Section 3.7.

Table 3.1 - Coefficients of Best-Fit Curves for Fixed-Areas		
Data Set	m_j (MPa)	y_j
Polar Sea - 1 Subpanel	0.230	0.152
Canmar Kigoriak - A1	0.373	-0.113
Canmar Kigoriak - A2	1.281	0.038

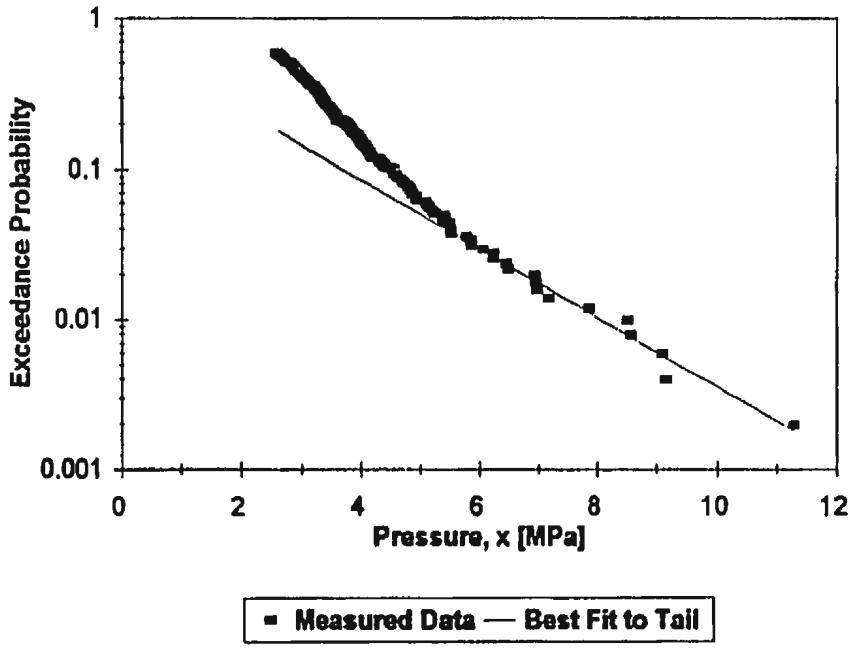

Figure 3.2 (a): Empirical Analysis of Local Pressure for the Polar Sea.

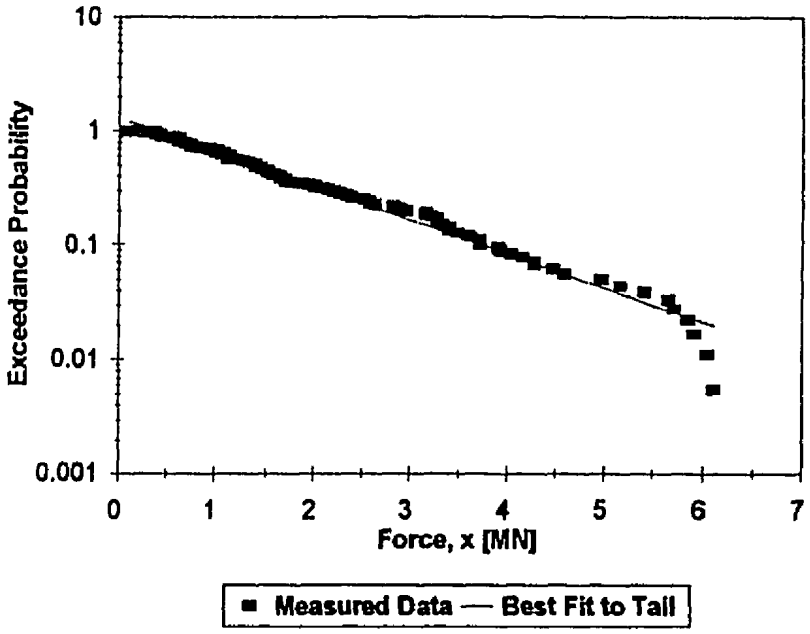

Figure 3.2 (b): Empirical Analysis of Local Pressure for the Canmar Kigoriak (A1 = 1.25 m^2).

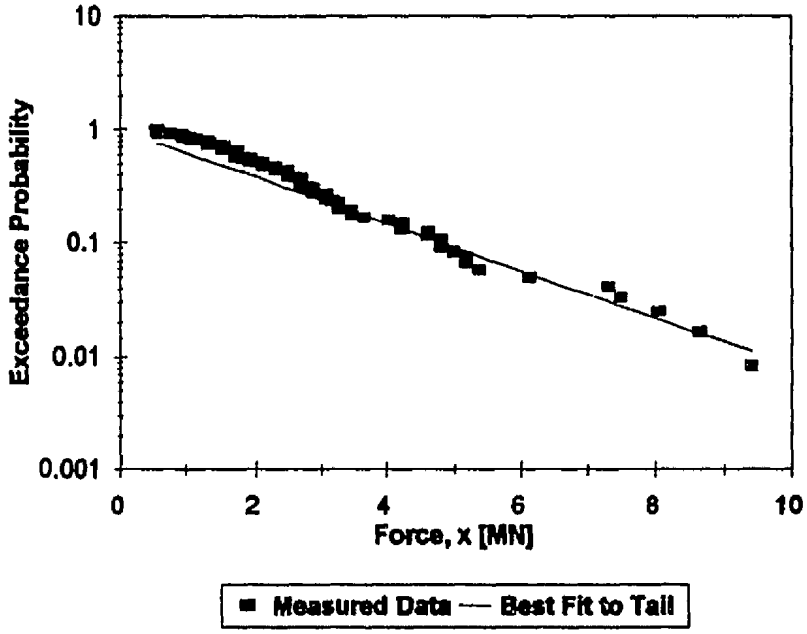

Figure 3.2 (c): Empirical Analysis of Local Pressure for the Canmar Kigoriak (A2 = 6.0 m^2).

3.3 Analysis of Canmar Kigoriak Small Panel Data

As mentioned earlier, the Canmar Kigoriak data presented the maximum force recorded during an impact and the area it was measured on. As a result, the data can be analyzed statistically using extreme statistics (Gumbel, 1958) in order to develop a pressure-area relationship for each of the subareas within the instrumented panel. The analysis used is based on the methodology presented by Maes and Hermans (1991).

3.3.1 Analysis of Measured Data

Using the data collected on A1 during the 1981 deployments, the following analysis was performed. The data were entered into a spreadsheet. Only hits were considered. The data are then grouped according to the area (number of subpanels) the force was measured on and transferred into separate spreadsheet pages. This grouping is referred to as the *moving* or *loaded* area class, k. A histogram of moving areas is presented in Figure 3.3.

The data are ranked (based on force) in ascending order and the probability of non-exceedance, p_{ne}, for each point is calculated. Again, straight lines are fitted to the tail of each curve (see Figure 3.4). It is noted that more weight is given to higher values in each set than to lower ones because it is these values which *drive* the extreme. These curves required some adjusting to achieve reasonable correlation between the slopes of the simulated curve for six subpanels and the original data curve fitted in Section 3.2.

While it is admitted that the data does not fit an exponential distribution, the tails of most distributions are exponential. This is considered appropriate for this analysis because the extremal load depends strongly on the tail of the parent distribution (Jordaan, 1985). These curves will be used to predict the design loads on each of the subpanels. The slope, m_k, and intercept, y_k, for each area class are presented in Table 3.2. It is noted that values calculated for low exposure conditions (i.e., a vessel operating in subarctic waters) should be checked against the original data to ensure their validity (i.e., that the values estimated are in the tail).

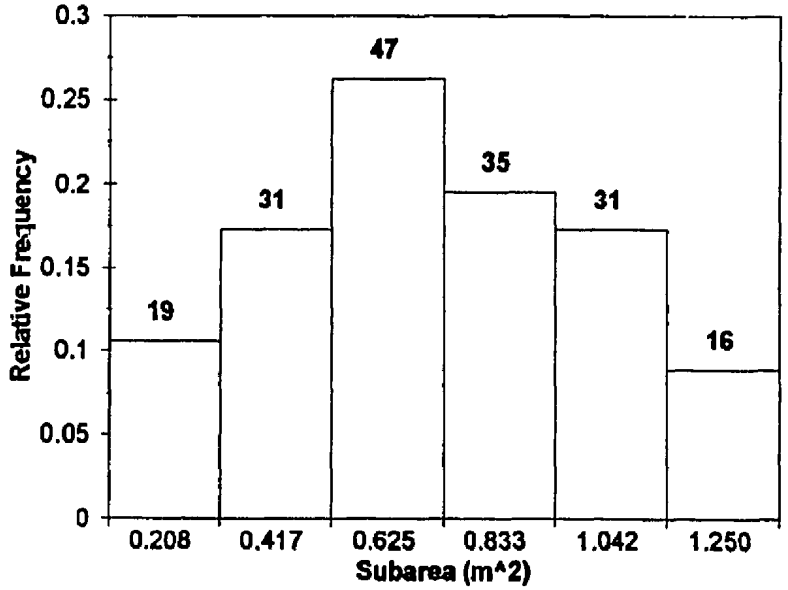

Figure 3.3: Histogram for 179 Rams of the Canmar Kigoriak During 1981 August and October Trials. Contact Area Between a Ship and Ice on a 1.25 m^2 Panel.

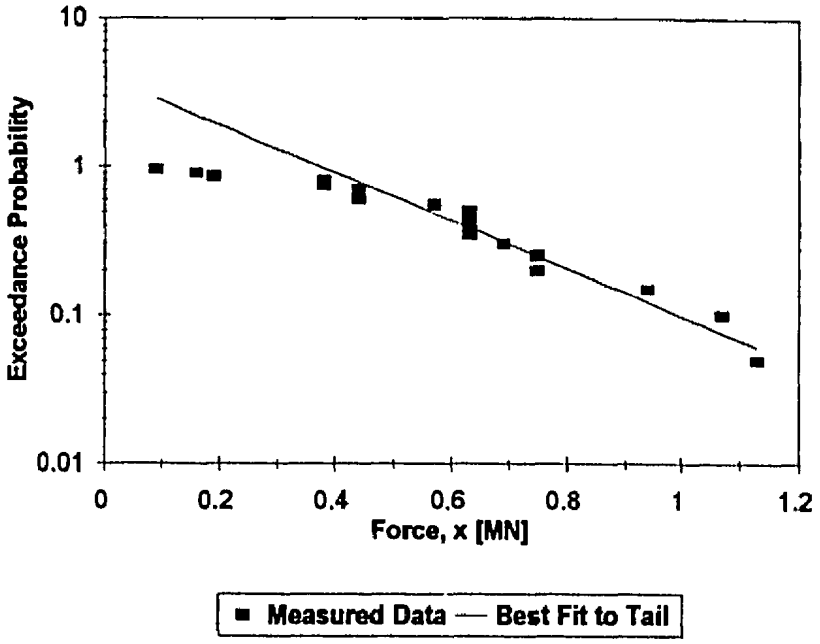

Figure 3.4(a): Distribution of Force on a 1 Subpanel Moving Area for the Canmar Kigoriak.

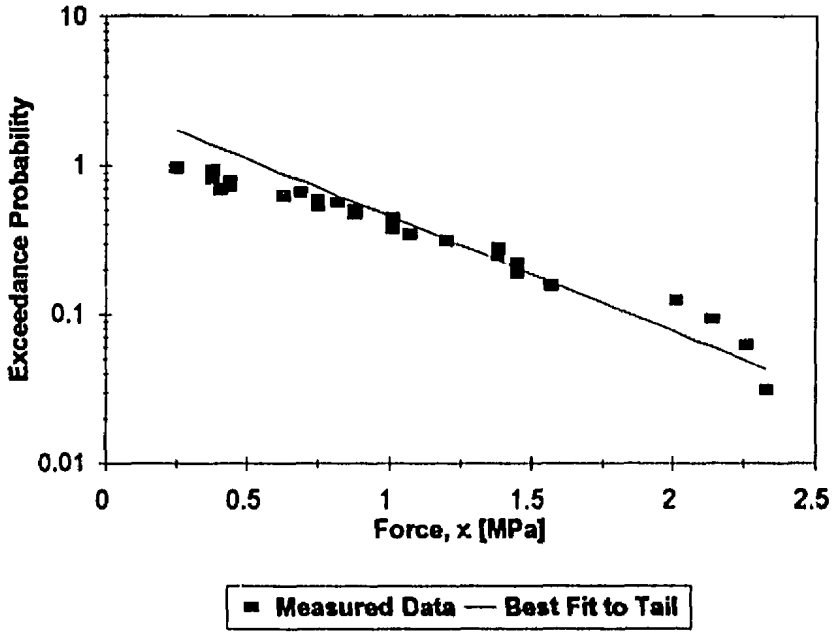

Figure 3.4(b): Distribution of Force on a 2 Subpanel Moving Area for the Canmar Kigoriak.

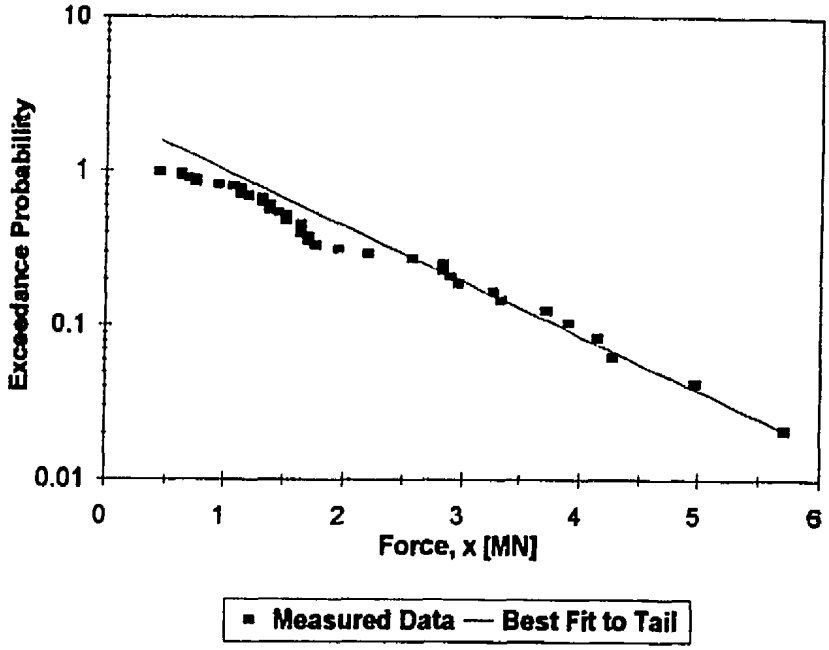

Figure 3.4(c): Distribution of Force on a 3 Subpanel Moving Area for the Canmar Kigoriak.

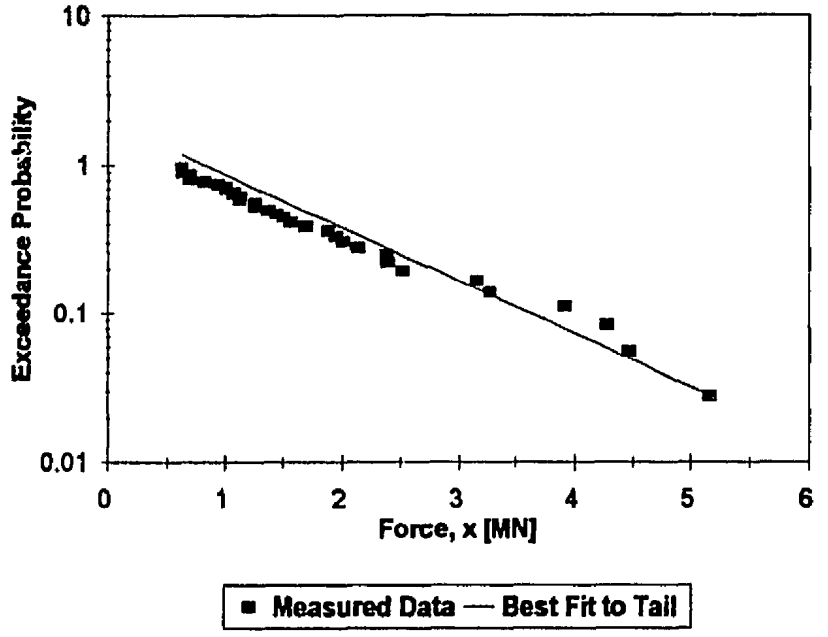

Figure 3.4(d): Distribution of Force on a 4 Subpanel Moving Area for the Canmar Kigoriak.

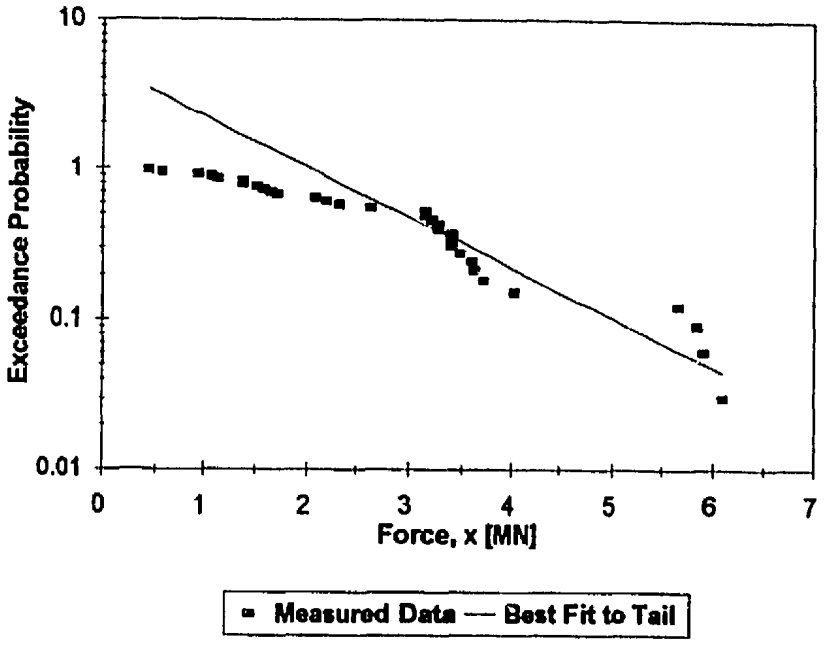

Figure 3.4(e): Distribution of Force on a 5 Subpanel Moving Area for the Canmar Kigoriak.

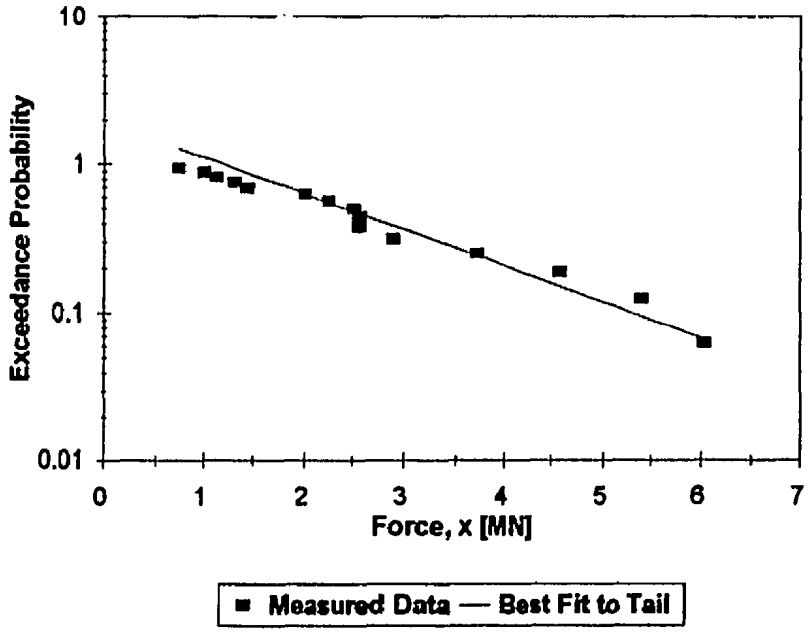

Figure 3.4(f): Distribution of Force on a 6 Subpanel Moving Area for the Canmar Kigoriak.

Table 3.2: Coefficients of Best-Fit Curves for Moving Areas, A1 = 1.25 m^2		
Area Class, k	m_k (MN^{-1})	y_k
1	1.600	-0.597
2	0.771	-0.429
3	0.356	-0.356
4	0.358	-0.298
5	0.332	-0.672
6	0.243	-0.289

It is noted for the 5 subpanel case (see Figure 3.4(e)) that the data is not linear in the extreme which implies a levelling off. There is no implication of such an effect in any of the other data. Furthermore, loads of up to 70 MPa have been measured during indenter tests (Frederking et al., 1990). Upon further study of Figure 3.4(e), another levelling off effect is found in the range of 3 MN and 4 MN. This is attributed to the difference in forces measured when 1 critical zone (Jordaan et al., 1991) is present as compared with 2 critical zones. As a result, it is assumed that if more impacts were performed, then impacts which produce 3 critical zones would be present resulting in increased loads. Hence, this anomalous behaviour is not considered further.

3.3.2 Coverage Analysis

As discussed above, the curves derived in the previous section are for loaded areas or moving areas and are a function of the impact between the ship and ice. The present

analysis is concerned with a fixed design area, i.e., to develop curves similar to those discussed in Section 3.2 for each of subarea. As a result, the probability of coverage must be considered.

We will consider the 2 × 3 design panel, presented in Figure 3.1(a), which was employed during the Canmar Kigoriak trials (Dome Petroleum Ltd., 1982). First we require the probability of coverage, p_c, for all combinations of fixed, j, and moving, k, panels sizes $p_c(j,k)$. Coverage, c, is defined as the overlap between the moving and fixed design areas (See Appendix A of Maes and Hermans (1991) for a full discussion). Possible fixed load and moving load patterns are found in Appendix 1(a). Similar assumptions to those used by Maes and Hermans (1991) were employed. These are as follows.

1. As a result of the instrumentation system employed during the trials, only integral numbers of subpanels are considered.
2. When selecting coverage possibilities, only contiguous combinations of subpanels are considered.
3. Since a given coverage may result from many combinations of fixed and moving areas, it is assumed that the load on the overlapping area is the same as that measured on the entire moving area.
4. It is assumed that all loading and design area *patterns* are equally likely.
5. All interactions are equally likely.
6. Combinations which require loading outside the instrumented panel are not considered.

The results of this analysis are found in Table 3.3. It should be noted that not all columns for a given $p_c(j,k)$ add up to one because $p_c(j,k)$ for $c = 0$ is not considered.

Table 3.3 - Probability of Coverage for Given j and k, $p_c(j,k)$

j	c	k					
		1	2	3	4	5	6
1	1	1/6	1/3	1/2	2/3	5/6	1
2	1	1/3	20/49	17/35	16/35	1/3	0
	2	0	1/7	2/7	16/35	2/3	1
3	1	1/2	17/35	9/25	9/50	0	0
	2	0	2/7	12/25	14/25	1/2	0
	3	0	0	1/10	13/50	1/2	1
4	1	2/3	16/35	9/50	0	0	0
	2	0	16/35	14/25	19/50	0	0
	3	0	0	13/50	13/25	2/3	0
	4	0	0	0	1/10	1/3	1
5	1	5/6	1/3	0	0	0	0
	2	0	2/3	1/2	0	0	0
	3	0	0	1/2	2/3	0	0
	4	0	0	0	1/3	5/6	0
	5	0	0	0	0	1/6	1
6	1	1	0	0	0	0	0
	2	0	1	0	0	0	0
	3	0	0	1	0	0	0
	4	0	0	0	1	0	0
	5	0	0	0	0	1	0
	6	0	0	0	0	0	1

3.3.3 Monte Carlo Simulation

Maes and Hermans (1991) developed the following closed form solution to calculate the design force distribution from the moving force distribution, and coverage probabilities:

$$1 - F_{Xj}(x) = \sum_{c=1}^{j} \sum_{k=c}^{n_i - j + c} p_c(j,k)\ Pr[K = k] \left[1 - F_{Xk}\left(\frac{k}{c}\, x\right)\right] \qquad (3.3)$$

where n_i is the total number of subpanels (i.e., 6 and 18 for A1 and A2 respectively), $\Pr[K = k]$ is the probability that a random quantity of moving panels, K, is equal to a specified number, k. $F_{Xj}(x)$ is the CDF for the fixed area curves and $F_{Xk}(x)$ is the CDF for the moving area curves.

As a means of verifying Equation (3.3), a Monte Carlo simulation was written and employed to develop fixed area load distributions. The program considered each fixed design area in sequence. Each iteration (there were 10,000 per fixed area class) consisted of:

1. randomly selecting k using the histogram of area data (see Figure 3.3);
2. randomly selecting $p_c(j,k)$ and then using the CDF for coverage probability to obtain c;
3. randomly selecting p_e;
4. calculating the moving pressure, P_k, using k and p_e; and
5. printing P_k, c and j to an output file if $P_k \geq 0$ and $c > 0$.

The output file was then input into another program which calculated the design area pressure, P_j, according to:

$$P_j = \frac{c}{j} P_k. \tag{3.4}$$

These data were then sorted in descending order according to P_j and the largest 6500 points were output to a file. The spreadsheet software allows approximately 8000 rows of data per file; 6500 was chosen for manageability.

These data were plotted against the exceedance probability and the tail was fit using least-squares linear regression. The α values calculated for these curves are plotted in Figure 3.5 along with those of Maes and Hermans (1991); see Section 3.7 for discussion of α. As can be seen, there is good correlation between the methods.

3.3.4 Analysis of Data

A program was written to perform the calculation specified in Equation (3.3). This program uses the coverage information (see Table 3.3), best-fit curve coefficients (see Table 3.2) and probability of moving area size (see Figure 3.3) data to perform the calculations.

The results of this analysis are presented in Figure 3.6. It is noted that the curves developed are not linear. The results can be presented as linear without great loss of accuracy (Maes and Hermans, 1991). Linear fits to the fixed area results are calculated

using least-squares regression are also presented in Figure 3.6. The coefficients of these curves are presented in Table 3.4.

As can be seen by comparing Tables 3.2 and 3.4, the slopes of the curves (plotted on semi-log paper) become smaller. This is an appropriate result as $P_j(k = 6)$ will temper the slope of the curves for smaller areas.

Table 3.4 - Coefficients of Best Fit Curves for Fixed-Areas, A1 = 1.25 m^2

Area Class, j	m_k (MN^{-1})	y_k
1	1.073	0.446
2	0.553	0.474
3	0.406	0.403
4	0.382	0.037
5	0.331	-0.039
6	0.289	-0.093

3.4 ANALYSIS OF CANMAR KIGORIAK LARGE PANEL DATA

There are a number of inconsistencies in the collection, interpretation and reporting of the A2 data set with respect to the A1 data set. These include the following.

1 Two subpanel sizes were used to measure data (see Figure 3.1(b)).

2. The subpanels used to measure the A2 data are significantly larger than for A1 (0.333 m^2 or 0.667 m^2 as regards 0.208 m^2).

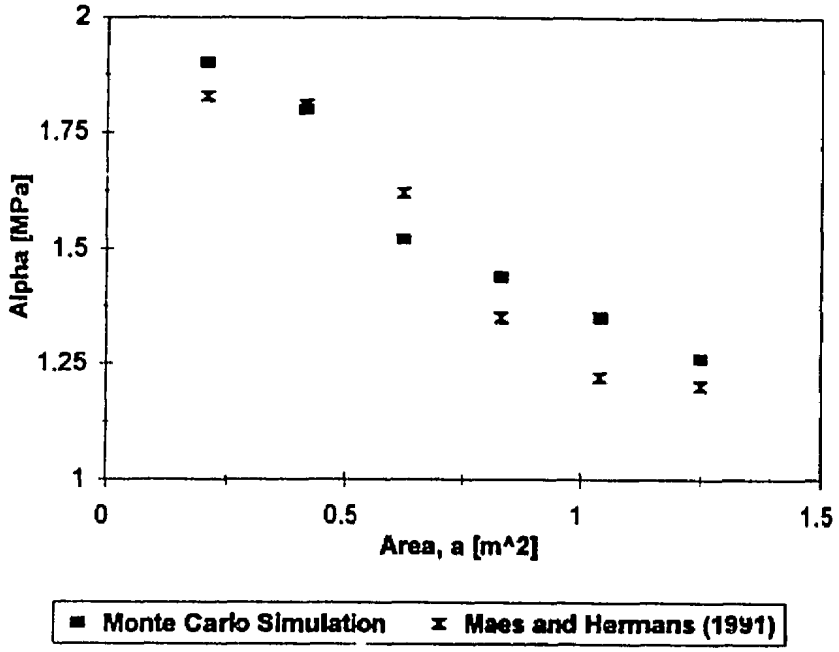

Figure 3.5: Comparison of Monte Carlo Simulation with Maes and Hermans (1991).

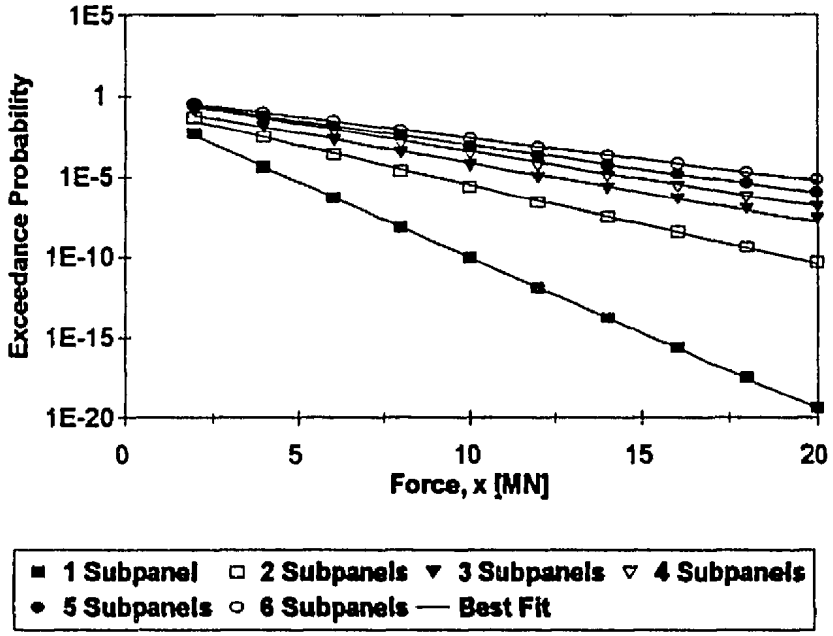

Figure 3.6: Fixed Area Force Distribution for Canmar Kigoriak, 1.25 m^2 Panel.

3. A large number of measured loads are not contained on an integral number of subpanels (as a result of items 1 and 2).

4. Many moving area classes have very few data points, if any, as a result of the large number of subpanels considered.

5. A2 is aft of A1 thus reducing the likelihood of a hit (especially with multiyear ice).

As a result, two additional assumptions were made in formulating the design area model.

a. The histogram of moving area class frequency was developed using standard statistical theory (for example, the 3 subpanel bin included data with moving areas of 2.5 to 3.5 subpanels). Hence, the uncertainty associated with this model is increased with respect to A1.

b. When necessary, two or more moving area classes are grouped together to produce a reasonable size data base to develop the moving area curves.

In addition to the two simplifications just mentioned, two further simplifications were made.

i. Only regular panel shapes (for both fixed and moving panels) are considered when developing the coverage model.

ii. Subpanels 1, 8 and 15 (see Figure 3.1(b)) cannot be subdivided.

These simplifications were made to reduce the amount of work required to formulate the coverage model. Schematic drawings of the load patterns are found in Appendix 1(b).

The model assumptions, just mentioned, were incorporated with the methodology used for A1 to develop the $p_c(j,k)$ table (see Appendix 1(b)) for A2, the probability of

moving area size (see Figure 3.7) and in developing the best fit curves (see Table 3.5). These results, along with the program referred to in Section 3.3.4 were used to estimate the fixed design force curves for each area class within A2. The coefficients of each of these curves are presented in Table 3.6.

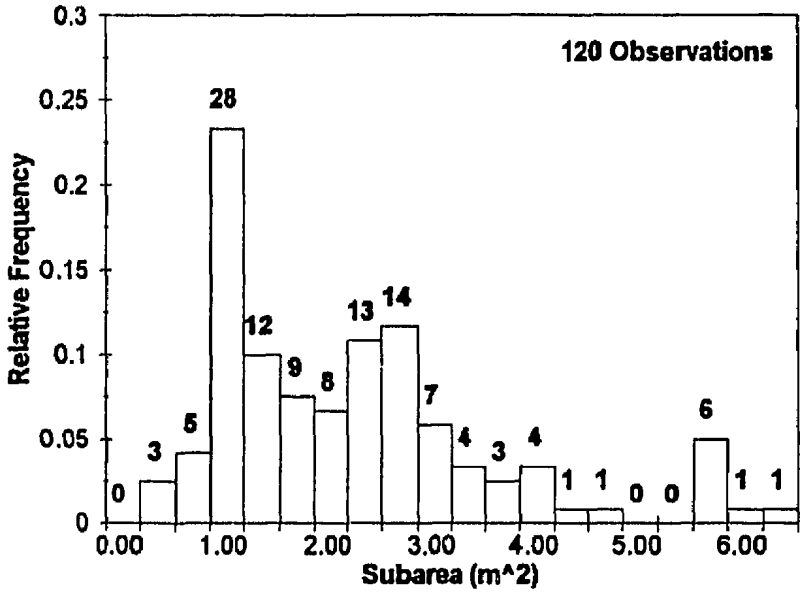

Figure 3.7: Histogram for 120 Rams of the Canmar Kigoriak During 1981 August and October Trials. Contact Area Between Ship and Ice on a 6.0 m^2 Area.

Table 3.5 - Coefficients of Best-Fit Curves for Moving Areas, A2 = 6.0 m^2		
Area Class, k	m_k (MN^{-1})	y_k
1,2	0.575	-0.253
3	0.668	-0.724
4	0.527	-0.604
5	0.262	-0.309
6	0.517	-0.390
7	0.521	-1.052
8	0.400	-0.700
9-10	0.151	-0.333
11-12	0.185	-0.477
13-18	0.154	-0.126

3.5 ANALYSIS OF THE POLAR SEA DATA

The data set used for the Polar Sea was collected during a winter, 1983, deployment of the vessel in the North Chukchi Sea. This data is found in Appendix A of Daley et al. (1986). Ice loads were measured on an instrumented panel measuring 9.2 m^2 in the bow of the ship. This panel was subdivided into sixty subpanels of 0.152 m^2.

The data set reported by Daley et al. (1986) consists of the highest force measured on a single subpanel during a ram. For larger areas (see Figure 6, Daley et al., 1984), peak pressure was calculated by taking the maximum force just mentioned and averaging it with the next largest contiguous subpanel at the time of the maximum force, and so on.

This method tends to give lower values at larger contact areas than the method employed by the Canmar Kigoriak. This can be seen in Figure 3.8. As a result, direct comparisons between the data for Canmar Kigoriak and Polar Sea is not possible for larger areas as the Polar Sea data will give lower than peak pressures. The pressure data measured on small areas (= 0.21 m^2) will be analyzed to see if the two data sets can be compared directly.

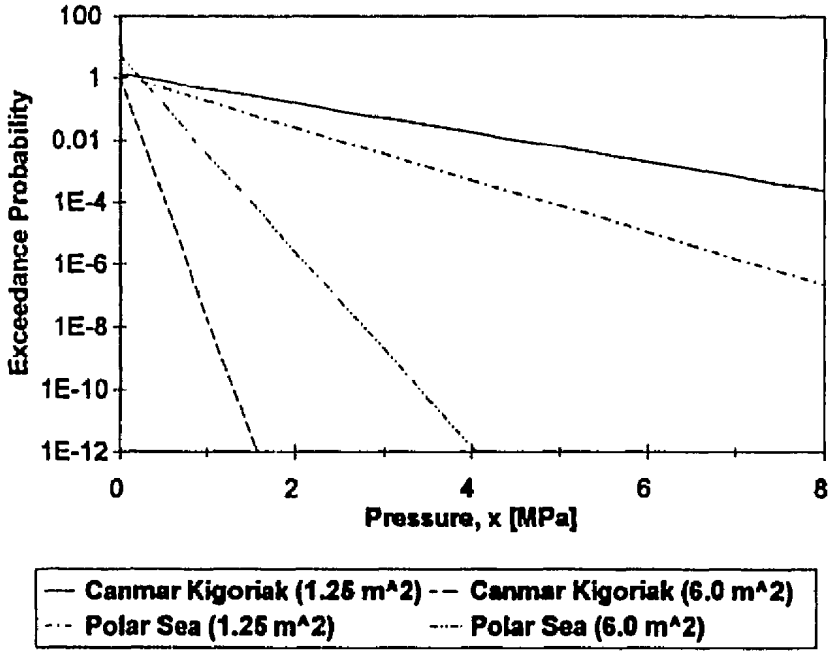

Figure 3.8: Comparison of Polar Sea and Canmar Kigoriak Data. Local Pressures on Fixed Areas.

Table 3.6 - Coefficients of Best-Fit Curve for Fixed-Areas, A2 = 6.0 m^2		
Area Class, j	m_j (MN^{-1})	y_j
1	0.586	2.261
2	0.627	1.030
3	0.481	0.756
4	0.362	0.714
5	0.306	0.629
6	0.269	0.555
7	0.241	0.476
8	0.224	0.434
9	0.210	0.340
10	0.201	0.330
11	0.193	0.271
12	0.190	0.228
13	0.187	0.188
14	0.183	0.158
15	0.182	0.137
16	0.179	0.113
17	0.183	0.122
18	0.175	0.096

3.5.1 Comparison of Small Area Data

The small area (≈ 0.21 m^2) pressure data for the Canmar Kigoriak and Polar Sea must be analyzed to ensure that the two data sets are directly comparable, i.e., that they can be assumed to come from the same parent distribution. Figure 3.9(a) presents the

pressure data, measured on an area of approximately 0.21 m^2, with respect to exceedance probability. Data presented here come from both the A1 and A2 data sets. It is noted that exceedance probability accounts for exposure (see Section 3.6) resulting from 397 impacts, 2 readings per ram, and a contact area of 0.21 m^2 within a 7.25 m^2 instrumented area.

Next, it is assumed that all of the pressure data can be used for this analysis. Carter et al. (1992) suggest that average pressure experienced by a large area is also experienced by a smaller area within it. Figure 3.9(b) presents all the local pressure measurements recorded on board the Canmar Kigoriak. Exposure has again been considered. The similarity between the two slopes is encouraging.

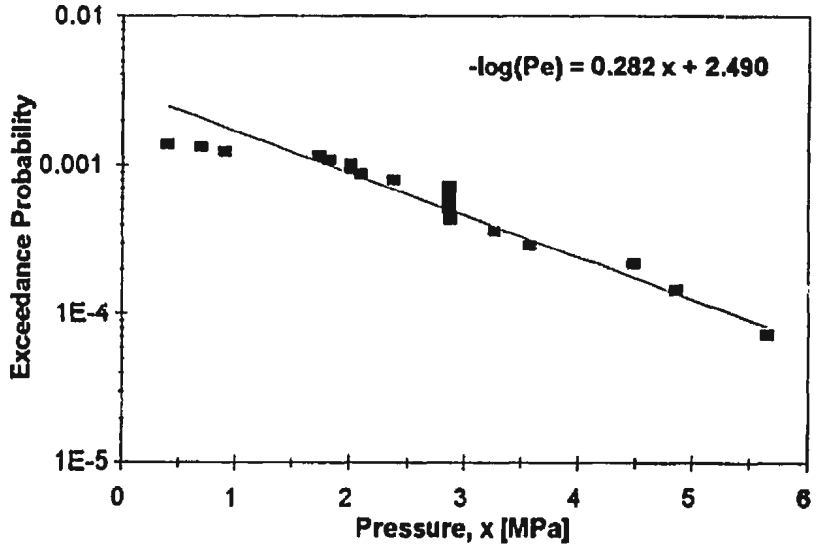

Figure 3.9(a): Analysis of Canmar Kigoriak Pressure on 0.15 - 0.30 m^2 Subpanels.

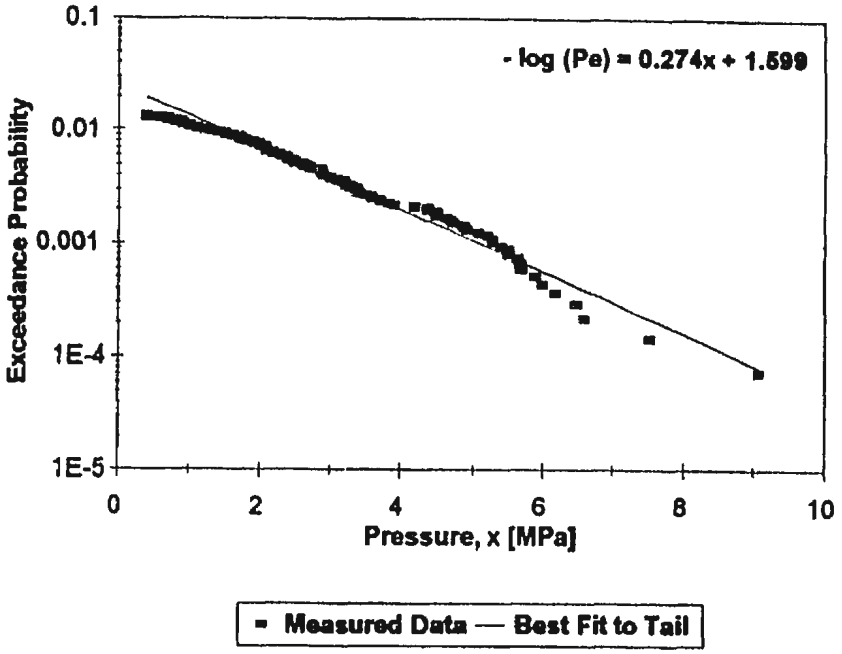

Figure 3.9(b): Pressure Analysis of the Canmar Kigoriak Using Results for A1 (= 1.25 m^2) for a Single Subpanel.

Figure 3.10 presents the Polar Sea data for one and two subpanels. There were 60 subpanels employed during the Polar Sea trials, hence, exceedance probability has been adjusted to incorporate this exposure. In addition, a best-fit curve was approximated for an area of 0.21 m^2 by linear interpolation. This is considered to be appropriate for the following reasons.

1. It is assumed that any deviations in the pressure curve for two subpanels, as regards the formulation of peak pressure on larger areas, is negligible for an area of two subpanels.
2. It is assumed that the relative differences between the two areas is small enough to allow a linear interpolation without significant error.

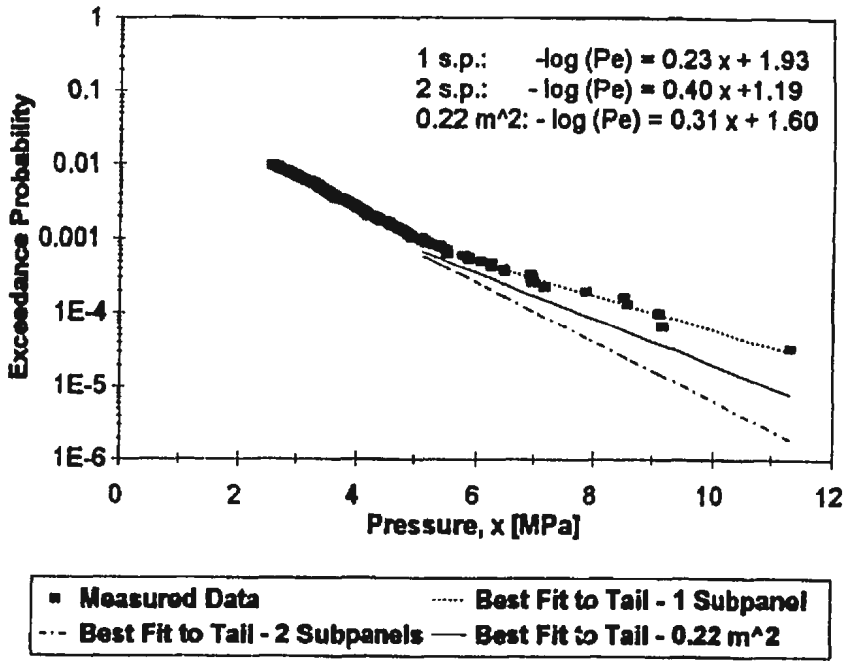

Figure 3.10: Empirical Analysis of Local Pressure on the Polar Sea, 0.22 m^2 Subpanels.

Figure 3.11 presents the Canmar Kigoriak best-fit curve (for all subareas) and that for the Polar Sea for an area of 0.21 m^2. The agreement between the slopes and the y-intercepts of both curves is encouraging and it is concluded that both data sets are similar.

3.6 EXPOSURE

When analyzing ship-ice interaction data, exposure must be considered. One example of exposure concerns the number of subpanels employed during the test programme. The data for the Polar Sea presented in Figure 3.12 is actually the peak pressure measured on one subpanel in an array of sixty subpanels. Hence, this actually

represents an exposure of 60 n_i. The Polar Sea data is replotted in Figure 3.12 accounting for this exposure. As can be seen, this results in a vertical shift in the data and lower probabilities.

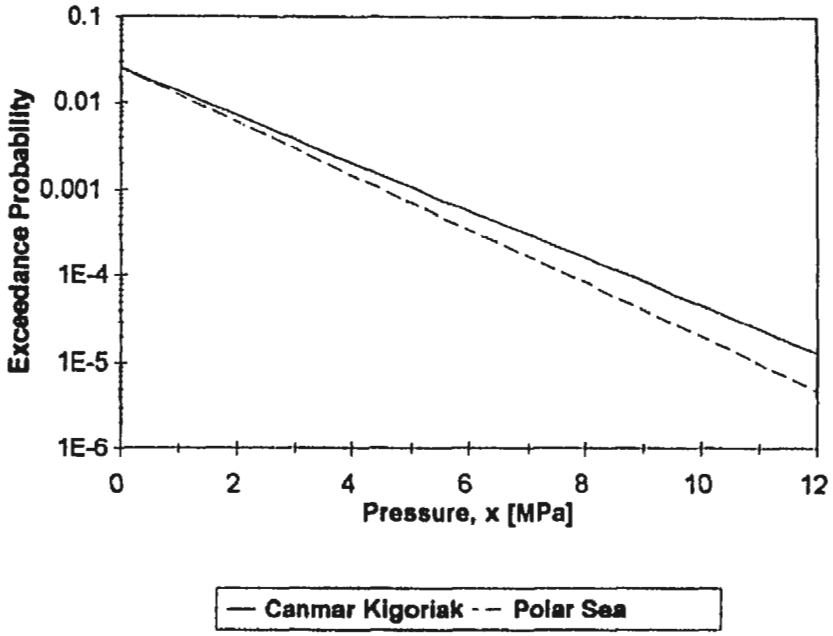

Figure 3.11: Comparison of Canmar Kigoriak and Polar Sea Data on 0.22 m^2 Subareas.

Another example of exposure concerns the length interaction of an event. For the case of continuous interaction (i.e., a few minutes, hours, days, ...) the probability of an extreme load being recorded is higher than for a ram (i.e., lasting a few seconds). As a result, duration must also be considered.

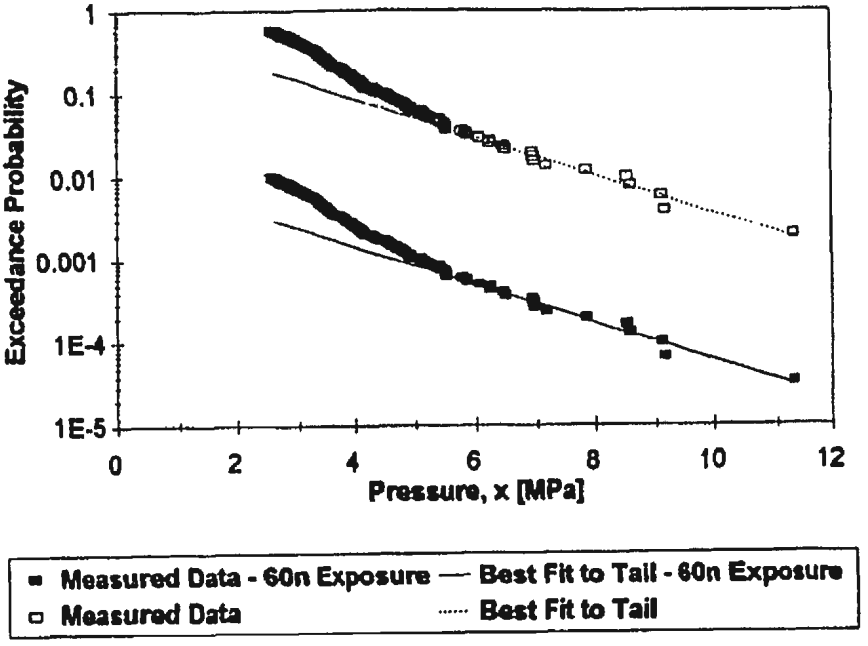

Figure 3.12: Effect of Exposure on Empirical Analysis of Local Pressure for Polar Sea.

A third example of exposure pertains to the location on the ship. For example, the bow of the ship is more prone to higher loads during a ram with multiyear ice than are the sides or bottom. This type of exposure is reflected in the ASPPR Proposals (Melville Shipping Ltd., 1989) by using area factors to increase or decrease the design pressure. The result of this, assuming 10,000 bow impacts per year, is presented in Figure 3.13. This results in somewhat exaggerated exposure values because impact quality (i.e., the magnitude of a bottom impact is not as large as that for the bow) is not considered.

A fourth example of exposure depends on the number, N, of events experienced by the vessel during a given period of time. This relates to the mission profile of the ship. For the case of an ice management vessel, N can be very large (thousands of

impacts per year) while N for a shuttle tanker servicing the Hibernia site will be very small (less than one impact per year). In addition, N need not be fixed (i.e., N may be Poisson-distributed).

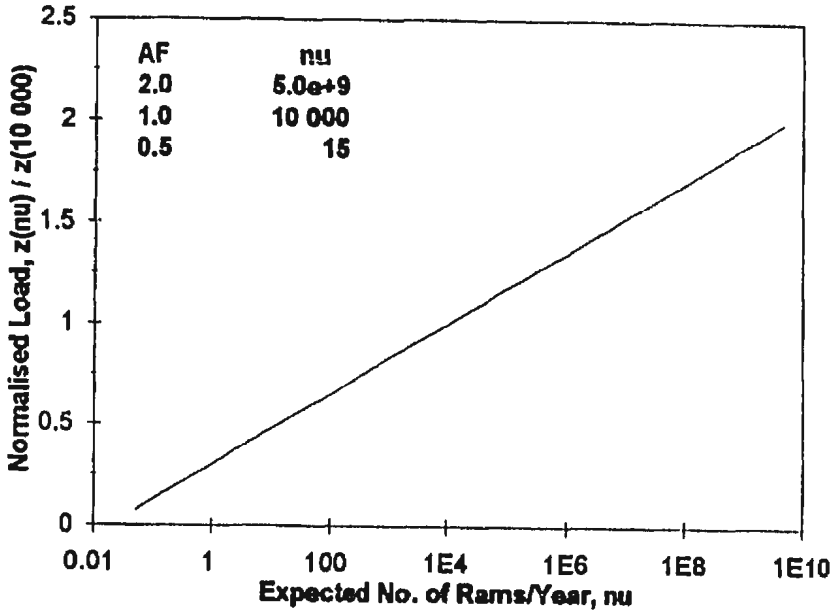

Figure 3.13: Evaluation of Expected Number of Annual Impacts Required for Area Factors Suggested by ASPPR Proposals (Melville Shipping Ltd., 1989).

3.7 Analysis of Reconstituted Data

The analysis to be discussed employs all the information discussed above. The best-fit curves calculated in Sections 3.3 and 3.4 (transformed from common logs to natural logs and from force to pressure) are of the form:

$$p_e = \exp(- b_j x + c_j) \tag{3.5}$$

where b_j and c_j are coefficients of slope and y-intercept for a given fixed area. We wish to perform the analysis in terms of pressure. Therefore, Equation (3.5) is written:

$$p_e = \exp[-(x - x_0)/\alpha] \tag{3.6}$$

where $\alpha = 1 / b_j$ and $x_0 = c_j / b_j$. It is noted that both α and x_0 are in units of MPa.

When concerning ourselves with safe design, we must ensure that the balance is maintained between structural integrity and economic efficiency. With regard to structural integrity, one must ensure that an appropriate design load is forecasted. We do this by combining the distribution of Equation (3.6) with information on the number of events per unit time (i.e., exposure of the vessel). In essence, we are considering the maximum pressure, Z, per unit time, generally taken to be a year.

The maximum pressure, Z, is arrived at as follows. If we wish to specify some load y, not to be exceeded, it can be described for one ram by:

$$Pr[Y \leq y] = F_Y(y) \tag{3.7}$$

where $Pr[Y \leq y]$ is the probability that a random load Y does not exceed a specified load y. Equation (3.7) may be extended for two rams as follows. Let:

$$Z = \max (Y_1, Y_2) . \tag{3.8}$$

Then:

$$Pr[Z \leq z] = Pr[Y_1, Y_2 \leq z] = F_Y^2(z) \tag{3.9}$$

and for n rams:

$$Pr[Z \leq z] = Pr[Y_1, Y_2, ..., Y_n \leq z] = F_Y^n(z) = F_Z(z) \qquad (3.10)$$

where Z is the max (Y_1, Y_2, ..., Y_n) and n is the number of rams.

We may wish to consider the case where n is a random quantity N. It may be assumed that N is Poisson-distributed (Jordaan et al., 1987) and may be expressed as:

$$Pr[N = n] = \frac{e^{-\nu} \nu^n}{n!} \qquad (3.11)$$

where ν is the expected number of collisions and $n = 1, 2, \ldots$. Let Z be the maximum of the N random rams.

The expected number of rams of magnitude $Y > z$, denoted ν', is given by:

$$\nu' = [1 - F_Y(z)]\nu \ . \qquad (3.12)$$

In the case that Equation (3.6) applies, we obtain:

$$\nu' = \nu \exp[-(x - x_0) / \alpha] \ . \qquad (3.13)$$

We may now develop the formula for the case where no collisions exceed pressure z, i.e., $n = 0$. This may be derived from Equations (3.10), (3.11) and (3.13) as follows:

$$F_Z(z) = \exp\{-\nu \exp[-(x - x_0) / \alpha]\} \ . \qquad (3.14)$$

It is noted that N includes both hits and misses (see discussion of exposure). However, the pressure equations derived earlier correspond to hits only. As a result, the methodology must be tempered to include hits only. If we let r be the proportion of hits to interactions, then the number of hits is defined by:

$$m = rn \qquad (3.15)$$

where m is the number of hits, or considering the case where M and N are random,

$$\mu = r\nu \tag{3.16}$$

where ν is the expected number of events, N, and μ is the expected number of hits, M, per unit time. As a result, Equation (3.14) can be expressed as:

$$F_Z(z) = \exp\{-\exp[-(z - x_0 - x_1) / \alpha]\} \tag{3.17}$$

where $x_1 = \alpha(\ln \nu + \ln r)$ and is in units of MPa.

3.8 APPLICATION OF RESULTS

Results of the analyses of the Canmar Kigoriak data and Polar Sea data performed in Sections 3.2 - 3.4 have to be expressed in a convenient format for use with Equation (3.16). This involves developing relationships or values for α, x_0, r and ν.

3.8.1 Development of the Pressure-Slope Relationship, α

The parameter, α, found in Equation (3.16) is a function of pressure [MPa]. It is also noted that Equation (3.16) is a function of natural logarithm while the coefficients of the fixed area design curves are a function of the common logarithm. As a result, α, is calculated according to:

$$\alpha = \frac{0.4343}{m_j \, j \, a_s} \tag{3.18}$$

where m_j is the slope of the fixed area force curve, j is the number of subpanels and a_s is the area of a subpanel. The parameter, α, is plotted with respect to area in Figure 3.14. The results of the analysis performed by Maes and Hermans (1991) are also plotted. Values for α were calculated for the fixed area analysis discussed in Section 3.2 and are also presented. In addition, the design curve presented by Jordaan et al. (1993) is presented. This equation, which will be used for design purposes forthcoming, is:

$$\alpha = 1.25a^{-0.70}, \; \alpha \leq 1.90 \tag{3.19}$$

where a is area. The very good correlation between the data sets is noted.

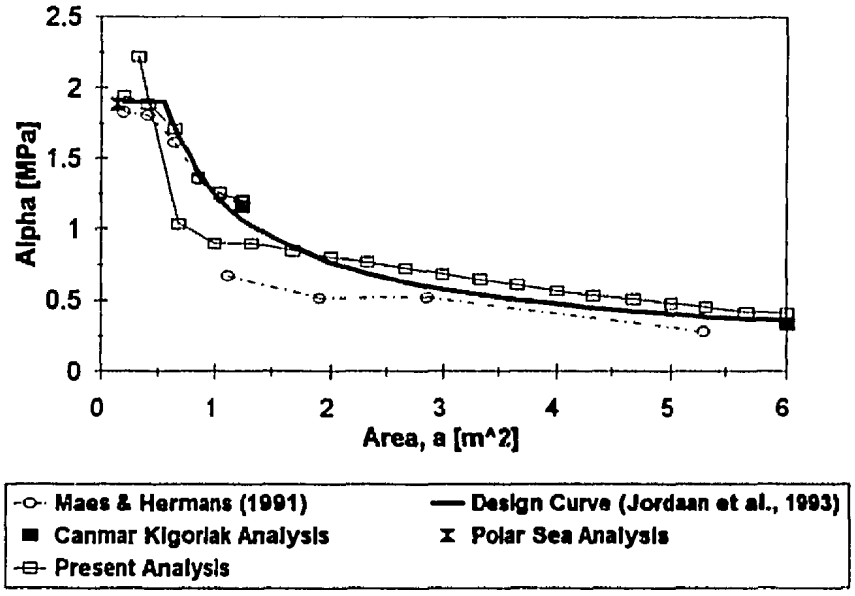

Figure 3.14: Results of Analysis of Slope, α.

Discrepancies between the present analysis and Maes and Hermans (1991) can be attributed to the following.

1. This analysis plotted the moving panel data against logarithm of exceedance probability while Maes and Hermans (1991) used the Gumbel distribution.
2. Maes and Hermans (1991) performed an approximate analysis of the 6.0 m^2 subpanel data (simplifying to four subareas), the present analysis was more exact.

3.8.2 Development of the x-Intercept Parameter, x_0

The y-intercept (for the fixed area force curve) data, y_j, was transformed to x_0 (the x-intercept of the design pressure curve) according to:

$$x_0 = \frac{-y_j}{m_j\, j\, a_s} \,. \tag{3.20}$$

Values for x_0 are plotted against area in Figure 3.15. As can be seen, the x_0 parameter is either negative or very small. As a result, it is assumed that $x_0 = 0$. This is supported by the analyses of A1 and A2 for the Canmar Kigoriak (see Section 3.2) which give intercept values, $x_0 \leq 0$ (see Figure 3.15).

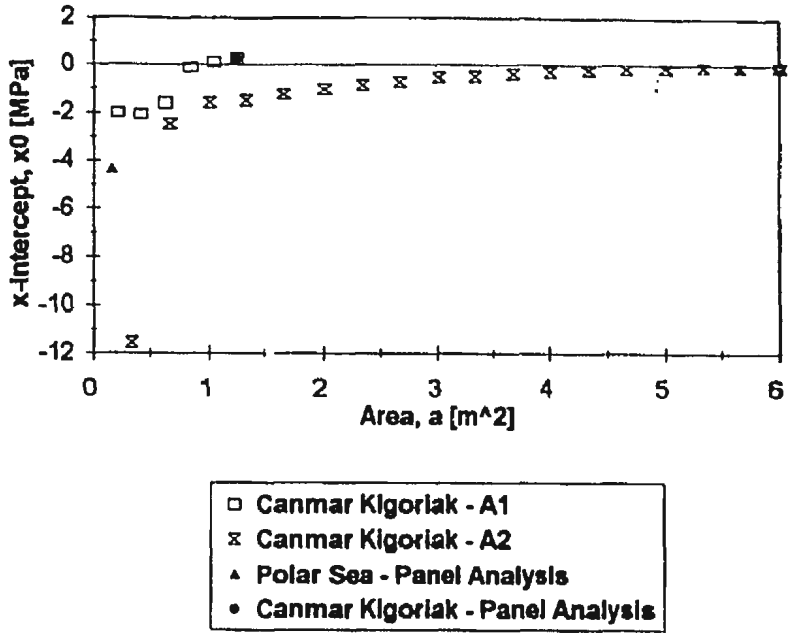

Figure 3.15 Results of Analysis of x-Intercept, x_0.

3.8.3 Development of the Exposure Parameter, r

The parameter, *r*, represents the number of rams which result in a hit (i.e., the panel being considered is loaded). This analysis is based on the Canmar Kigoriak data (Dome Petroleum Ltd., 1982). Polar Sea data were recorded only when a minimum force threshold on a panel was exceeded (Daley et al., 1986). During August and October, 1981, a total of 397 rams were conducted on board the Canmar Kigoriak. Table 3.7 presents the exposure level of the panels to impact.

Table 3.7 - Exposure of Canmar Kigoriak Instrumented Panels to Impact				
Data Set	Total Number of Rams	Number of Hits A1	Number of Hits A2	Total
August	157	88	90	178
October	240	91	30	121
TOTAL	**397**	**179**	**120**	**299**

It can be determined from Table 3.7 that the Canmar Kigoriak data sets contain a significant number of misses. For example, only 57% of August rams and 25% of the October rams produced loads on the instrumented panels. In total, only 38% of the Canmar Kigoriak rams produced hits. Hence, r will be taken as 0.4 for this analysis.

3.8.4 Estimation of the Number of Rams, ν

The ASPPR Review Committee (Carter et al., 1992) determined, after consultation with those who developed the regulations, that the following annual allocation of rams for each Canadian Arctic Class (CAC) is considered reasonable:

1. CAC1 - several thousand;
2. CAC2 - hundreds;
3. CAC3 - decades; and
4. CAC4 - several.

To show the effect of number of impacts on the load, a range of annual impacts between $\nu = 5$ and $\nu = 10{,}000$ is considered.

4 OPTIMISATION OF BOW PLATING

4.1 BACKGROUND

As noted in Section 1.1, the strength of a ship can be classified into three categories: primary, secondary and tertiary (Paulling, 1988). The primary, or global, strength classification is concerned with the *hull girder*. The secondary, or semi-local, strength classification is concerned with the strength of a ship panel, generally taken between two bulkheads or deep web frames. The tertiary, or local, strength classification is concerned with the strength of the plating between two frames. This is the region considered in this chapter. The localised ice load model established in Chapter 3 will be used for the present analysis. This model encompasses pressure-area distributions up to 6 m^2.

4.2 HULL PLATING LIMIT STATES

In order to optimize the bow plating, one must first consider the probability of failure of the shell to the estimated ice loading (see Chapter 3). Three limit states (i.e., failure conditions) were selected for this analysis. They are flexural plastic collapse, permanent set and plate rupture.

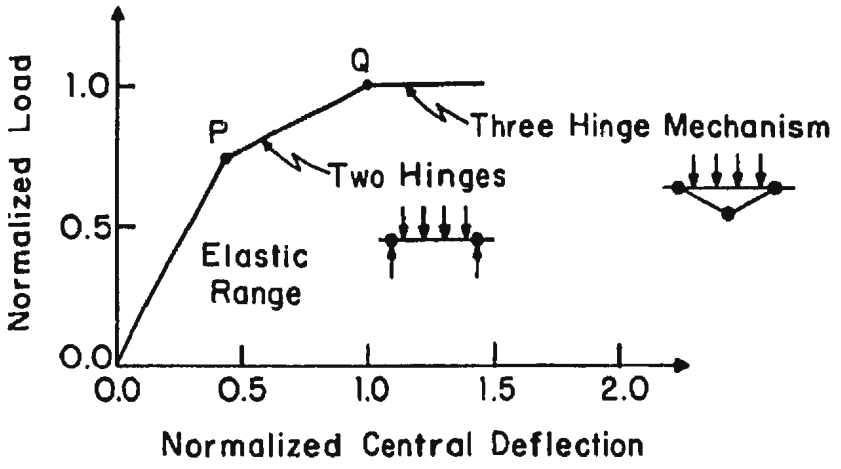

(a) Schematic Diagram Showing Development of Plastic Mechanism

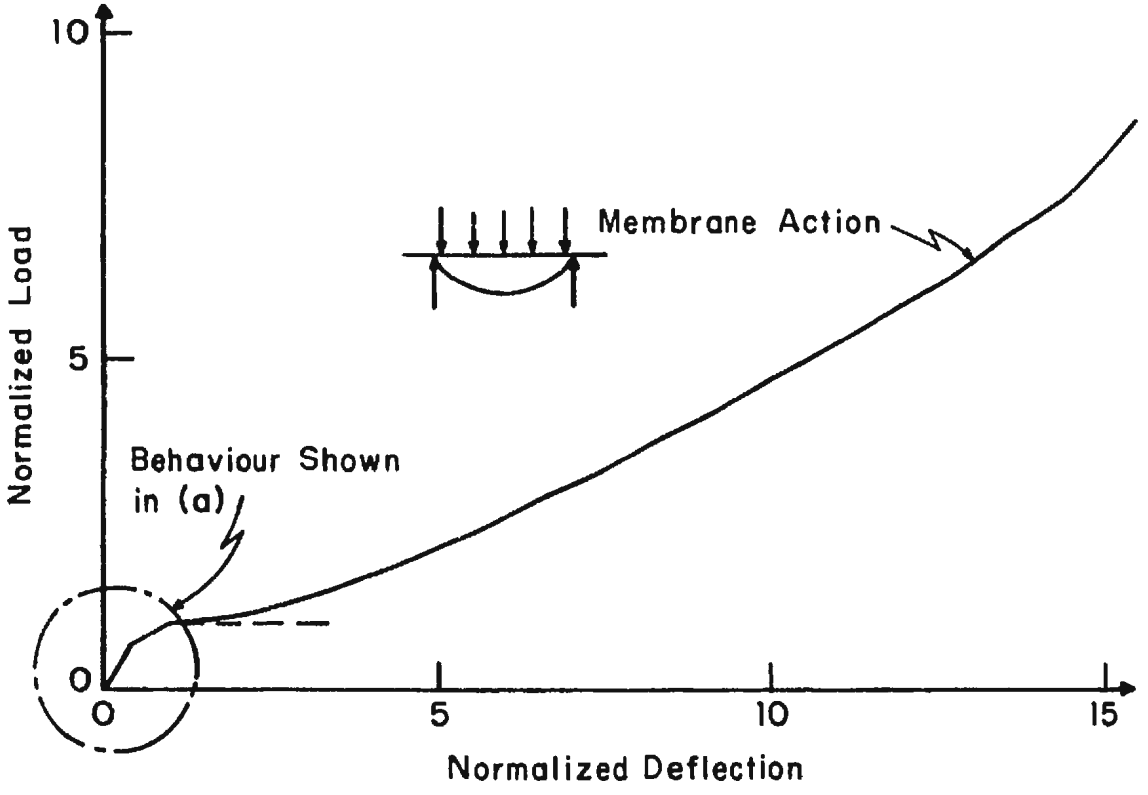

(b) Membrane Action

Figure 4.1: Schematic Diagram of Plate Failure Mechanisms (Carter et al., 1992).

Flexural plastic collapse is defined as the formation of a three-hinge mechanism and results when the plate is assumed to have no in-plane resistance against the load (i.e., the edges are clamped but free to slide). This is presented in Figure 4.1(a). With fully supported, ductile steels, this mechanism usually results in minor denting and is used in the present analysis to represent aesthetic damage. It can be seen from Figure 4.1(b) that there is a considerable reserve of strength beyond the three-hinge limit in steel plating provided by membrane effects. Reliance on membrane action assumes that the adjoining structure provides adequate resistance against freedom to slide. This is considered a reasonable assumption for the bow plating of an ice class vessel. It is assumed (Carter et al., 1992) that this reserve of strength is responsible for the level of safety inherent in ship plating.

Derivation of the three-hinge limit state assumes that the ice load is uniformly distributed over the entire span of the plate and that plane strain conditions exist in the plane normal to the supporting frames. The flexural plastic collapse load capacity, q_{3H}, calculated from plastic beam theory (assuming the von Mises yield criterion) is as follows:

$$q_{3H} = 4.62\ \sigma_y \left(\frac{t}{s}\right)^2 \tag{4.1}$$

where t is plate thickness, s is the plate span and σ_y is the yield stress (Nessim et al., 1992).

Permanent set is defined (Hughes, 1988) as the deflection of a plate involving plastic bending strain along its boundaries, i.e., frames and stringers. This limit state

represents significant damage which requires repair. Ratzlaff and Kennedy (1985) derived an analytical expression for the load-deflection relationship with only plastic membrane strength. The relationship is:

$$q_P = \frac{8\ \sigma_y\ W_{max}\ t}{(1 - \nu_p^2)\ s^2 \sqrt{1 + \left(\frac{4\ W_{max}}{s}\right)^2}} \qquad (4.2)$$

where ν_p is the plastic Poisson's ratio (taken as 0.5) and W_{max} is the deflection at midspan. This formula is based on the elastic load-deflection relationship for a transversely loaded, infinitely long, isotropic membrane assuming uniform strain. This assumption is considered reasonable for large deflections because the plastic hinges have been *pulled out* (Ferregut and Daley, 1988). It is suggested by Ayuub et al. (1989) that a reasonable level of permanent set to be taken as a limit state is $2t$. Substituting $W_{max} = 2t$ and $\nu_p = 0.5$ into Equation (4.2), one obtains the permanent set load capacity, q_p, from:

$$q_P = \frac{21.3\ \sigma_y \left(\frac{t}{s}\right)^2}{\sqrt{1 + 64\left(\frac{t}{s}\right)^2}}\ . \qquad (4.3)$$

An alternative formula for permanent set was derived by Wiernicki (1987) based on yield line theory (see Wood, 1961; Johansen, 1962). This analysis assumes the structure to be a perfectly plastic body thus simplifying the analysis. Wiernicki's formula accounts for both membrane and bending effects and is as follows:

$$q_P = 4\ \sigma_y \left(\frac{t}{s}\right)^2 \left(\frac{2W_{max}}{t} + 1\right). \qquad (4.4)$$

Again, an infinitely long, isotropic plate is assumed. For an allowable permanent set of $2t$, Equation (4.4) simplifies to:

$$q_P = 20\,\sigma_y \left(\frac{t}{s}\right)^2. \qquad (4.5)$$

The equations for permanent set, developed using yield line theory and plastic membrane theory, are both plotted in Figure 4.2 with respect to q. It can be seen that the equation developed using yield line theory gives more optimistic results than does the one developed using plastic membrane theory for higher stiffness ratios. This is attributed to the effects of bending (see Figure 4.2) which is less important at lower stiffness ratios. Weimicki (1987) further states that yield-line theory presents an upper-bound solution and hence should not be exceeded. Plastic membrane theory will be used for this analysis.

Plate rupture is defined as reaching the ultimate membrane capacity of the plating and is used in the present analysis to represent the breaching of the hull. In most cases this limit state results in repair; structural redundancy, double skin design and two compartment subdivision required for the Canadian Arctic (Melville Shipping Ltd., 1989) will reduce incidents of foundering. However, on some occasions loss of the vessel and perhaps the crew will result. It will be assumed that 0.1% of hull ruptures will result in ship loss. This value is consistent with Hughes (1988) who suggests that the probability of a severe accident leading to the loss of a vessel is 4.14×10^{-4}. The ultimate capacity

of the plate, q_U, is derived semi-empirically by Nessim et al. (1992) from static equilibrium of the plate after it deforms into a membrane (see Figure 4.3).

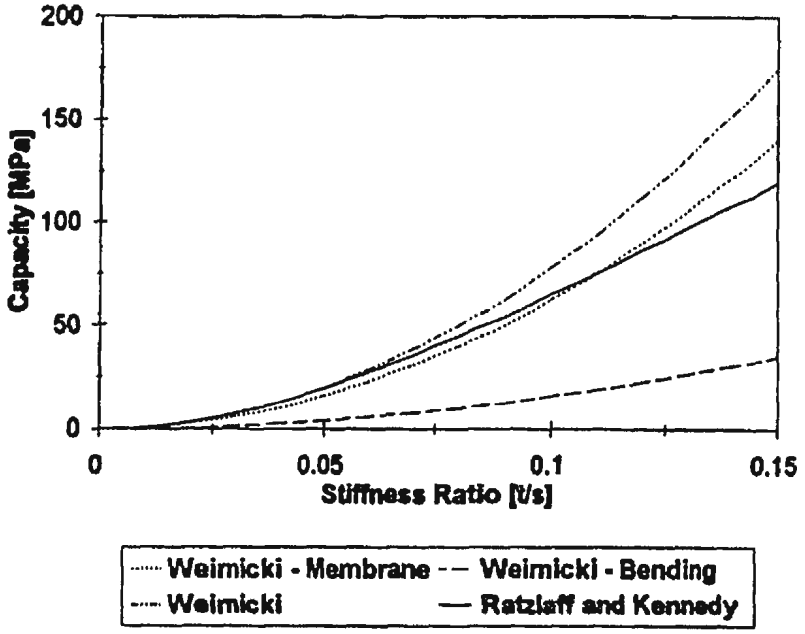

Figure 4.2: Load-Deflection Behaviour for $2t$ Permanent Set.

It is assumed that the crushed ice generates a uniform pressure on the shell plate when deflection approaches its maximum value. Assuming static equilibrium:

$$2P\sin\theta = qs \tag{4.6}$$

where $P = \sigma t$ and σ is the plate stress.

For uniform pressure, ignoring flexural stiffness of the plate, the plate is assumed to take the shape of a circular arc (Ratzlaff and Kennedy, 1986). This is defined by:

$$\frac{\sin\theta}{\theta} = \frac{\pi}{180(1 + \varepsilon_s)} \tag{4.7}$$

where $\varepsilon_s \approx 0.05$ is the nominal membrane strain in the shell at rupture (Egge and Böckenhauer, 1991). The authors base this assumption on collision tests carried out by Woisin (1976) at Gesellschaft für Kernenegieverwertung in Schiffbau und Schiffahrt mbH.

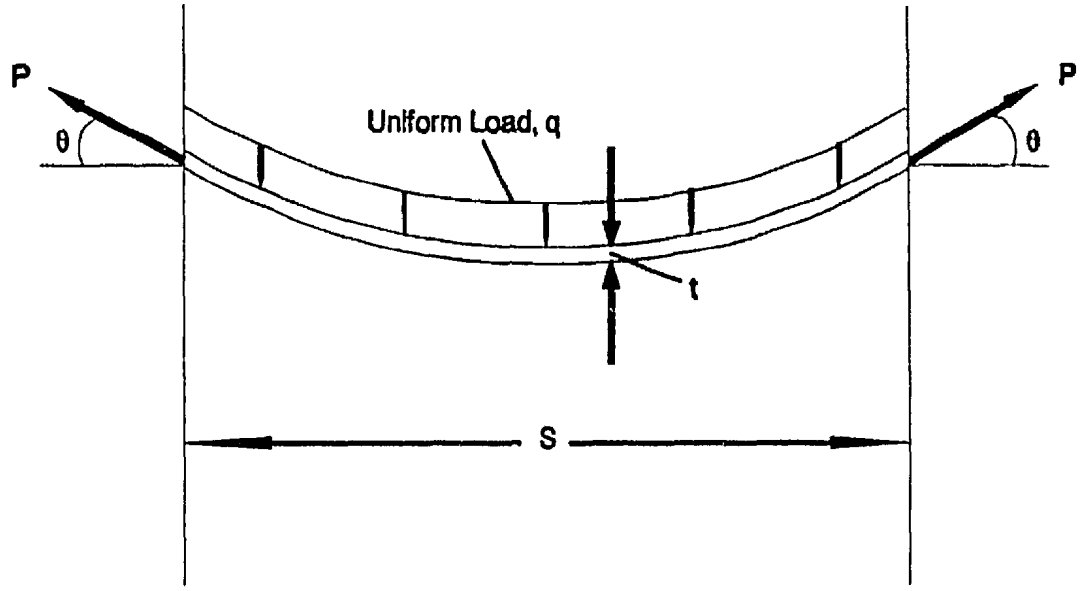

Figure 4.3: Schematic Diagram of Membrane Failure Mechanism.

Substituting $\varepsilon_s = 0.05$ into Equation (4.7) gives $\theta \approx 31^\circ$. Substituting this value of θ into Equation (4.6) and rearranging gives:

$$q_U = \frac{2P_U \sin(31)}{s} = \frac{1.03P_U}{s}. \tag{4.8}$$

Recalling that $P_U = \sigma t$ and letting $\sigma = (\sigma_y + \sigma_u) / 2$, the *effective strength* one obtains:

$$q_U = 0.515(\sigma_y + \sigma_u)\left(\frac{t}{s}\right). \tag{4.9}$$

The effective strength is a dynamic strength characteristic based on structural analysis for minor collisions by McDermott et al. (1974; see also Egge and Böckenhauer, 1991).

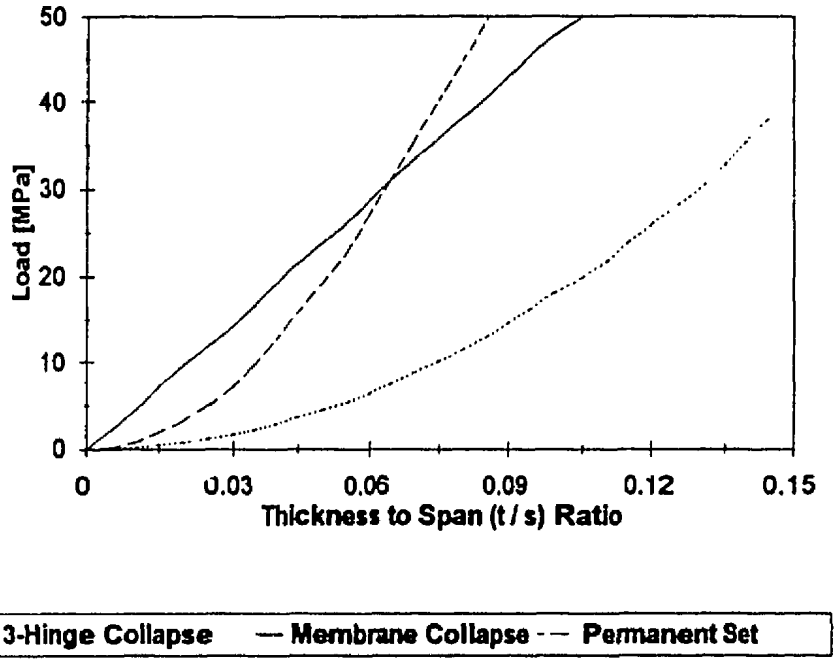

Figure 4.4: Comparison of Limit States.

The structural capacity, q, of each of these limit states is presented with respect to panel stiffness, t / s, in Figure 4.4. It can be seen in Figure 4.4 that the equation for permanent set gives optimistic results for stiff panels (high t / s ratios), even higher than that required to produce membrane failure. To ensure that the permanent set limit state remains realistic throughout the full range of panel stiffness, an alternate criterion, W_{max}

= 0.1s (Daley et al., 1991), is also considered. Substituting $W_{max} = 0.1s$ and $\nu_p = 0.5$ into Equation (4.2) gives:

$$q_P = 0.99\,\sigma_y\left(\frac{t}{s}\right). \tag{4.10}$$

Figure 4.5 presents the permanent set limit state equation with $W_{max} = 2t$ and $W_{max} = 0.1s$.

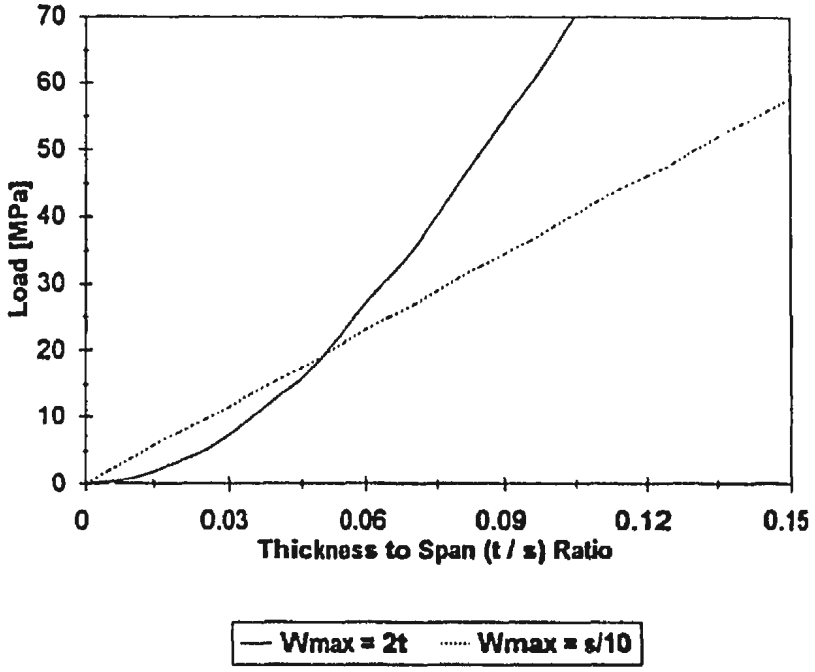

Figure 4.5: Comparison of Permanent Set Limit State Equations with $W_{max} = 0.1s$ and $W_{max} = 2t$.

It can be seen in Figure 4.5 that Equation (4.3) gives more conservative results for stiffness ratios below about 0.05 while Equation (4.10) does for stiffness ratios above 0.05. To accommodate these two limits, the more conservative is selected in each case. To ease the transition between the two equations, a linear blending function

$$q_P = C_i q_{P,2t} + (1 - C_i) q_{P,s/10}, \tag{4.11}$$

where C_i = 1 - [(t/s) - 0.025] / 0.05, is employed between t/s = 0.025 and 0.075. Figure 4.6 presents the three limit states (three-hinge, permanent set and membrane collapse) including the blended permanent set function.

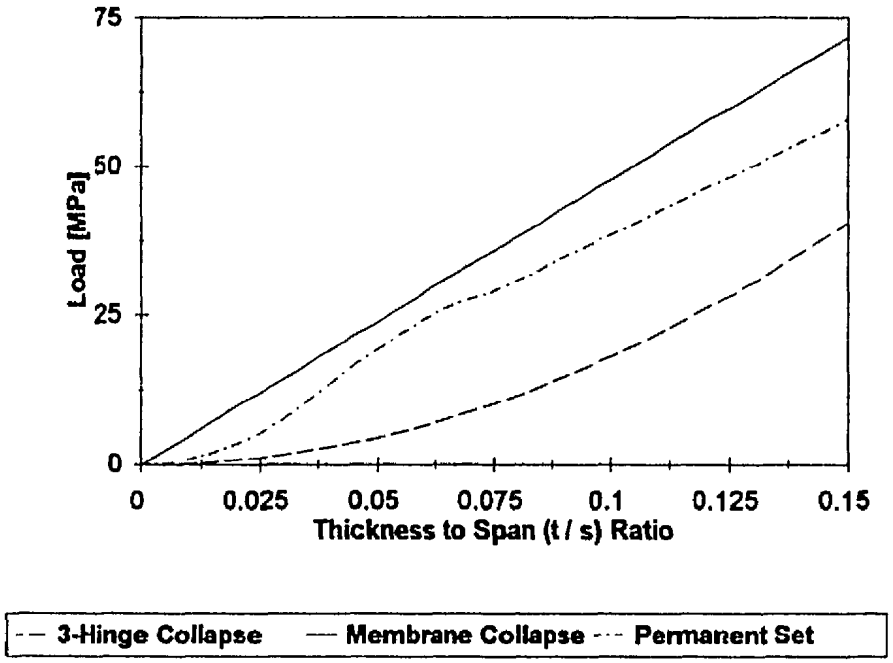

Figure 4.6: Comparison of Limit States Including Blended Permanent Set Criterion.

4.3 OBJECTIVE FUNCTION

To develop an optimal bow structure, an objective function must be developed. The objective function selected is minimum cost as a function of construction (C), aesthetics (A), repair (R) and replacement (L); the symbols in brackets are subscripts. Safety is also of great concern; i.e., the probability of plate rupture must be kept very low. The following variables are considered:

1. plate thickness (10 - 60 mm);
2. frame spacing (400 - 800 mm);
3. expected annual number of impacts (5 - 10,000);
4. steel grade (EH-36);
5. temperature (-5°C); and
6. strain rate (10^{-2} s^{-1}).

The three limit states just discussed are also considered.

The cost function will be minimised subject to all constraints. Steel is assumed to cost $0.35/lb. (Lilly, 1993) and labour rates are assumed for convenience to be 150% of steel cost. In addition, the cost of framing designed to meet the ASPPR Proposals (Melville Shipping Ltd., 1989) will be included in the cost of construction.

The objective function is of the form:

$$E(C) = C_C + \Phi_A C_A + \Phi_R C_R + \Phi_L C_L \qquad (4.12)$$

where $E(C)$ is the overall expected cost to be minimised, C_C is the initial cost of construction, C_A is the cost associated with aesthetics, C_R is the cost of repair, C_L is the

cost of replacement or loss and Φ is the probability that a particular outcome occurs. The cost of construction, C_C, is the initial cost and is equal to the cost of plating, framing and associated labour. Each of the other cost groups is calculated for a single panel based on the probability of failure and the associated cost per failure. Expected cost is discussed in greater detail in Section 4.7.

To make use of the model just stated, the probability of failure must be calculated for each limit state and design parameter discussed earlier in this chapter. Hence, the distributions for each of the design parameters must be defined. These distributions are described in the following section.

4.4 PROBABILITY DISTRIBUTION OF INPUT PARAMETERS

There is uncertainty in many of the parameters used in the limit state equations just discussed. In addition, parameters such as yield stress and ultimate stress must account for temperature and strain rate. The temperature selected for this analysis is -5°C and the strain rate is 10^{-2} s^{-1} based on the ASPPR Proposals (Melville Shipping Ltd., 1989)

4.4.1 Dynamic Yield Stress

Calculation of the dynamic yield stress for steel is based on the work of Nessim et al. (1992). The dynamic yield stress of structural steel is dependent on temperature,

T, and strain rate, $\dot{\varepsilon}$. The results presented by Soroushian and Choi (1987) were used to calculate the mean value of the dynamic yield stress, $\sigma_y(\dot{\varepsilon})$ from the static yield stress, $\sigma_y(0)$. The relationship between these values is:

$$\frac{\sigma_y(\dot{\varepsilon})}{\sigma_y(0)} = \left[-0.311\times10^{-8}\sigma_y(0) + 1.46\right] + \left[-0.634\times10^{-8}\sigma_y(0) + 0.093\right]\log(\dot{\varepsilon}) \tag{4.13}$$

The dependence of dynamic yield stress on temperature is characterised using data presented by Malik and Tomin (1991). This data is provided for EH-36 steel which has a specified yield stress of 355 MPa and for tests which were carried out at a strain rate of 5×10^{-2} s^{-1}. The ratio of the actual yield stress at a given temperature, $\sigma_y(T)$, to the specified yield stress, σ_{ys}, can be calculated according to Nessim et al. (1992) using:

$$\frac{\sigma_y(T)}{\sigma_{ys}} = 1.14 - 0.004T \tag{4.14}$$

where T is measured in °C. Equations (4.13) and (4.14) can be used to estimate the mean value of yield stress for any combination of temperature and strain rate. Equation (4.14) is first used to calculate the yield stress, $\sigma_y(T)$, for a given temperature and $\dot{\varepsilon} = 5\times10^{-2}$. Noting that $\sigma_y(T) = \sigma_y(\dot{\varepsilon})$ at the specified temperature and $\dot{\varepsilon} = 5\times10^{-2}$, Equation (4.13) can be used to calculate the static strain rate at the reference temperature $\sigma_y(0)$. Equation (4.13) is again used to calculate $\sigma_y(\dot{\varepsilon})$ for the strain rate being considered, 10^{-2} s^{-1} for this analysis.

A lognormal probability density function (PDF) is used to model yield stress (Kennedy and Baker, 1984) with mean value just mentioned and coefficient of variation

(COV) equal to 0.05 (Galambos and Ravindra, 1978). It is assumed that the COV is independent of temperature and strain rate (Nessim et al., 1992).

4.4.2 Dynamic Ultimate Stress

The ultimate strength of steel, σ_u, under dynamic loading is obtained using a method similar to that described in Section 4.4.1 (Nessim et al., 1992). Temperature effects are again based on data reported by Malik and Tomin (1991) and the ratio between $\sigma_u(T)$ and σ_{ys} is:

$$\frac{\sigma_u(T)}{\sigma_{ys}} = 1.62 - 0.003T \qquad (4.15)$$

where $\sigma_u(T)$ is the ultimate strength at a specified T (see Nessim et al., 1992). The strain rate effect, based on Soroushian and Choi (1987), is:

$$\frac{\sigma_u(\dot{\varepsilon})}{\sigma_u(0)} = \left[-0.471\times10^{-7}\sigma_y(0) + 1.72\right] + \left[-0.944\times10^{-8}\sigma_y(0) + 0.144\right]\log(\dot{\varepsilon}) \qquad (4.16)$$

where $\sigma_y(0)$ and $\sigma_u(0)$ are the static yield and ultimate strengths respectively. Equations (4.15) and (4.16) can be used in the same manner as Equations (4.13) and (4.14) to calculate the ultimate strength for a given combination of strain rate and temperature. Similar to Section 4.4.1, a constant COV of 0.05 and a lognormal PDF are used.

4.4.3 Plate Thickness

The PDF for the actual thickness is based on information presented by Kennedy and Aly (1980). The authors report the ratio between actual and specified thickness is 1.014 and that the COV is 0.01. A normal PDF is used for this parameter (Nessim et al., 1992).

4.4.4 Frame Spacing

The frame spacing parameter is assumed to be normally distributed. The mean value is assumed equal to the specified value with a COV of 0.05 (Allen, 1975; see also Daley et al., 1991).

4.4.5 Area of Unsupported Plating

The plate in question will be supported by transverse frames. The area used in calculating the design load is taken as $s \times 1.5s$ since this corresponds reasonably to one-way action (see Figure 4.7). Yield lines calculated according to the method presented by Wiernicki (1987) show that the central region of a plate with this aspect ratio will fail according to one way action (i.e., as a long plate). Since this region of the plate is generally where the maximum deflection occurs, limit states based on long plate theory

can be used. For the purpose of calculating the loaded area, i.e., to find the coefficients of the pressure curve, the dimensions just mentioned are assumed to be exact.

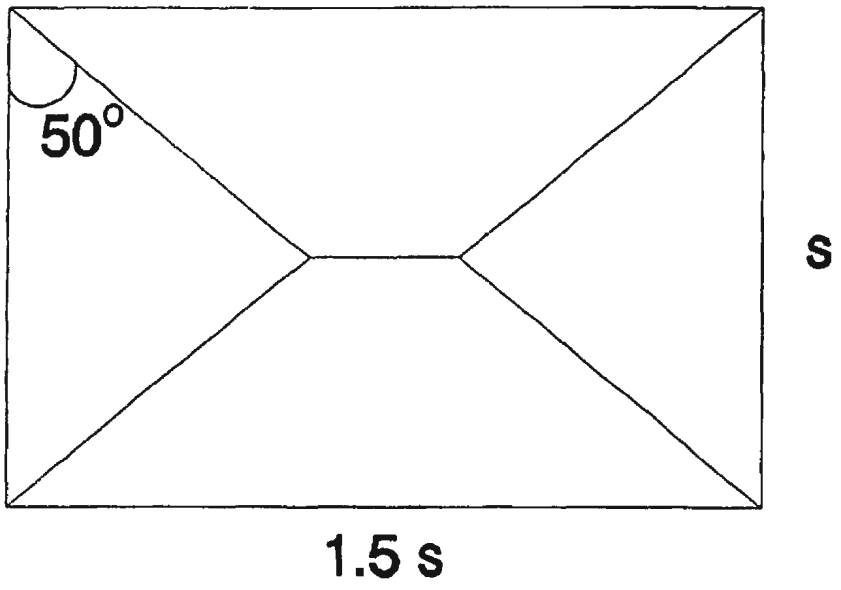

Figure 4.7: Schematic Diagram of Plating Showing Yield Lines.

4.5 Analysis of Plate Failure

The risk or probability of failure, Φ, of a system is defined by:

$$\Phi = Pr[R - L < 0] \tag{4.17}$$

where R is the capacity, or resistance, of the system and L is the load applied to it. For the present analysis, that the ice load intensity exceeds the load carrying capacity of the plate. Variabilities in the ice load and structural criteria are modelled using the criteria discussed in Sections 3.8 and 4.4 for the structural criteria presented in Table 4.1. These

uncertainties in the model form a joint distribution function which is tedious to solve, especially with so many unknowns. As a result, the probabilities were calculated using the FORM software package (Gollwitzer et al., 1988).

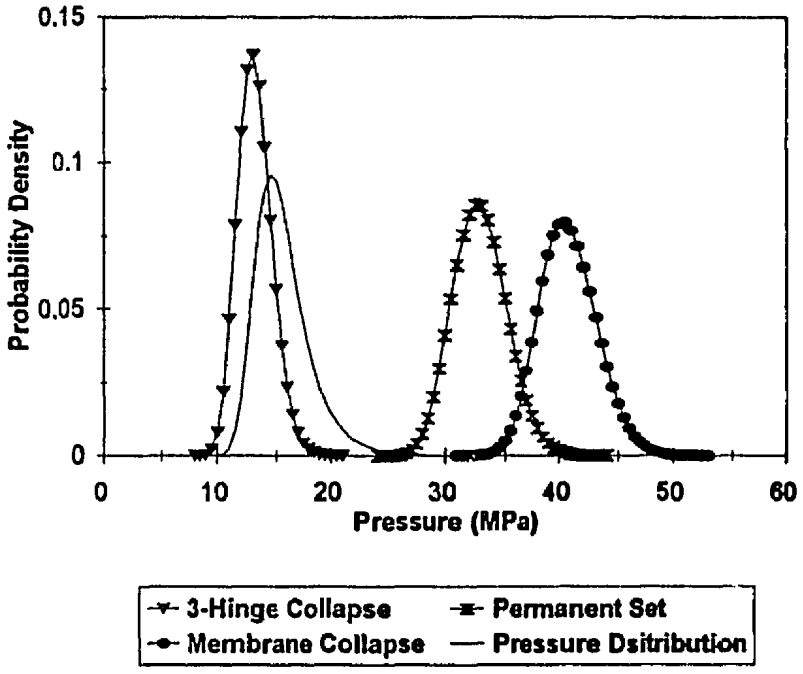

Figure 4.8(a): Probability Distributions for Loading Condition with ν = 5000 and a = 0.54 m^2 and Limit States with t = 50 mm and s = 600 mm.

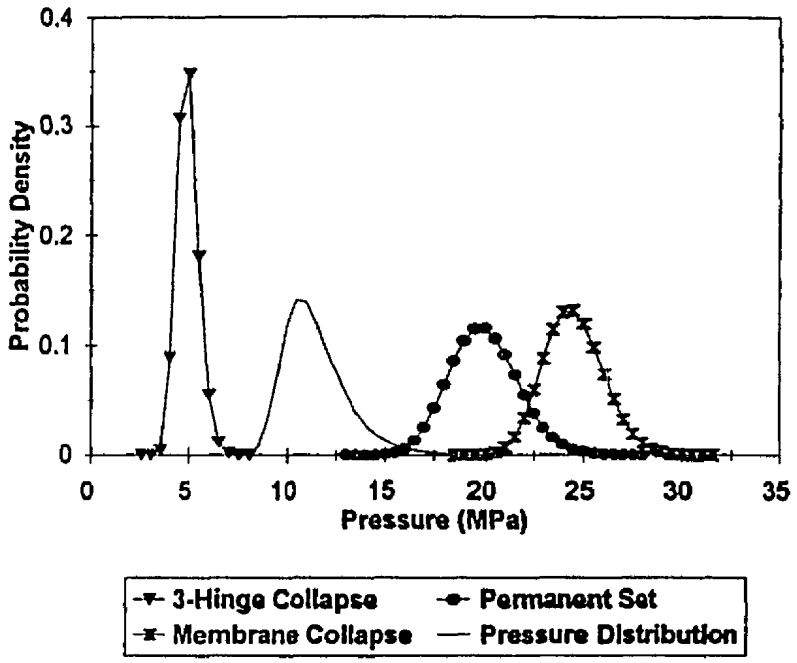

Figure 4.8(b): Probability Distributions for Loading Condition with ν = 10,000 and a = 0.96 m^2 and Limit States with t = 40 mm and s = 800 mm.

As discussed in Chapter 3, a range of expected annual impacts will be considered, ν = 5 - 10,000. This range accounts for a wide range of shipping activities from servicing the Hibernia Site off the east coast of Canada to ice management in the Beaufort Sea. For illustrative purposes, the PDF of a loading condition with ν = 5000 and a = 0.54 m^2 is presented in Figure 4.8(a) with PDF's for each of the three limit states with t = 50 mm and s = 600 mm. A similar PDF for ν = 10,000 and a = 0.96 m^2 is presented in Figure 4.8(b) with the PDF's for each of the three limit states with t = 40 mm and s = 800 mm. Shifts in the distributions, resulting from the change of parameters, can be seen.

Routines were developed to evaluate the capacity of the structure for the selected failure condition and structural parameters, the load according to the operation profile of

the ship and contact area and the risk of failure, Φ, according to Equation (4.17). These routines were linked to the appropriate FORM modules.

Table 4.1 - Structural Parameters

Item	Specified Value	Statistical Values	
		Expected Value	Standard Deviation
t (mm)	10	10.14	0.101
	20	20.28	0.203
	30	30.42	0.304
	40	40.56	0.406
	50	50.70	0.507
	60	60.84	0.608
s (mm)	400	400.00	20.00
	600	600.00	30.00
	800	800.00	40.00
σ_y (MPa)	355	390.3	19.5
σ_u (MPa)		542.3	27.1
T (°C)	-5	-5	0
$\dot{\epsilon}$ (s^{-1})	10^{-2}	10^{-2}	0
area (m^2)	0.240	0.240	0
1.5 s^2	0.540	0.540	0
	0.960	0.960	0

It can be seen in Figure 4.8 that the permanent set and membrane collapse failure distributions overlap significantly; i.e., it is possible to have failure due to rupture before failure due to permanent set. Hence, it is necessary to calculate the probability of this

occurring, $\Phi_{U|\bar{P}}$. To calculate this probability, the permanent set and membrane collapse limit states were approximated by normal distributions (see Figure 4.9) which is appropriate according to the central limit theorem. The probability that the plate fails due to rupture without first failing due to permanent set can be written as:

$$\Phi_{U|\bar{P}} = Pr[L > q_U] \cap Pr[q_P > L] \tag{4.18}$$

recalling that q_U and q_P are the resistance to membrane collapse and permanent set failure, respectively, provided by the structure. This can be calculated using:

$$\Phi_{U|\bar{P}} = \int_0^{\infty} f_L(l)[1 - F_P(l)] F_U(l)\, dl \tag{4.19}$$

where $f_L(l)$ is the PDF for load derived in Chapter 3, $F_P(l)$ is the CDF for failure due to permanent set and $F_U(l)$ is the CDF for failure due to membrane collapse. Equation (4.19) can be solved easily using numerical methods.

For each limit state discussed in Section 4.3, the risk of failure, Φ, was evaluated for each combination of t, s and ν. These can be visualised using a Venn diagram (see Figure 4.10). It can be seen from Figure 4.10 that the probability of no damage, Φ_0, can be calculated by:

$$\Phi_0 = 1 - \Phi_{3H}, \tag{4.20}$$

the risk of aesthetic damage, Φ_A, can be found according to:

$$\Phi_A = \Phi_{3H} - \Phi_P - \Phi_{U|\bar{P}}, \tag{4.21}$$

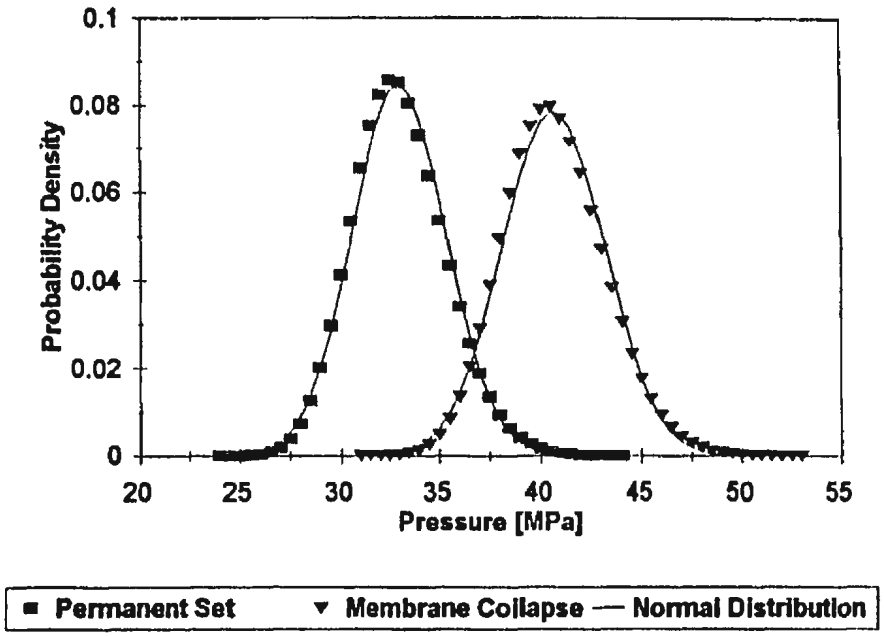

Figure 4.9: Probability Distributions for Permanent Set and Membrane Collapse Limit States with t = 50 mm and s = 600 mm.

the risk of damage needing repair, Φ_R, can be found according to:

$$\Phi_R = \Phi_P + \Phi_{U|\bar{P}} - 0.001\,\Phi_U, \tag{4.22}$$

and the risk of loss, Φ_L, can be found according to:

$$\Phi_L = 0.001\,\Phi_U. \tag{4.23}$$

As expected,

$$\Phi_0 + \Phi_A + \Phi_R + \Phi_L = 1. \tag{4.24}$$

Making use of Equations (4.20 - 4.23) and the probabilities for each load, configuration and limit state, the probability of no damage, aesthetic damage, repair and loss can be calculated for a randomly selected plate panel in the bow of a ship.

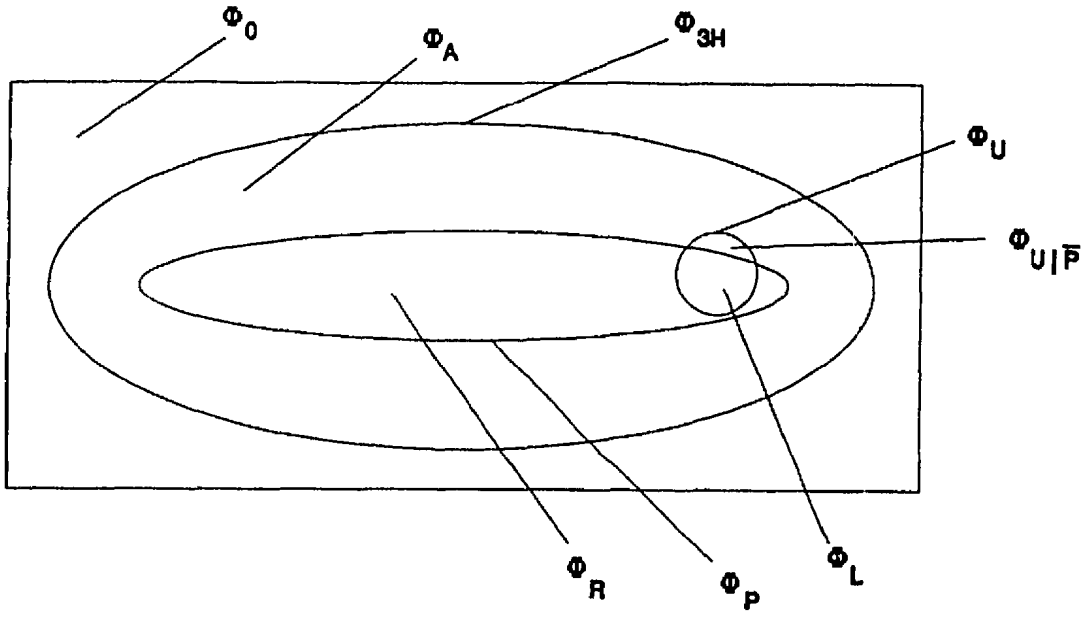

Figure 4.10: Schematic Diagram of Failure Space.

4.6 SAFETY

Safety is of great importance. Therefore, certain minimum standards must be set. The CSA Standard S.471 for fixed offshore structures considers two limit states (Jordaan and Maes, 1991), Class 1 (great risk to life and the environment) and Class 2 (small risk). Suggested values for these safety classes are 10^{-5} for Class 1 and 10^{-3} for Class 2. These values are considered reasonable as lower bounds for Φ_U and Φ_P respectively.

The ASPPR Proposals (Melville Shipping Ltd., 1989) require that all pollutants be stored a minimum of 760 mm from the outer shell of the ship. Furthermore, all CAC

vessels must be designed to meet the two compartment stability criterion. As a result, the probability of a severe impact, resulting in membrane collapse, leading to loss of the ship or damage to the environment is small. However, one must consider the consequences of polluting the Canadian Arctic, hence, $\Phi_U = 10^{-5}$ will be used as a lower bounds.

Table 4.2 - Minimum Allowable Plate Thickness

ν [per year]	Frame Spacing [mm]		
	400	600	800
10,000	34	50	46
5000	32	48	44
2000	30	46	42
1000	30	44	40
500	28	42	38
200	26	40	36
100	26	38	36
50	24	36	34
20	22	34	32
10	22	32	30
5	20	30	28

The risk of failure for a structure as a result of permanent set and rupture are plotted in Figure 4.11, for $\nu = 1000$, with respect to thickness. It can be seen in Figure 4.11(a) that probability failure due to permanent set decreases approximately linearly with thickness when plotted on semi-log paper. This result is also true for risk of failure due to membrane collapse (see Figure 4.11(b)). Hence, the minimum allowable thickness required to maintain the safety requirements just mentioned can be calculated using linear

regression. The minimum allowable plate thicknesses are presented in Table 4.2. It is noted that a 2 mm resolution for plate thickness is used.

4.7 OPTIMISATION OF PLATING

The primary interest of the present analysis is to develop an optimising function for the design of bow plating for ice capable ships. This is performed by minimising the cost function discussed in Section 4.3. To this end, the present analysis considers cost of construction, aesthetics, repair and loss. For illustrative purposes, a simple example is developed.

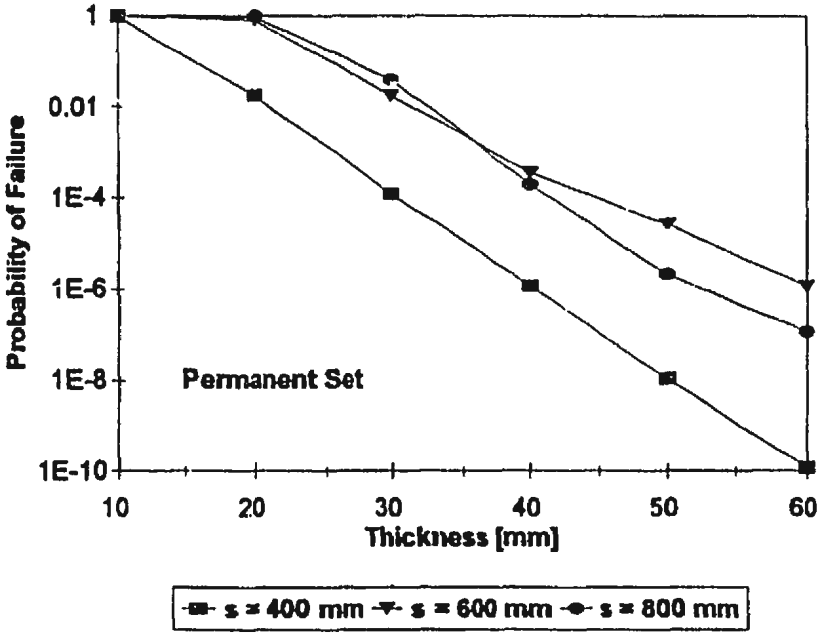

Figure 4.11(a): Effect of Thickness on Risk of Failure Due to Permanent Set for v = 1000.

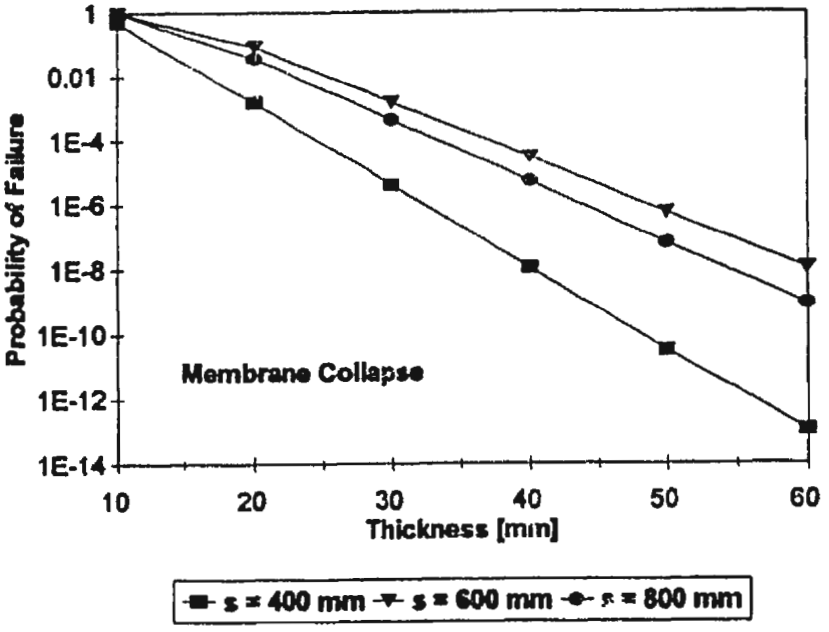

Figure 4.11(b): Effect of Thickness on Risk of Failure Due to Rupture, $\nu = 1000$.

4.7.1 Cost of Construction

Cost of construction considers the cost of labour and materials required to construct the bow section of the ship. Material cost will be limited to steel and will be assumed to cost \$0.35 per pound (Lilly, 1993). For simplicity, labour costs will be assumed to be 150% of material cost.

Steel costs will be limited to cost of the hull shell plating and cost of the support frames. Support frames will be designed to meet the requirements of the ASPPR Proposals (Melville Shipping Ltd., 1989). This will allow for a reasonable comparison

between the various configurations considered. In addition to frame spacing and span criteria discussed earlier, the following assumptions are made.

1. 2000 to 10,000 impact/year is treated to be a CAC1 vessel, 200 to 1000 impacts/year a CAC2 vessel, 20 to 100 impacts/year a CAC3 vessel and 5 to 10 impacts/year a CAC4 vessel.
2. Deep web frames will be placed every fourth frame and will have a span of 3.0 m.
3. A 10,000 tonne vessel will be considered for the purpose of calculating frames sizes. Shaft power is assumed to be 20 MW, 16 MW, 12 MW and 8 MW for CAC1-4 respectively (Carter et al., 1992).

The cost of construction is treated as a present cost that is not amortised.

4.7.2 Cost of Aesthetics

The expected cost due to minor denting for one year is calculated according to:

$$N \Phi_A C_A \tag{4.25}$$

where N is the number of panels making up the bow of the ship, Φ_A is the risk of aesthetic damage and C_A is the cost per damaged panel; the bow is assumed to be 500 m^2. Each panel is assumed to be independent. For the present analysis, C_A is taken to be \$0, i.e., minor denting is acceptable.

4.7.3 Cost of Repair

It is assumed that to repair a damaged panel, the entire steel plate must be replaced. In Canada, a typical steel plate is 4′ × 8′ (2.9729 m^2; Lilly, 1993). Hence, the cost to repair one panel is:

$$C_R = 2.5\left(2.9729\frac{t}{1000}\rho C_s\right) \tag{4.26}$$

where t is the plate thickness (mm), ρ is the density of the material (t / m^3) and C_s is the cost of steel ($ / t). This function assumes that labour costs are still 150% of material costs. The assumption to replace an entire plate poses another problem. What if more than one damage occurs on the same plate? Hence, we need the probability that a plate needs replacement; i.e., the probability that one or more panels within the plate needs to be replaced. This is calculated using:

$$Pr[\textit{plate needs replacement}] = 1 - (1 - \Phi_R)^{n_P} \tag{4.27}$$

where Φ_R is the probability that a panel within the plate is damaged and n_p is the number of panels which make up a plate. This assumes that each panel is independent. The expected annual cost of damage is:

$$N_p C_R\left[1 - (1 - \Phi_R)^{n_P}\right] \tag{4.28}$$

where N_p is the number of plates making up the bow. Each plate is assumed to be independent.

4.7.4 Cost of Replacement

The cost of replacing a ship, C_L, is assumed to be \$1,000,000,000. This is considered an average cost which accounts for either replacement of the ship or replacement of the ship and loss of life. The expected annual cost of replacement can be calculated using Equation (4.25) substituting values associated with aesthetics with values associated with loss. This is again considered an annual cost which is converted to a present value using Equation (4.26

4.7.5 Results of Cost Estimate

The expected annual cost for damages, $E(C_D)$, (aesthetics, repair and replacement) are presented with respect to v in Figure 4.12(a) and t in Figure 4.12(b) for the case where s = 600 mm. Figure 4.12 shows that $E(C_D)$ and v are linearly related when plotted on log paper and that $E(C_D)$ and t are linearly related when plotted on semi-log paper; a maximum value of \$1.0 × 10^6 is also seen. As a result, a plane can be fit to the data to simplify calculation of $E(C_D)$. The plane was fit using the multiple linear regression method (Walpole and Myers, 1972). The equation of the best-fit plane, recall that plane is fit to log[$E(C_D)$], log(v) and t, is of the form:

$$E(C_D) = v^{a_0} e^{a_1 + a_2 t} \tag{4.29}$$

where a_0, a_1 and a_2 are coefficients of the curve. For the aesthetic, repair and replacement models just discussed, the coefficients of the plane are presented in Table 4.3.

Table 4.3 - Coefficients of Best-Fit Plane to Expected Annual Cost of Damage.

s [mm]	Coefficients		
	a_0	a_1	a_2
400	0.972	19.362	-0.560
600	0.965	19.121	-0.389
800	0.964	18.674	-0.435

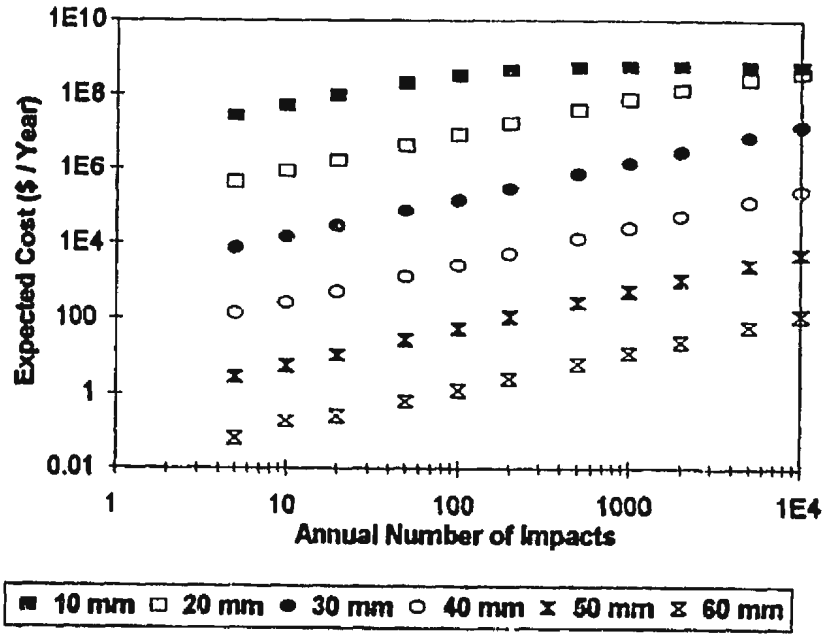

Figure 4.12(a): Effect of Annual Number of Impacts on Expected Annual Cost of Damage for s = 600 mm.

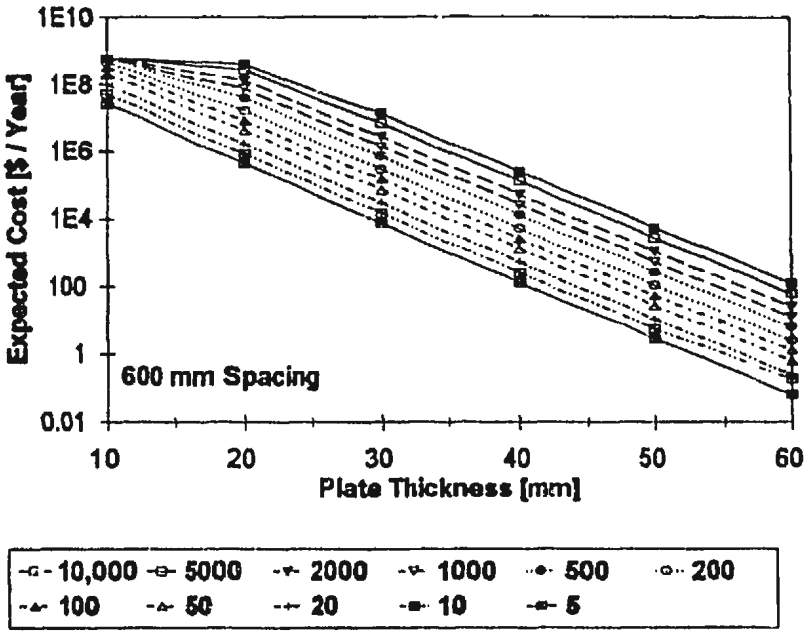

Figure 4.12(b): Effect of Thickness on Expected Annual Cost of Damage for s = 600 mm

The annual expected cost of damage, $E(C_D)$ is assumed to be an annual cost. This cost is converted to a present value assuming a 20-year vessel life, a 7% annual rate of inflation and a 10% rate of interest on investments. Converting an annual expense to a present value is calculated according to:

$$P_V = \frac{A}{1 + i_g} (P/A, i, n) \tag{4.30}$$

where P_V is the present value of the payment, A is the annual payment in today's dollars, i_g is the rate of inflation and $(P/A, i, n)$ is the present worth factor for net interest rate, $i = i_i - i_g$ and number of payments, n (Riggs et al., 1986). For the present case $(P/A, i, n) = 15.1614$.

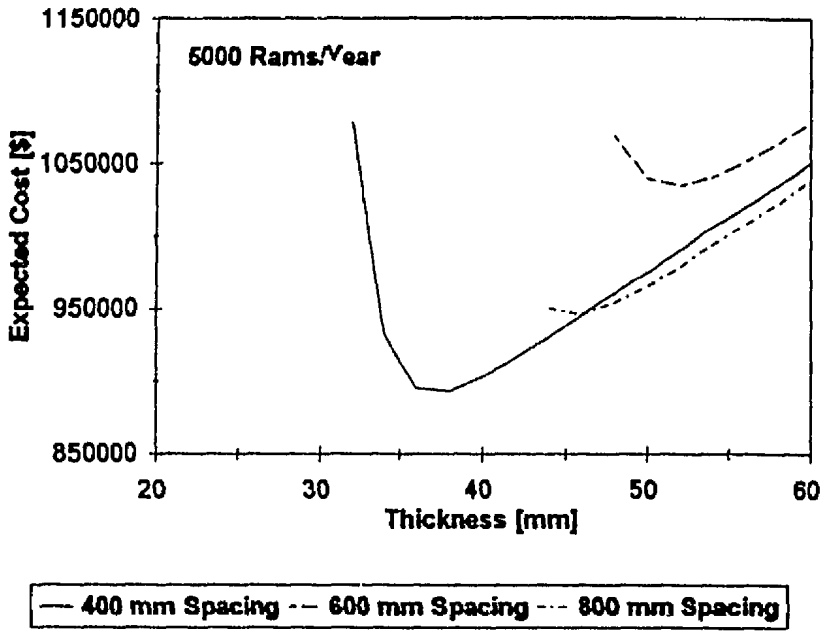

Figure 4.13(a): Expected Cost of the Bow Structure for a Ship Designed for $\nu = 5000$.

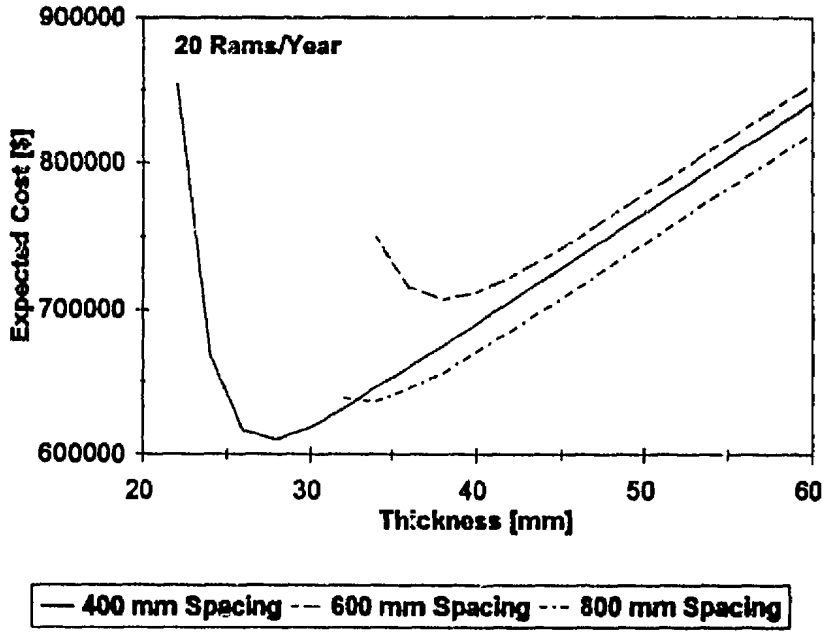

Figure 4.13(b): Expected Cost of the Bow Structure for a Ship Designed for $\nu = 20$.

The expected cost, $E(C)$, is presented in Figure 4.13(a) for $\nu = 5000$ and in Figure 4.13(b) for $\nu = 20$. It can be seen from these figures that 400 mm spacing is optimal and that 600 mm spacing is the least cost effective. This result is consistent for each value of ν. Expected cost plots for each value of ν can be found in Appendix 2.

Table 4.4 - Minimised Cost Function Results

ν [rams/yr]	s = 400 mm		s = 600 mm		s = 800 mm	
	t [mm]	C [$M]	t [mm]	C [$M]	t [mm]	C [$M]
10,000	38	0.9013	54	1.0480	48	0.9591
5000	38	0.8933	52	1.0390	46	0.9465
2000	36	0.8803	50	1.0180	44	0.9312
1000	34	0.7494	48	0.8612	42	0.7920
500	34	0.7413	46	0.8481	40	0.7806
200	32	0.7283	44	0.8310	38	0.7652
100	30	0.6313	42	0.7376	36	0.6638
50	30	0.6233	40	0.7247	36	0.6520
20	28	0.6103	38	0.7074	34	0.6367
10	26	0.5293	36	0.6121	32	0.5567
5	26	0.5212	34	0.5994	30	0.5449

The results presented in Table 4.4 are consistent with those required by the ASPPR Proposals (Melville Shipping Ltd., 1989) which are presented in Table 4.5. For 400 mm spacing, the optimal thickness resulting from the present analysis and the thickness required by the ASPPR Proposals are the same. For 600 mm spacing, the optimal thickness resulting from the present analysis is approximately 4-6 mm greater than that

required by the ASPPR Proposals. For 800 mm spacing, the optimal thickness resulting from the present analysis is approximately 4-8 mm less than that required by the ASPPR Proposals. This is presented in Figure 4.14. It can also be seen that the optimal cost for ships designed with 800 mm frame spacings occurs at a lower plate thickness than does the optimal cost for ships designed with 600 mm frame spacings. This results because both designs have approximately the same cost of construction while the expected cost of damage for a ship with 600 mm frame spacing is projected to be higher than that for a ship with 800 mm frame spacing. This is presented in Figure 4.15 for ν = 5000.

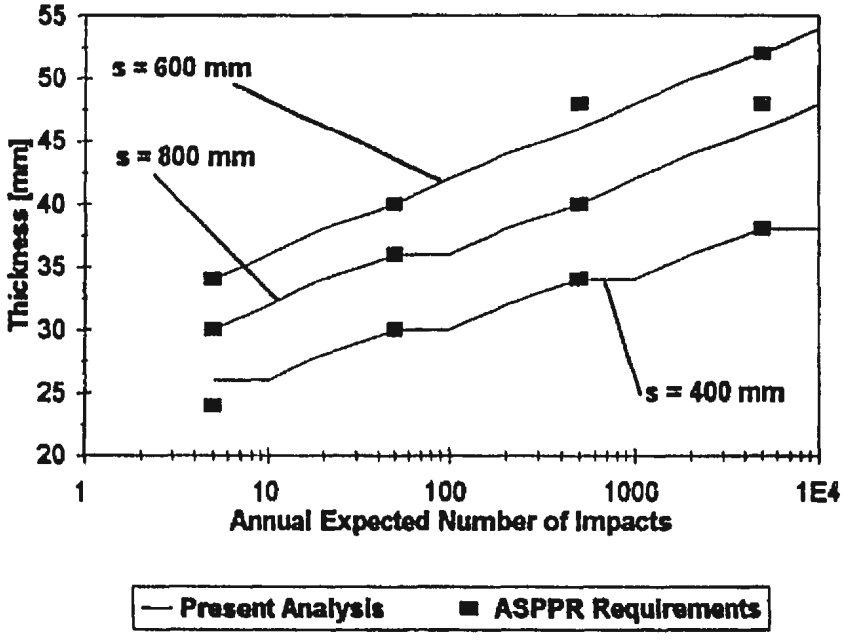

Figure 4.14: Comparison of Optimum Thickness from the Present Analysis with the Minimum Thickness Required by the ASPPR Proposals.

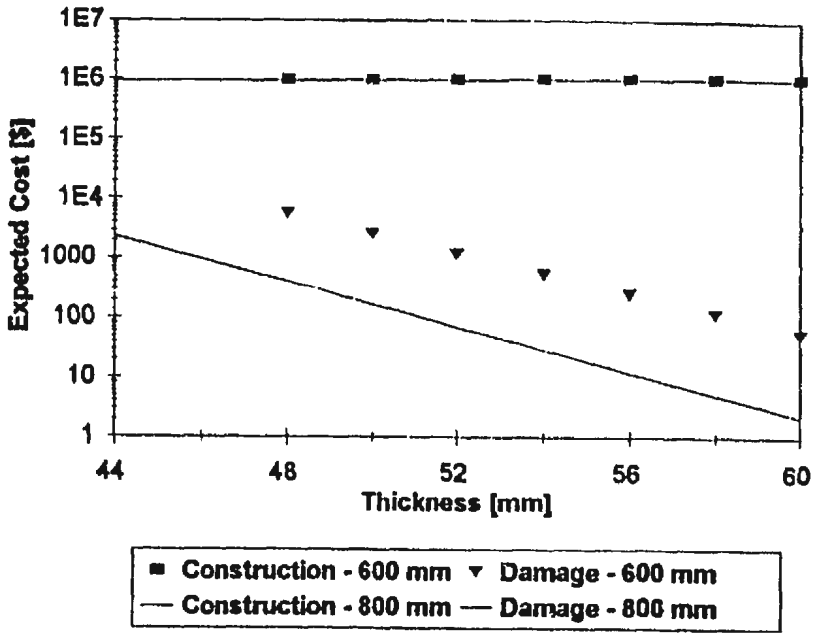

Figure 4.15: Comparison of Initial Cost and Expected Cost of Damage for s = 600 mm and s = 800 mm for ν = 5000.

Table 4.5: Plating Requirements for a 10,000 t Vessel as Specified by the ASPPR Proposals (Melville Shipping Ltd., 1989)

Class	Frame Spacing		
	400	600	800
CAC1	38	46	52
CAC2	34	40	48
CAC3	30	36	40
CAC4	24	30	34

The results presented are for a simplified model which is not specific to any particular mission profile. Should this algorithm be used for design purposes, more

attention would have to be given to the following when assessing cost or the effects of damage.

1. Labour costs should be computed more rigorously. It may be reasonable to assume that the 400 mm design may result in higher labour costs per unit steel mass than a larger spacing due to increased labour costs (e.g. more welding is required). As a result, a lower bound on frame spacing may be defined
2. The cost of construction can be amortised over the useful life of the ship.
3. The limit state functions can be enhanced to include the supporting structure.
4. Balance of structure, between plating and supports, can be optimised.
5. A penalty function for excessive weight or down-time, especially for cargo carrying vessels, can be incorporated.

5 CONCLUSIONS AND RECOMMENDATIONS

5.1 PRINCIPAL CONCLUSIONS

The present analysis provides the designer with an algorithm to optimize plate thickness for the bow region of ice capable vessels. The methodology presented is deterministic in format but is based on probabilistic methods. The present analysis can be divided into two distinct sections: analysis of local pressure and optimisation of bow plating. Optimisation of bow plating includes an assessment of structural integrity.

To develop the local ice load model, full scale data sets for the Canmar Kigoriak and Polar Sea are considered. It is shown that for small areas, the Polar Sea and Canmar Kigoriak data can be assumed to come from the same parent distribution. Hence, both data sets are compared directly. The data sets are analyzed as a function of area using a method similar to that of Maes and Hermans (1991). Exposure is also considered. This analysis results in the verification of the local pressure curve presented by Jordaan et al. (1993). It is recognised that this model is based on fairly limited data sets. Future test programmes would provide a larger data base and greater reliability in an ice load model. The use of data from small and medium scale indentor tests can be used to supplement the data set but are difficult to analyse statistically.

Structural integrity is based on the assessment of risk, i.e., the probability that the applied load exceeds the capacity of the structure. The capacity of the structure is assessed using three limit states. These are three-hinge collapse, permanent set and

membrane collapse. Minimum safety levels are set for membrane collapse and permanent set. The choice of limit states used in the present analysis encompasses a reasonable scope of plastic design methodologies. Three-hinge collapse is an aesthetic case which is not meant to correspond to repairable damage; permanent set criteria was selected to provide a reasonable damage criteria for the bow of an ice strengthened vessel; membrane collapse provides a more severe damage criterion which includes the possibility of loss. Three-hinge collapse is ignored for the design of bow plating because it is assumed that the bow provides significant in-plane resistance to three-hinge collapse. More information is necessary to better define reasonable limit states for the design of ship structure. Analysis of scale models of structural panels would be useful to define useful limit states.

A simple objective function is employed to optimize the thickness of the bow plating. This objective function minimises cost. The total cost of the vessel is composed of the initial cost, aesthetic cost, cost of repairs and cost of replacement. The results of this analysis are presented. For the objective function considered it is found that a 400 mm frame spacing consistently results in an optimal design. Optimal plate thicknesses, for s = 400 mm, range between 26 mm for v = 5 up to 38 mm for v = 10,000 . These results will likely change as the model is made more specific to the design.

The plate thicknesses calculated using the present analysis are in excess of those required by the ASPPR Proposals (Melville Shipping Ltd., 1989). This is assumed to be due to differences in methodology, differences in the objective of the work, and the small

amount of full scale data available. A more elaborate objective function may result in more consistent results between the two methods.

5.2 RECOMMENDATIONS

Upon completion of the present analysis, a number of recommendations for future work are made. These are as follows.

1. More data is needed to improve the reliability of the ice load model. In addition, the data history for each subpanel is required. This will give designers more confidence in the model.
2. More work is required with regard to global loads and their relationship to local loads. This will allow development of an ice load model which is representative of all three components of the response of a ship.
3. The cost of aesthetics, repair and replacement should be made more specific to the vessel in question and relevant costs. It is further suggested that other costs (down-time, excess weight penalty, etc.) be assessed as required.
4. Confidence distributions for all the functions being considered (i.e., load, limit states, objective function, ...) should be derived and implemented.
5. Labour costs can be computed more rigorously.

6. The limit state functions can be enhanced to include the supporting structure. This will allow structural balance (between plating and supporting frames) to be assessed and optimised.

REFERENCES

Allen, D.E. (1975). "Limit States Design - a Probabilistic Study," *Canadian Journal of Civil Engineering*, Vol. 2, No. 1, pp. 36-49.

Arnell, N.W., Beran, M. and Hosking, J.R.M. (1986). "Unbiased Plotting Positions for the General Extreme Value Distribution," *Journal of Hydrology*, Vol. 86, pp. 59-69.

Ayyub, B.M. and White, G.J. (1987). "Reliability-Conditioned Partial Safety Factors," *Journal of Structural Engineering*, ASCE, Vol. 113, No. 2, pp. 279-294.

Ayyub, B.M., White, G.J. and Purcell, E.S. (1989). "Estimation of Structural Service Life of Ships," *Naval Engineers Journal*, ASNE, Vol. 101, No. 3, pp. 156-166.

Ayyub, B.M., White, G.J., Bell-Wright, T.F. and Purcell, E.S. (1990). "Comparative Structural Life Assessment of Patrol Boat Bottom Plating," *Naval Engineers Journal*, ASNE, Vol. 102, No. 3, pp. 253-262.

Carter, J.E., Frederking, R.M.W., Jordaan, I.J., Milne, W.J., Nessim, M.A. and Brown, P.W. (1992). *Review and Verification of Proposals for the Revision of the Arctic Shipping Pollution Prevention Regulations - Final Report*, Transport Canada Report No. TP 11366E, Memorial University of Newfoundland, St. John's, NF.

Clarkson, J. (1956). "A New Approach to the Design of Plates to Withstand Lateral Pressure," *Transactions, Institution of Naval Architects*, London, UK, Vol. 98, pp. 443-463.

Daley, C.G., St. John, J.W., Seibold, F. and Bayly, I. (1984). "Analysis of Extreme Ice Loads Measured on USCGC Polar Sea," *Transactions, Society of Naval Architects and Marine Engineers*, New York, NY, Vol. 92, pp. 241-252.

Daley, C.G., St. John, J.W., Brown, R. and Glen, I. (1986). *Consolidation of Local Ice Impact Pressures Measured Aboard USCGC Polar Sea (1982-1984)*, Transport Canada Report No. TP 8533E, Arctec Canada Ltd., Kanata, ON and Arctec Engineering Inc., Columbia, MD.

Daley, C.G., Ferregut, C. and Brown, R. (1991). "Structural Risk Model of Arctic Shipping," *Proceedings, IUTAM-IAHR Symposium on Ice-Structure Interaction*, Springer-Verlag, St. John's, NF, 1989, pp. 507-540.

Dome Petroleum Ltd. (1982). *Full Scale Measurements of the Ice Impact Loads and Response of the Kigoriak - August and October, 1981*, Dome Petroleum Ltd., Calgary AB.

Egge, E.D. and Böckenhauer, M. (1991). "Calculation of the Collision Resistance of Ships and its Assessment for Classification Purposes," *Marine Structures: Design, Construction and Safety*, Vol. 4, No. 1, pp. 35-56.

Ferregut, C. and Daley, C. (1988). *Final Report - ASPEN - Structural Modelling Using Limit States*, Transport Canada Report No. TP 9472E, Fleet Technology Ltd., Kanata, ON.

Frederking, R.M.W., Jordaan, I.J. and McCallum, J.S. (1990). "Field Tests of Ice Indentation at Medium Scale: Hobson's Choice Ice Island, 1989," *Proceedings, 10th International Symposium on Ice*, IAHR, Espoo, Finland, Vol. 2, pp. 931-944.

Frederking, R.M.W., Jordaan, I.J., Milne, W.J., Muggeridge, D.B. and Brown, P.W. (1991). *Review and Verification of Proposals for the Revision of the Arctic Shipping Pollution Prevention Regulations - Report on Phase 1: Concept Review*, Transport Canada Report No. TP 11472E, Memorial University of Newfoundland, St. John's, NF.

Galambos, T. and Ravindra, M.K. (1978). "Properties of Steel for Use in LFRD," *Journal of the Structural Division*, ASCE, Vol. 104, No. ST9, pp. 1459-1468.

German, J.G. and Sukselainen, J. (1984). *MV Arctic Test Results and Analysis*, Transport Canada Report No. TP 6727E, German and Milne Inc., Ottawa, ON and Technical Research Centre of Finland, Helsinki, Finland.

Glen, I.F. and Blount, H., (1984). "Measurements of Ice Impact Pressures and Loads Onboard CCGS Louis S. St. Laurent," *Proceedings, 3rd Offshore Mechanics and Arctic Engineering Symposium*, ASME, New Orleans, LA, Vol. III, pp. 246-252.

Gollwitzer, S., Abdo, T. and Rackwitz, R. (1988). *FORM (First Order Reliability Method) Manual*, RCP GmbH, Munich, Germany, 47 pages.

Grandy, L.D. (1991). *Development of Statistical Interface Systems for Both Wellsite and IIP Databases*, Centre for Cold Oceans Resources Engineering, St. John's, NF.

Gumbel, E.J. (1958). *Statistics of Extremes*, Columbia University Press, New York, NY, 375 pages.

Hooke, R. and Rawlings, B. (1969). "An Experimental Investigation of the Behaviour of Clamped, Rectangular, Mild Steel Plates Subjected to Uniform Transverse Pressure," *Proceedings, Institution of Civil Engineers*, London, UK, Vol. 42, pp. 75-103.

Hughes, O.F. (1981). "Design of Laterally Loaded Plating - Uniform Pressure Loads," *Journal of Ship Research*, SNAME, Vol. 25, No. 2, pp. 77-89.

Hughes, O. (1983). "Design of Laterally Loaded Plating - Concentrated Loads," *Journal of Ship Research*, SNAME, Vol. 27, No. 4, pp. 252-264.

Hughes, O.F. (1988). *Ship Structural Design - A Rationally-Based, Computer-Aided Optimization Approach*, 2nd edition, The Society of Naval Architects and Marine Engineers, Jersey City, NJ, 566 pages.

Johansen, K.W., (1962). *Yield-Line Theory*, 2nd ed., Cement and Concrete Association, London, U.K., 181 pages.

Jordaan, I.J., (1985). *A Probabilistic Approach to the Estimation of Ice Loads in Arctic Shipping*, Internal Report, Det norske Veritas (Canada) Ltd., Calgary, AB.

Jordaan, I.J. (1987). "Probabilistic Analysis of Environmental Data for Design of Fixed and Mobile Arctic Offshore Structures," *Reliability and Risk Analysis and Civil Engineering, Proceedings, 5th International Conference on Applications of Statistics and Probability in Soil and Structural Engineering*, Vancouver, BC, Vol. 2, pp. 1130-1137.

Jordaan, I.J., Nessim, M.A., Ghoneim, and Murray, A.M. (1987). "A Rational Approach to the Development of Probabilistic Design Criteria for Arctic Shipping," *Proceedings, 6th Offshore Mechanics and Arctic Engineering Symposium*, ASME, Houston, TX, Vol. IV, pp. 401-406.

Jordaan, I.J., Kennedy, K.P., McKenna, R.F. and Maes, M.A. (1991). "Loads and Vibration Induced by Compressive Failure of Ice," *Cold Regions Engineering, 6th International Specialty Conference*, ASCE, Hanover, NH, pp. 638-649.

Jordaan, I.J. and Maes, M.A. (1991). "Rationale for Load Specifications and Load Factors in the New CSA Code for Fixed Offshore Structures," *Canadian Journal of Civil Engineering*, Vol. 18, No. 3, pp. 454-464.

Jordaan, I.J., Maes, M.A., Brown, P.W. and Hermans, I.P. (1993). "Probabilistic Analysis of Local Ice Pressures," *Journal of Offshore Mechanics and Arctic Engineering*, ASME, Vol. 115, No. 1, pp. 83-89.

Keinonen, A.J., Revill, C.R. and Brown, P. (1991). *Review of Proposed Revisions to CASPPR - Study Area C: Damages*, AKAC Inc., Calgary, AB.

Kennedy, D.J.L. and Aly, M.G. (1980). "Limit States Design of Steel Structure - Performance Factors," *Canadian Journal of Civil Engineering*, Vol. 7, No. 1, pp. 45-77.

Kennedy, D.J.L. and Baker, K. (1984). "Resistance Factors for Steel Highway Bridges," *Canadian Journal of Civil Engineering*, Vol. 11, No. 2, pp. 324-334.

Køhler, P.E. and Jørgensen, L. (1985). "Ship Ice Impact Analysis," *Proceedings, 4th Offshore Mechanics and Arctic Engineering Symposium*, ASME, Dallas, TX, Vol. II, pp. 344-350.

Kujala, P.J. (1991). "Safety of Ice-Strengthened Ship Hulls in the Baltic Sea," *Transactions, Royal Institution of Naval Architects*, London, UK, Vol. 133, Part A, pp. 83-94.

Kulak, G.L., Adams, P.F. and Gilmor, M.I. (1990). *Limit States Design in Structural Steel*, 4th Edition, Canadian Institute of Steel Construction, Markham, ON, 358 pages.

Lilly, M. (1993). *Private Communication*, May 6, Russell Drummond, Paradise, NF.

Maes, M.A. and Jordaan, I.J. (1986). "Arctic Environmental Design Using Short Data Extremal Techniques," *Proceedings, 5th Offshore Mechanics and Arctic Engineering Symposium*, ASME, Tokyo, Japan, Vol. IV, pp. 13-19.

Maes, M.A. and Hermans, I.P. (1991). *Review of Methods of Analysis of Data and Extreme Value Techniques for Ice Loads*, Dept. of Civil Engineering and Statistics, Queen's University, Kingston, ON.

Malik, L. and Tomin, M. (1991). *Evaluation of Toughness of Conventional Ship Steels at Intermediate Loading Rate and its Implications*, Unsolicited Proposal A7-025, Marine Technology Centre Report No. E73331C, Fleet Technology Ltd., Kanata, ON and Reltec Advisory Services Inc., Calgary, AB.

Mansour, A.E. (1972). "Probabilistic Design Concepts in Ship Structural Safety and Reliability," *Transactions, Society of Naval Architects and Marine Engineers*, New York, NY, Vol. 80, pp. 64-97.

Mansour, A.E., Jan, H.Y., Zigelman, C.I., Chen, Y.N. and Harding, S.J. (1984). "Implementation of Reliability Methods to Marine Structures," *Transactions, Society of Naval Architects and Marine Engineers*, New York, NY, Vol. 92, pp. 353-382.

Masterson, D.M. and Frederking, R.M.W (1993). "Local Contact Pressures in Ship and Structure/Ice Interactions," *Journal of Cold Regions Science and Technology*, Vol. 21, No. 2, pp. 169-185.

McDermott, J.F., Kline, R.G., Jones, Jr., E.L., Maniar, N.M. and Chiang, W.P. (1974). "Tanker Structural Analysis," *Transactions, Society of Naval Architects and Marine Engineers*, New York, NY, Vol. 82, pp. 382-414.

Melville Shipping Ltd., (1989). *Proposals for the Revision of the Arctic Shipping Pollution Prevention Regulations*, Transport Canada Report No. TP 9981E, Melville Shipping Ltd., Ottawa, ON.

Minorsky, V.U. (1959). "An Analysis of Ship Collisions With Reference to Protection of Nuclear Power Plants," *Journal of Ship Research*, SNAME, Vol. 3, No. 2, pp. 1-4.

Moan, T. and Amdahl, J. (1989). "Catastrophic Failure Modes or Marine Structures," *Structural Failure*, ed. T. Wierzbicki, John Wiley and Sons, Inc., New York, NY, Chapter 14, pp. 463-510.

Nessim, M.A., Appleby, J.R., Jordaan, I.J. and Maes, M.A. (1984). *State-of-the-Art Description of Methods for Computation of Global and Local Loads in Ice-Structure Interaction*, Veritas Report No. 84-CGY-018, Det norske Veritas Canada, Calgary, AB.

Nessim, M.A., Hong, H.P. and Stephens, M.S. (1992). *Reliability-Based Assessment of Hull Failure and Brittle Fracture of Ships Designed to ASPPR*, C-FER Report No. 90-35, Centre for Frontier Engineering Research, Edmonton, AB.

Paulling, J.R. (1988). "Strength of Ships," *Principles of Naval Architecture*, ed. E.V. Lewis, The Society of Naval Architects and Marine Engineers, Jersey City, NJ, Vol. I, Chapter IV, pp. 205-299.

Ratzlaff, K.P. and Kennedy, D.J.L. (1985). "Analysis of Continuous Steel Plates Subjected to Uniform Transverse Loads," *Canadian Journal of Civil Engineering*, Vol. 12, No. 3, pp. 685-699.

Ratzlaff, K.P. and Kennedy, D.J.L. (1986). "Behaviour and Ultimate Strength of Continuous Steel Plates Subjected to Uniform Transverse Loads," *Canadian Journal of Civil Engineering*, Vol. 13, No. 1, pp. 76-85.

Riggs, J.L., Rentz, W.F., Kahl, A.L. and West, T.M. (1986). *Engineering Economics*, 1st Canadian Edition, McGraw-Hill Ryerson Ltd., Toronto, ON, 746 pages.

Scarborough, R.H. (1974). *Report of the International Ice Patrol Service in the North Atlantic, Season of 1973*, Bulletin No. 59, USCG Report No. CG-188-28, United States Coast Guard, Washington, DC.

Soroushian, P. and Choi, K. (1987). "Steel Mechanical Properties at Different Strain Rates," *Journal of Structural Engineering*, ASCE, Vol. 113, No. 4, pp. 663-672.

St. John, J.W., Daley, C., Blount, H. and Glen, I.F. (1984). *Ice Loads and Ship Response to Ice - USCGC Polar Class 1982/83 Deployment*, Transport Canada Report No. TP 6039E, Arctec Canada Ltd., Kanata, ON and Arctec Engineering Inc., Columbia, MD.

Varsta, P. (1984). "Determination of Ice Loads Semi-Empirically," *VTT Symposium 52*, Helsinki, Finland, pp. 177-182.

Walpole, R.E. and Myers, R.H. (1972). *Probability and Statistics for Engineers and Scientists*, Macmillian Publishing Co., Ltd., New York, NY, 506 pages.

White, G.J. and Ayyub, B.M. (1985). "Reliability Methods for Ship Structures," *Naval Engineers Journal*, ASNE, Vol. 97., No. 4, pp. 86-96.

White, G.J. and Ayyub, B.M. (1987). "Reliability-Based Design Format for Marine Structures," *Journal of Ship Research*, SNAME, Vol. 31, No. 1, pp. 60-69.

Wiernicki, C.J. (1987). "Damage to Ship Plating Due to Ice Impact Loads," *Marine Technology*, SNAME, Vol. 24, No. 1, pp. 43-58.

Woisin, G. (1976). "Die Kollisionsversuche der GKSS (Collision Tests of the GKSS)," *Jahrbuch der Schiffbautechnischen Gesellschaft*, 70, pp. 465-491.

Wood, R.H., (1961). *Plastic and Elastic Design of Slabs and Plates with Particular Reference to Reinforced Concrete Floor Slabs*, Thames and Hudson, London, UK, 344 pages.

Xiao, J. and Jordaan, I.J. (1991). *Modelling of Fracture and Production of Discrete Ice Pieces, Development and Verification of New Ice Load Models, Phase IV*, Ian Jordaan and Associates, St. John's, NF.

Young, A.G. (1959). "Ship Plating Loaded Beyond the Elastic Limit," *Transactions, Institution of Naval Architects*, London, UK, Vol. 101, pp. 143-165.

APPENDICES

Appendix 1 COVERAGE ANALYSIS

1A COVERAGE PATTERNS FOR THE CANMAR KIGORIAK SMALL PANEL, A1

1 Subpanel:

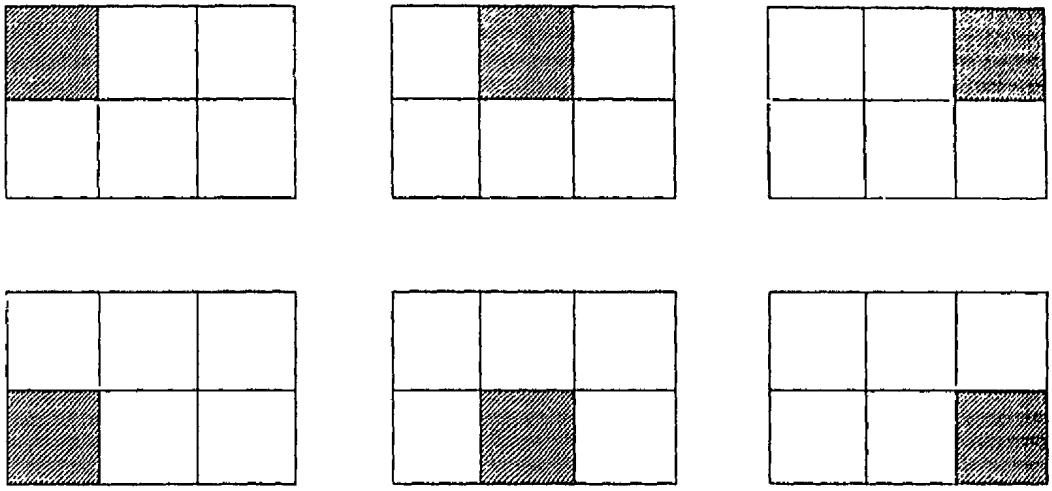

2 Subpanels:

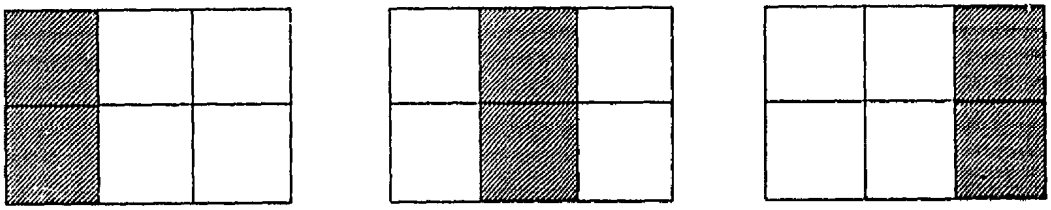

2 Subpanels (cont'd):

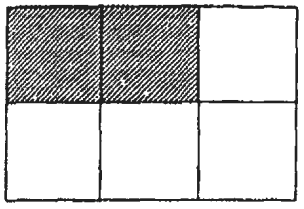

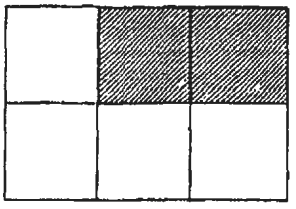

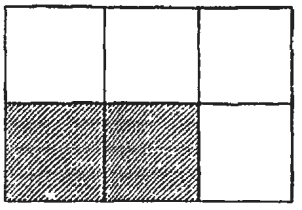

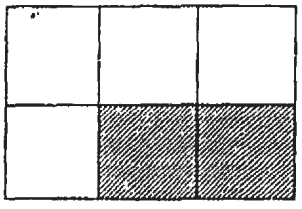

3 Supanels:

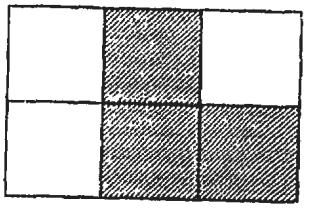

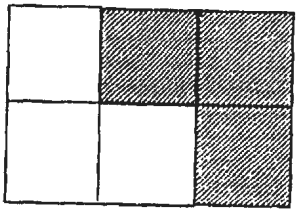

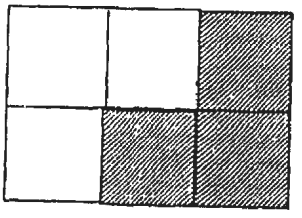

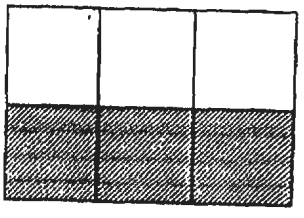

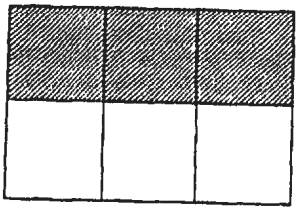

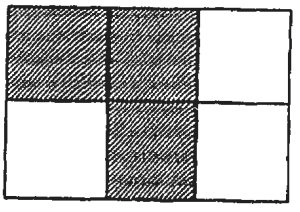

3 Subpanels (cont'd):

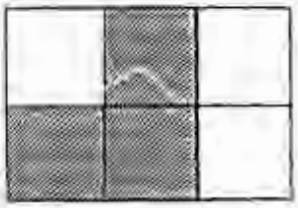

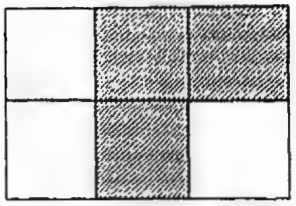

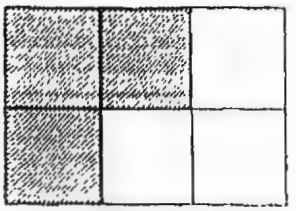

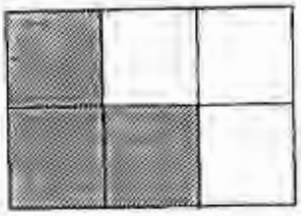

4 Subpanels:

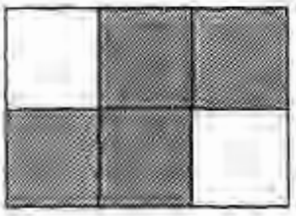

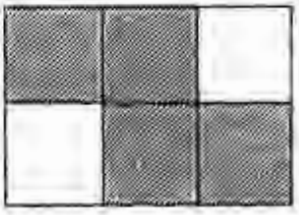

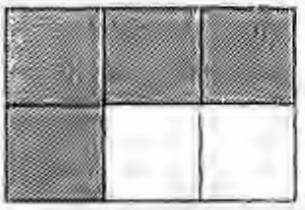

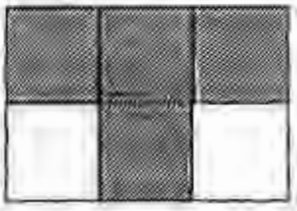

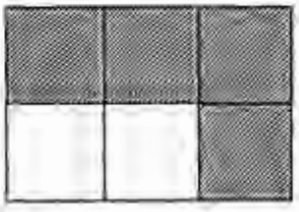

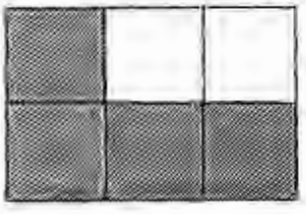

4 Subpanels (cont'd):

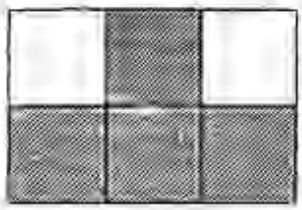

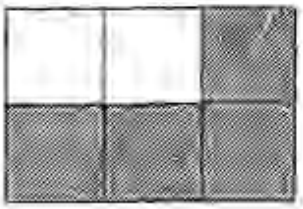

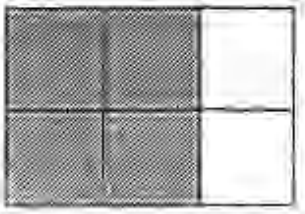

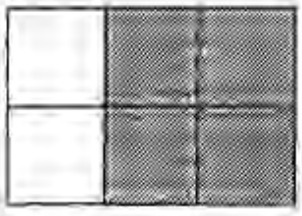

5 Subpanels:

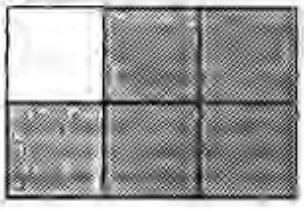

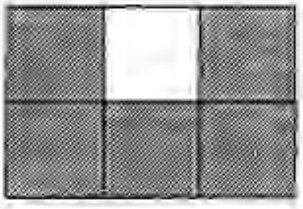

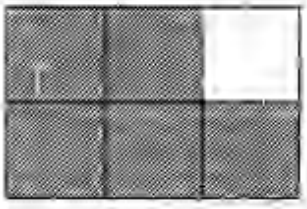

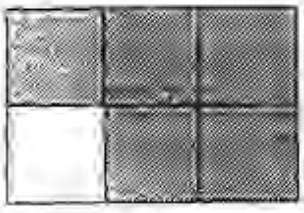

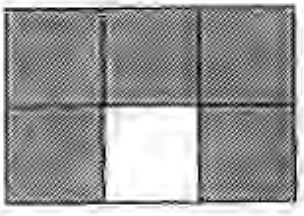

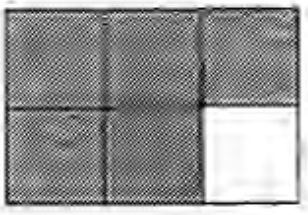

6 Subpanels:

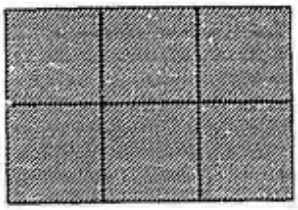

1B COVERAGE PATTERNS FOR THE CANMAR KIGORIAK LARGE PANEL, A2

1 Subpanel:

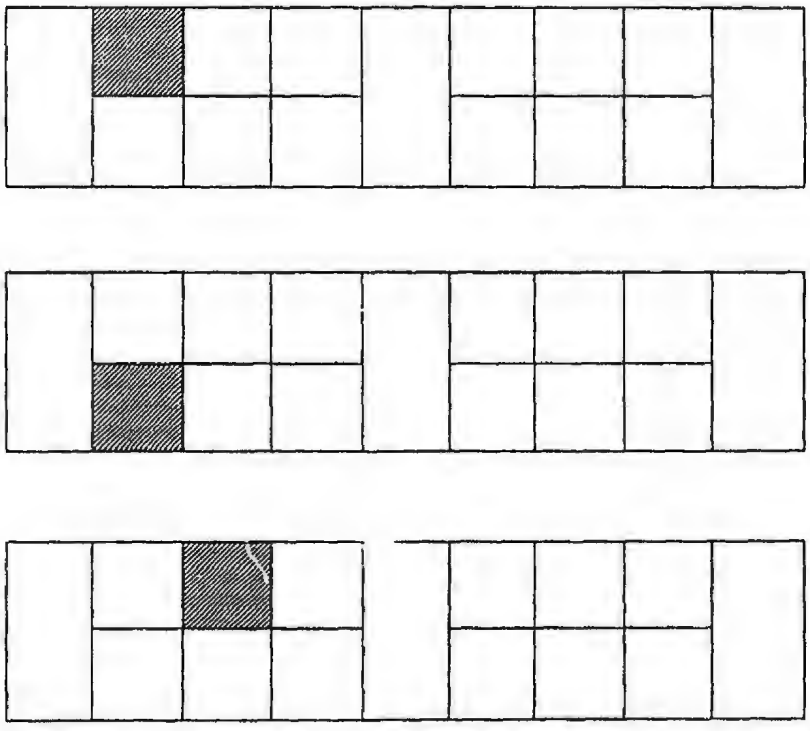

1 Subpane! (cont'd):

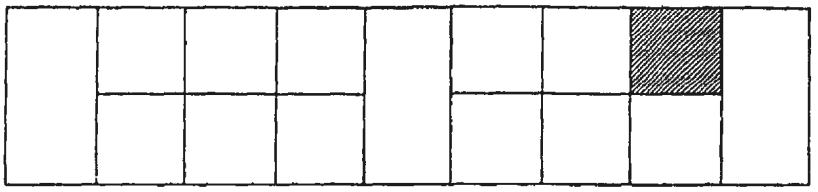

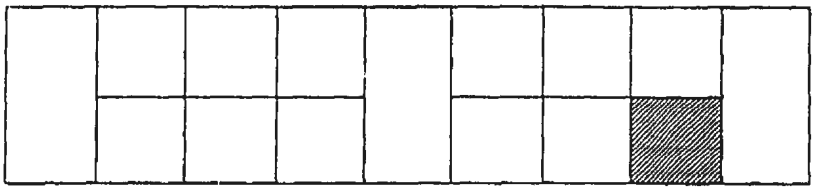

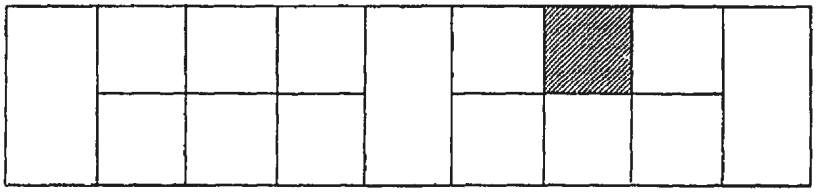

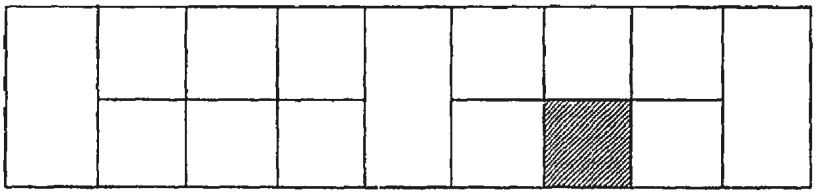

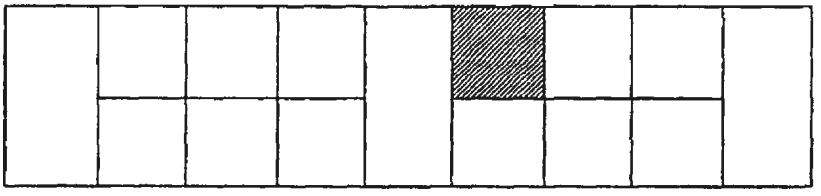

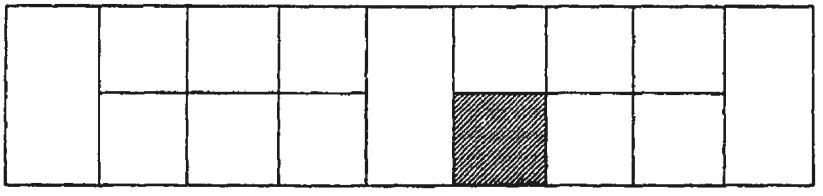

1 Subpanel (cont'd):

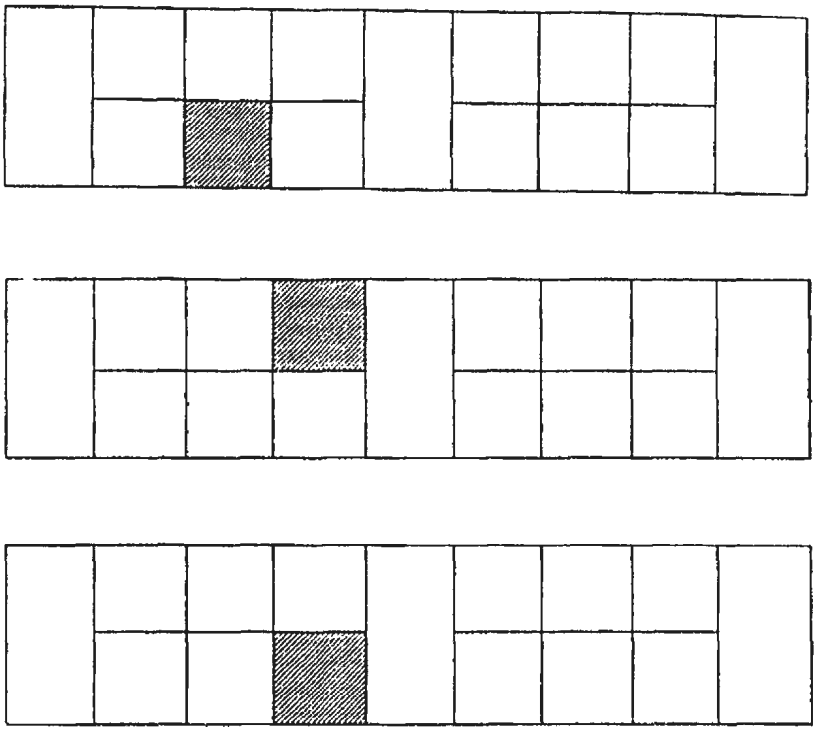

2 Subpanels:

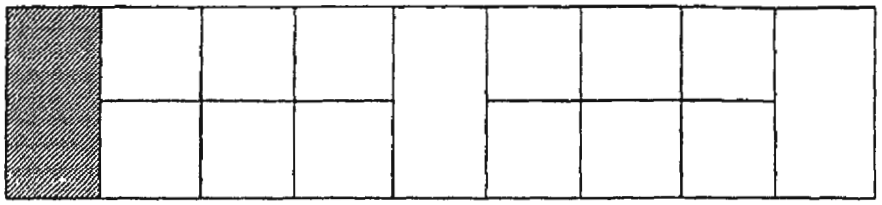

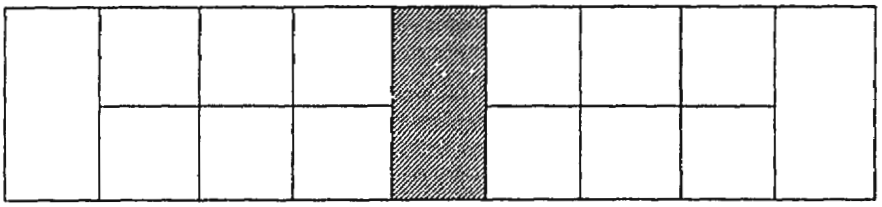

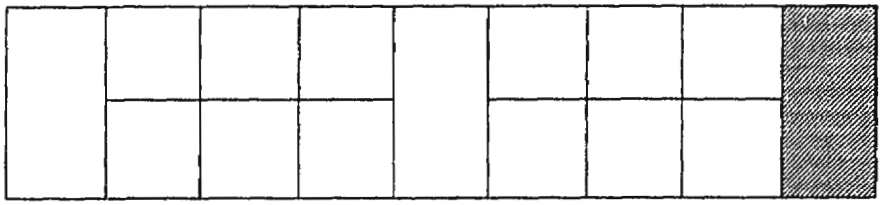

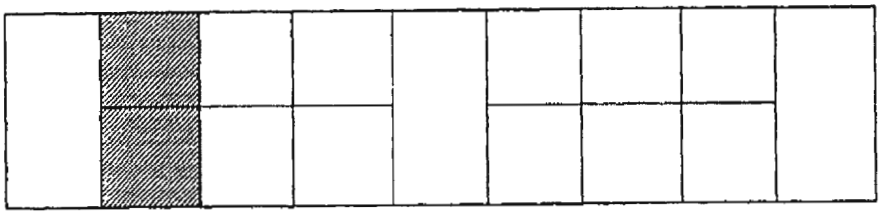

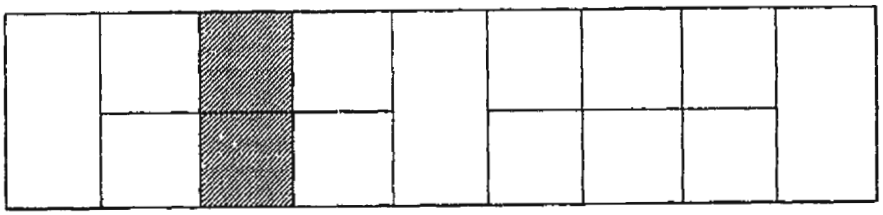

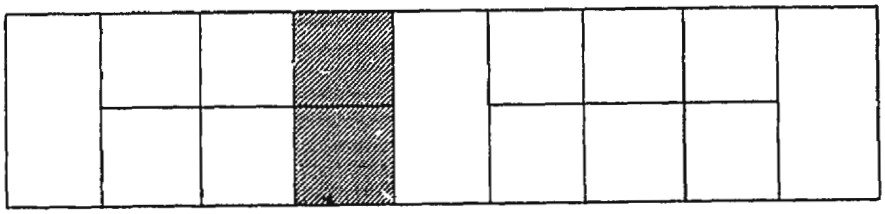

2 Subpanels (cont'd):

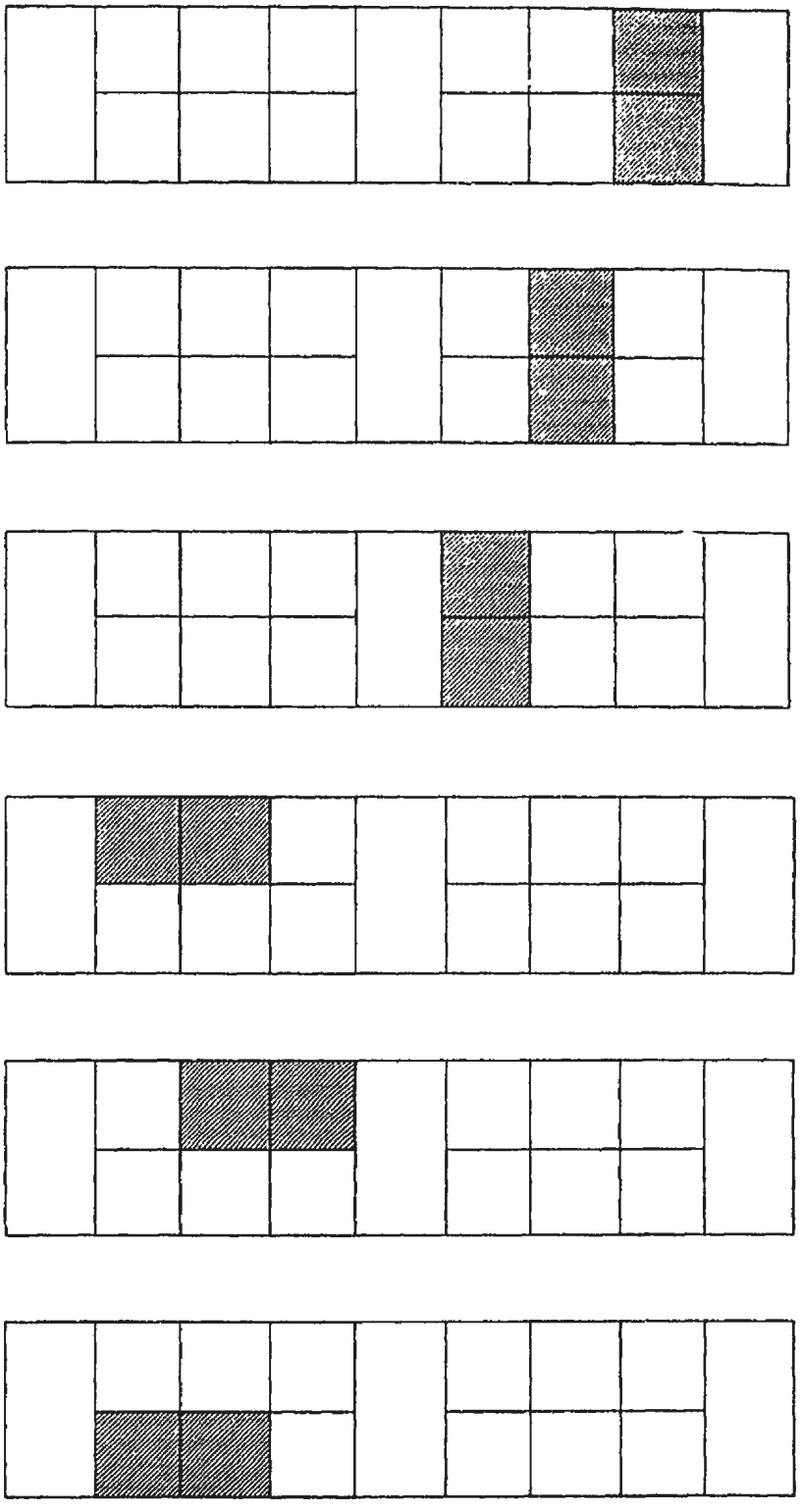

2 Subpanels (cont'd):

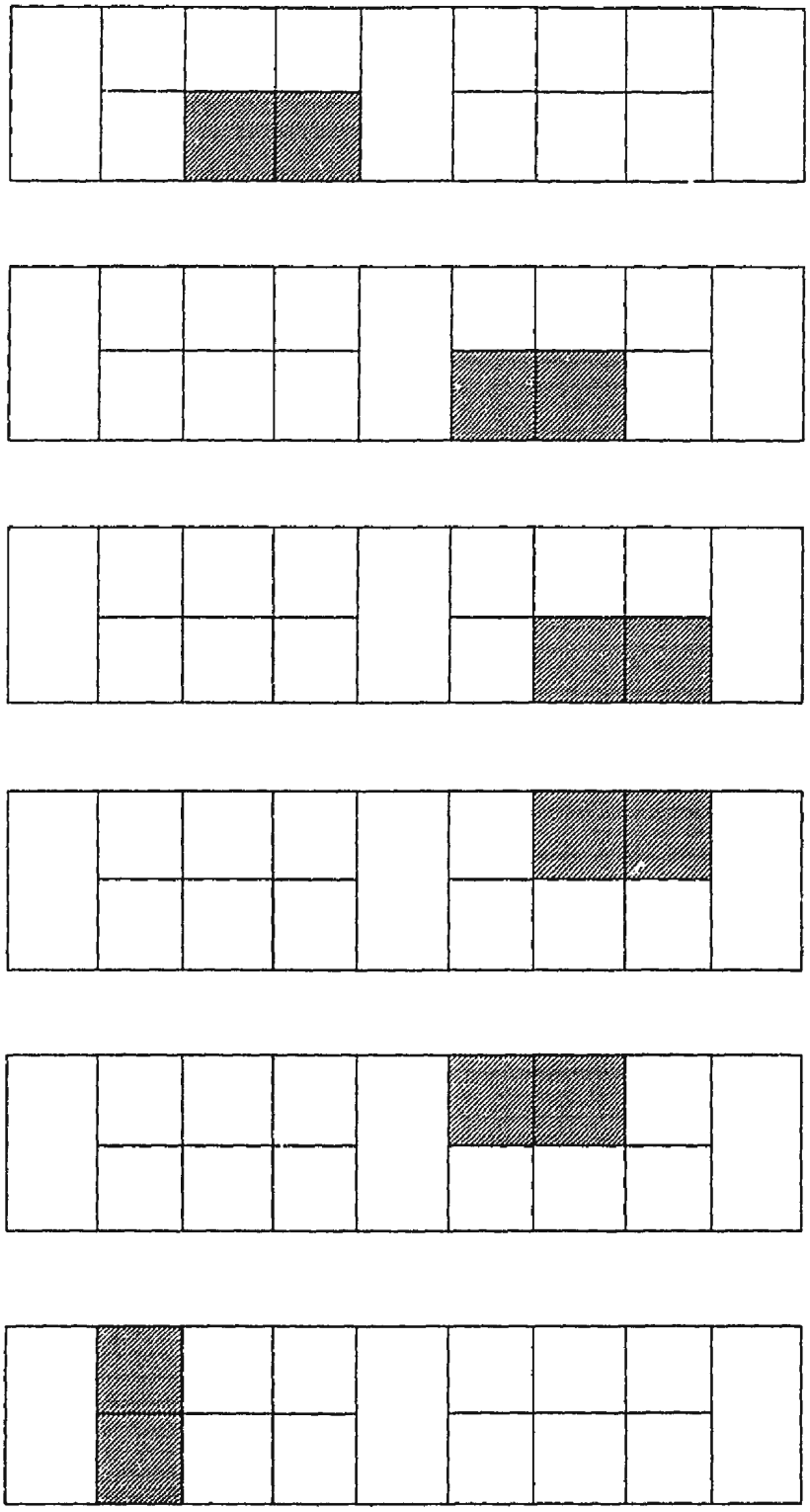

2 Subpanels (cont'd)

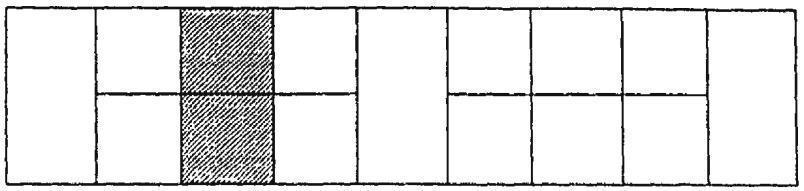

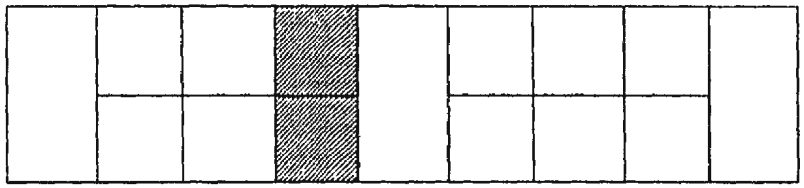

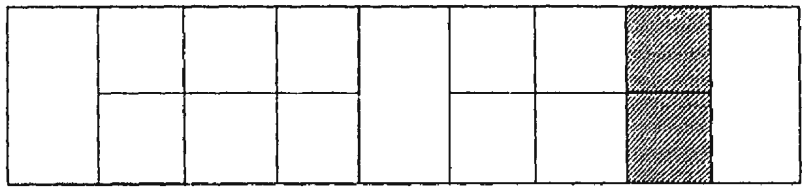

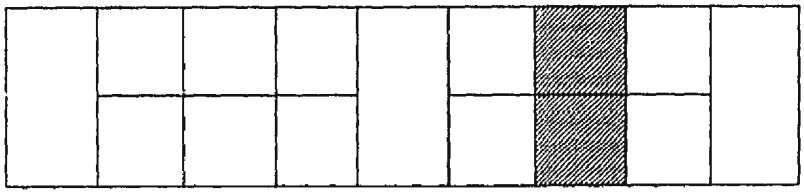

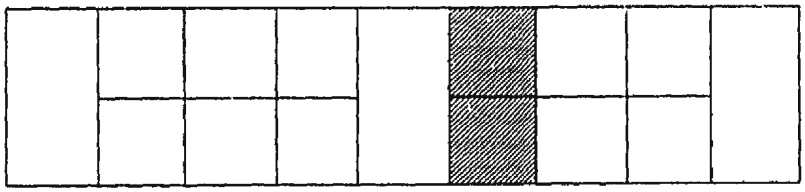

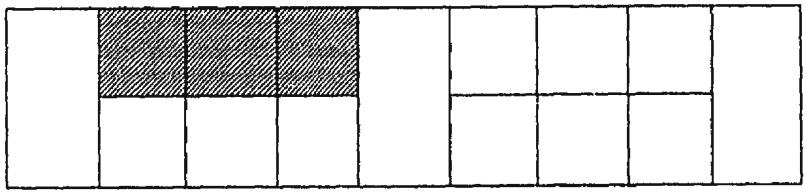

3 Subpanels:

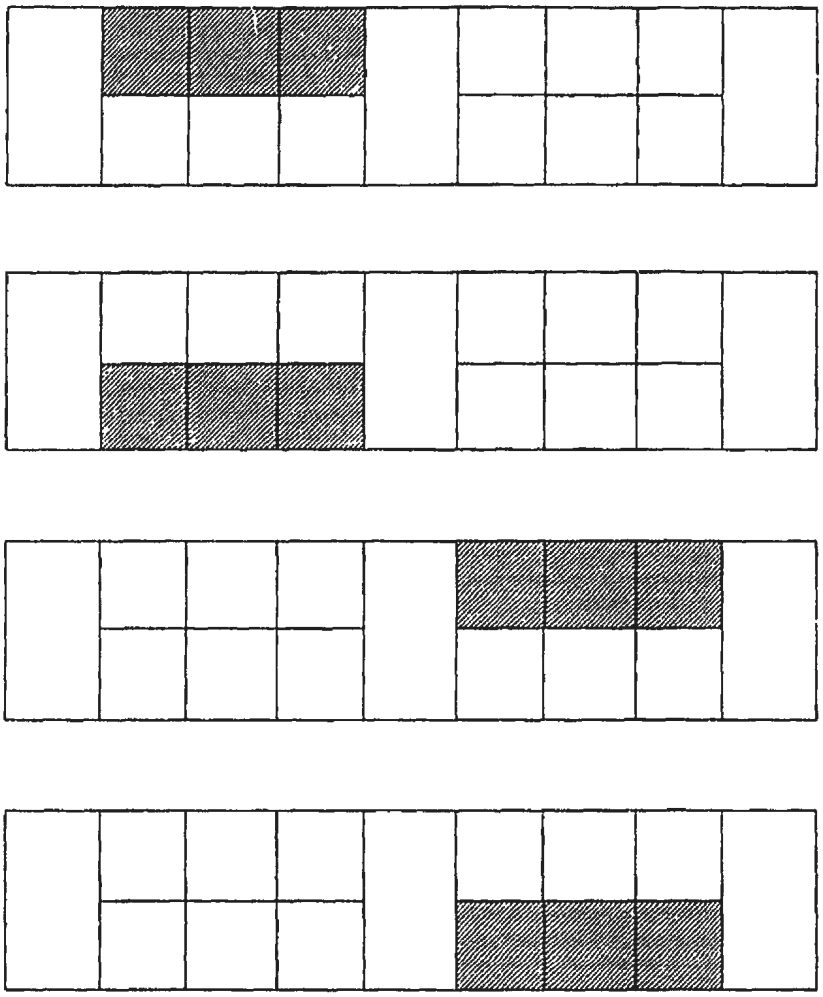

4 Subpanels:

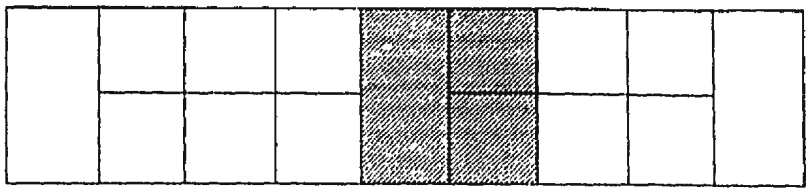

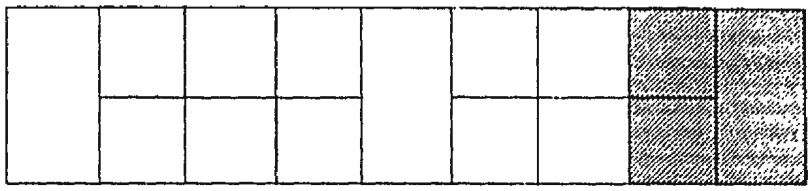

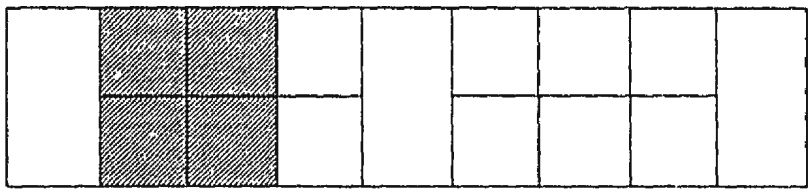

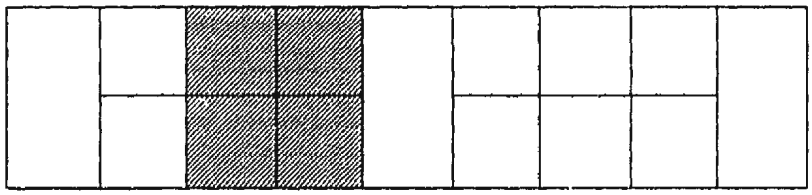

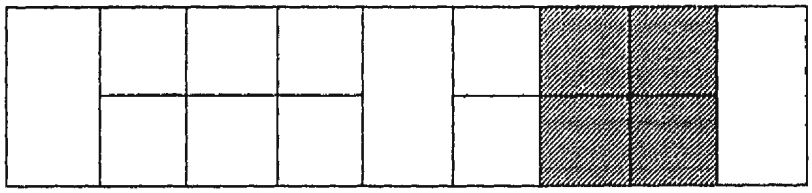

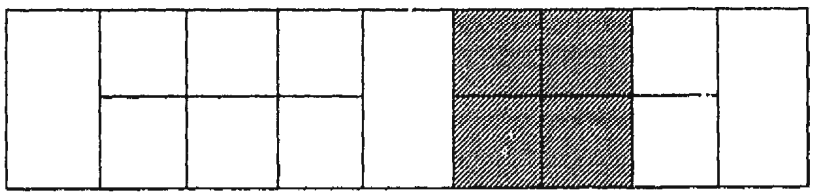

4 Subpanels (cont'd):

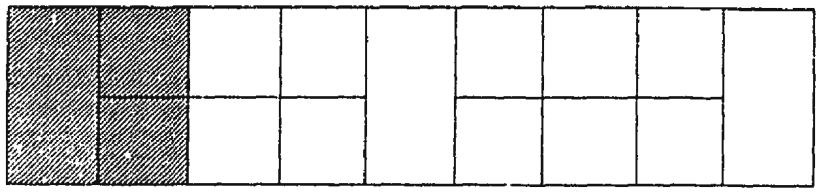

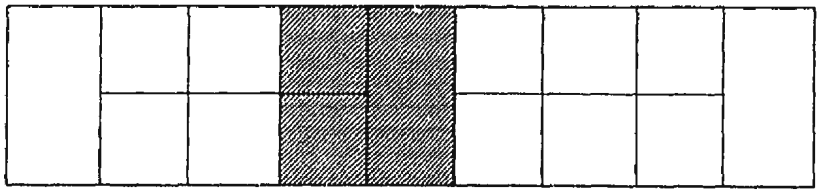

5 Subpanels:

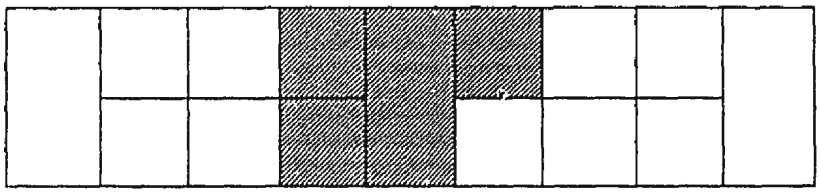

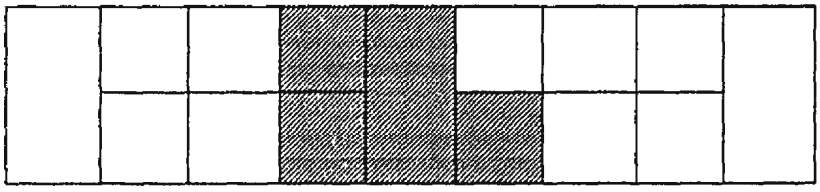

5 Subpanels (cont'd):

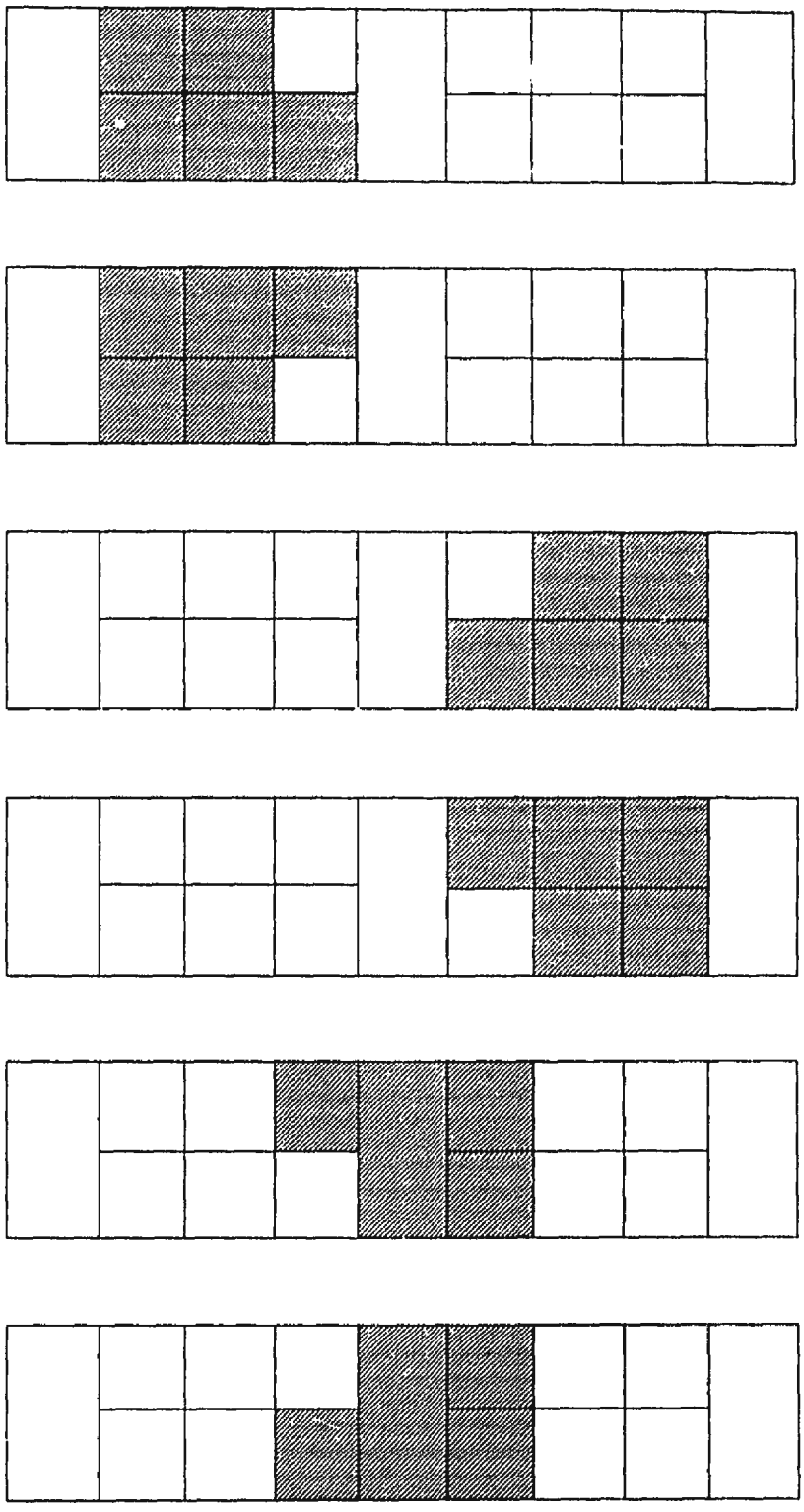

5 Subpanels (cont'd):

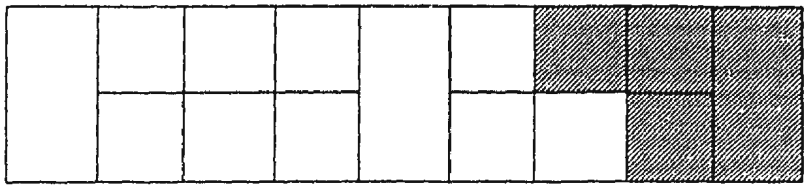

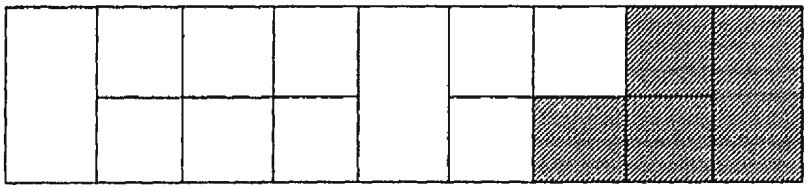

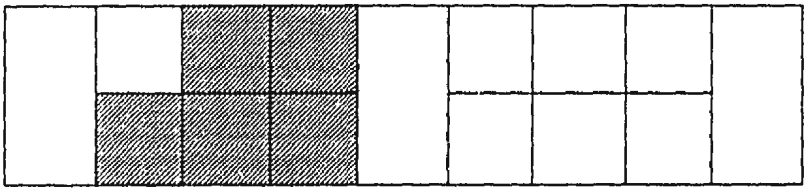

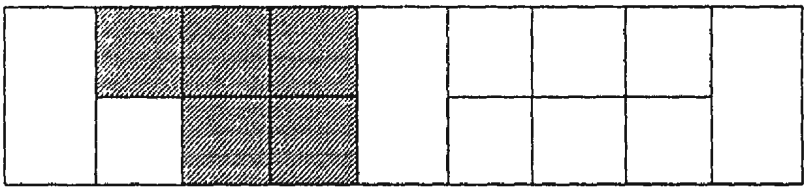

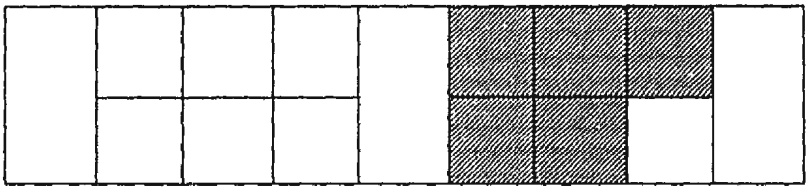

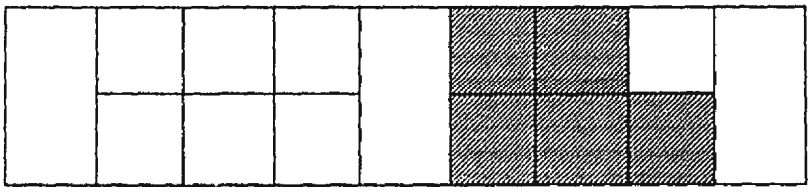

6 Subpanels:

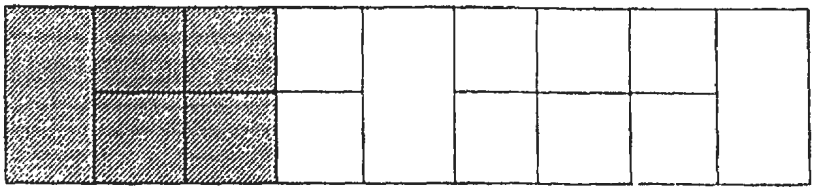

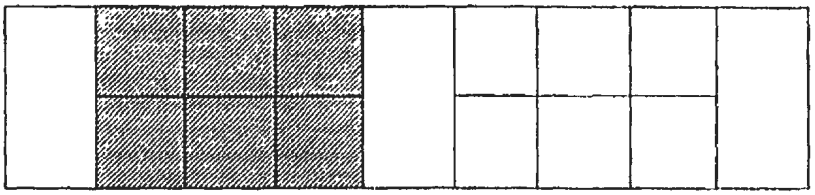

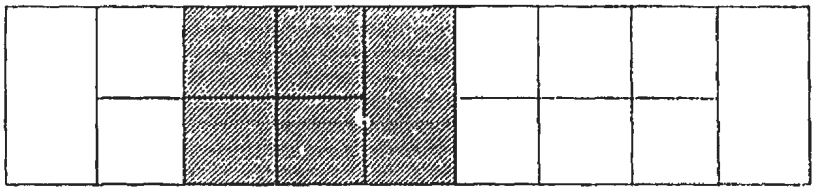

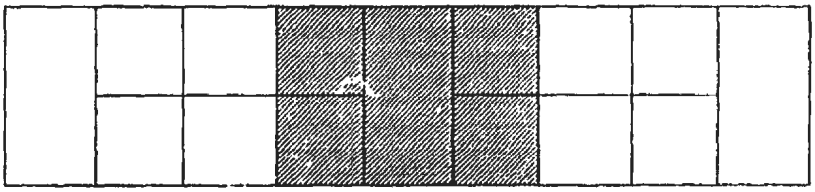

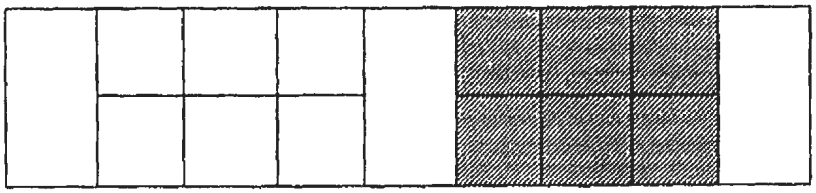

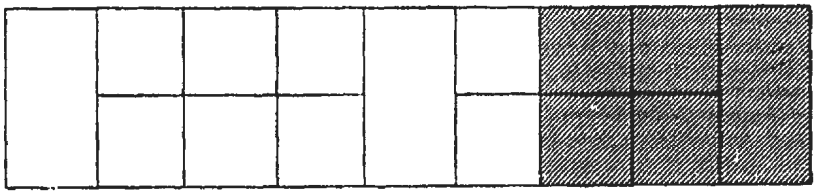

7 Subpanels:

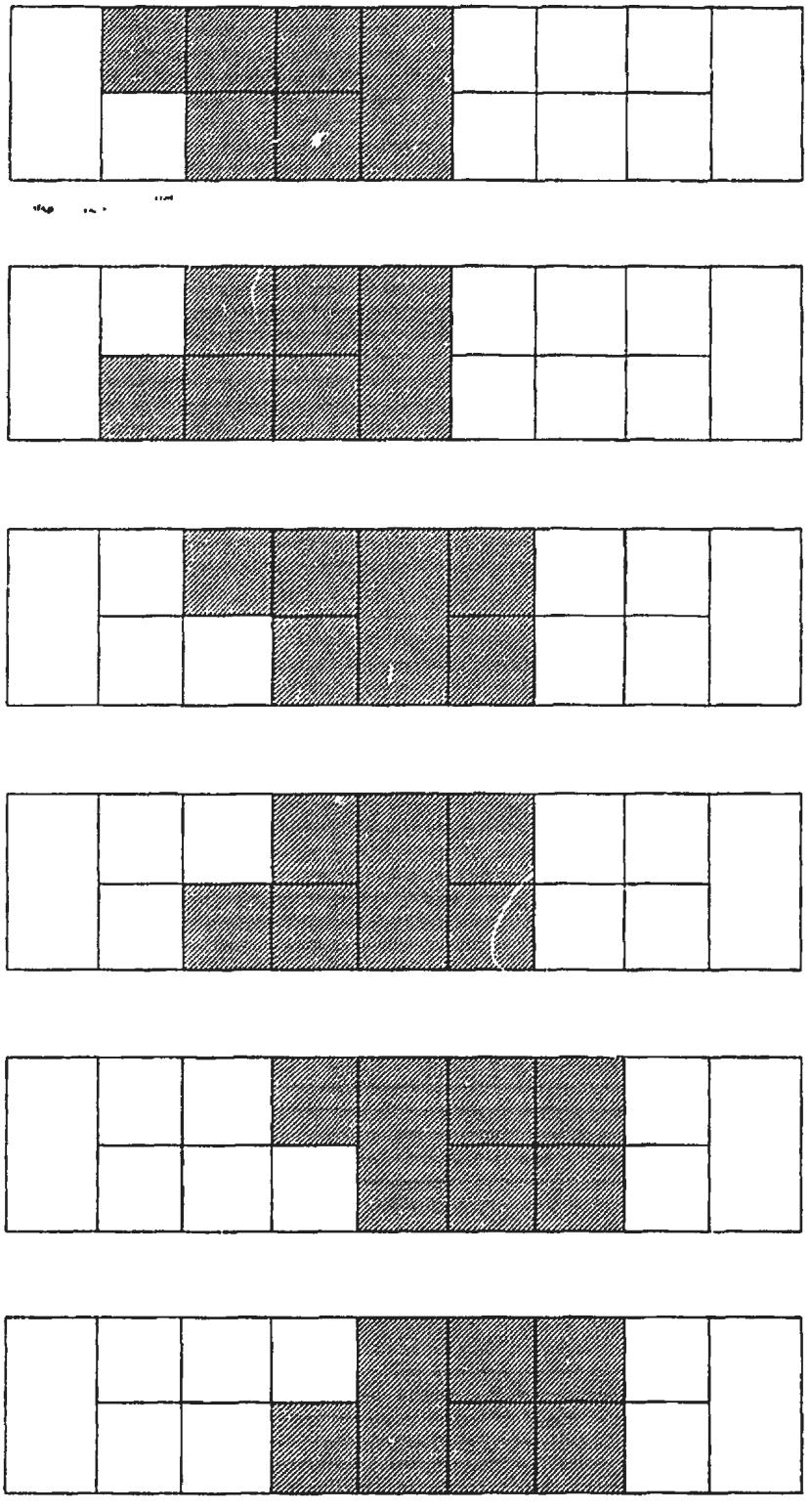

7 Subpanels (cont'd):

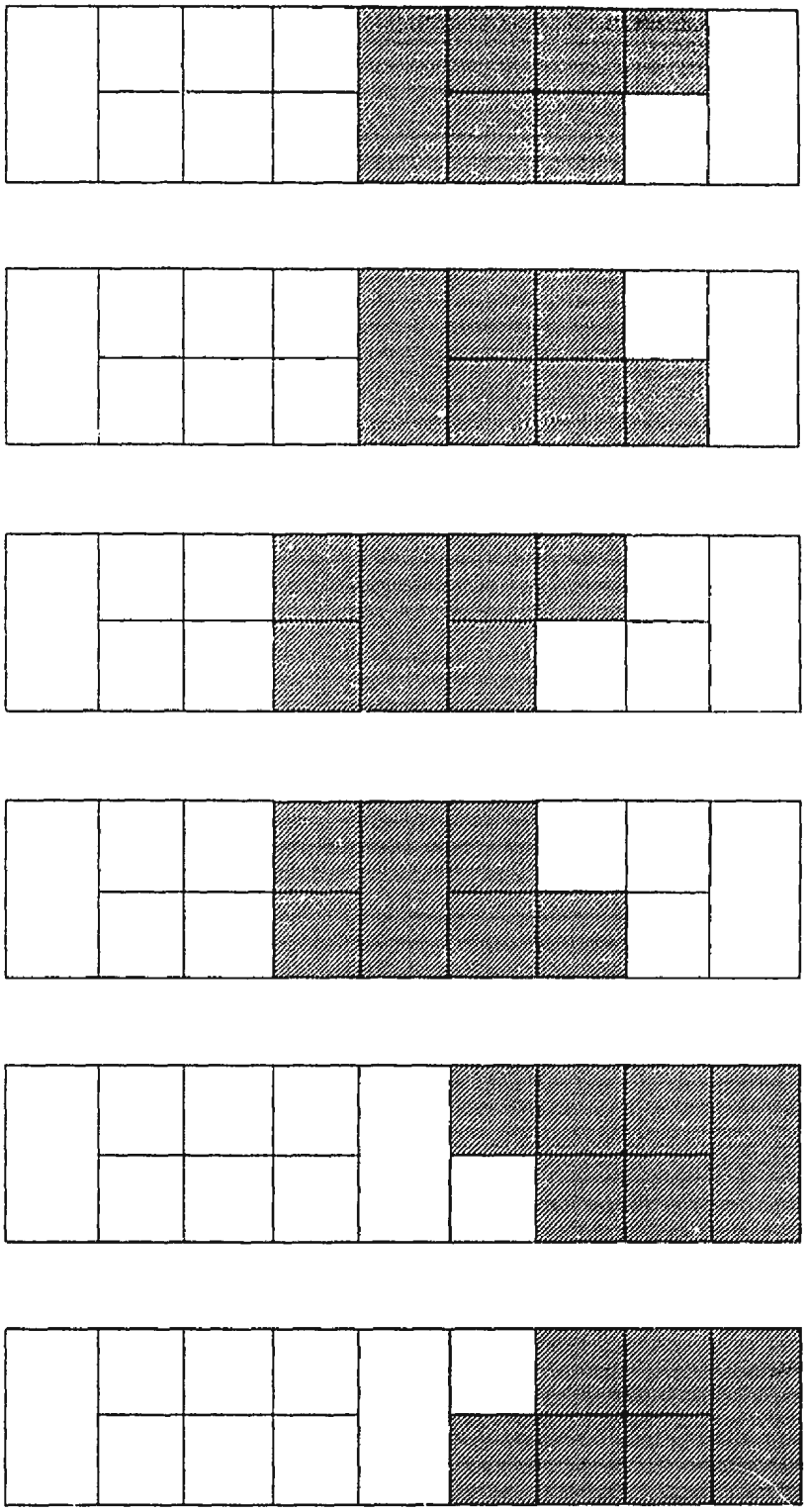

7 Subpanels (cont'd):

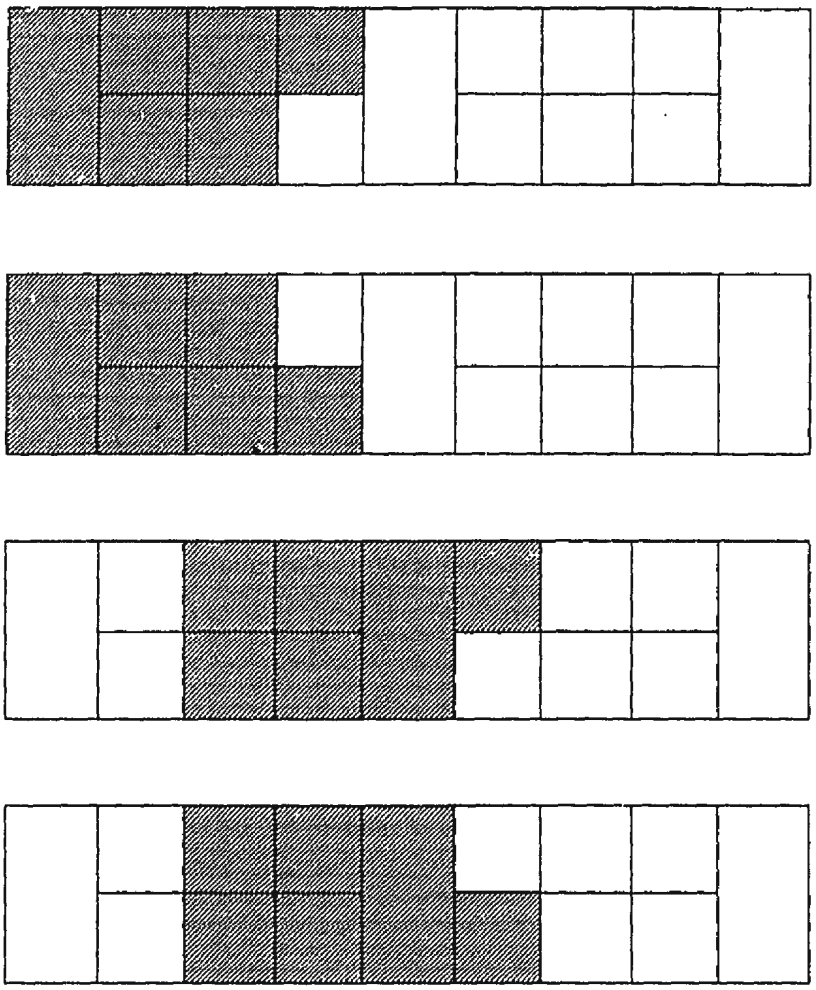

8 Subpanels:

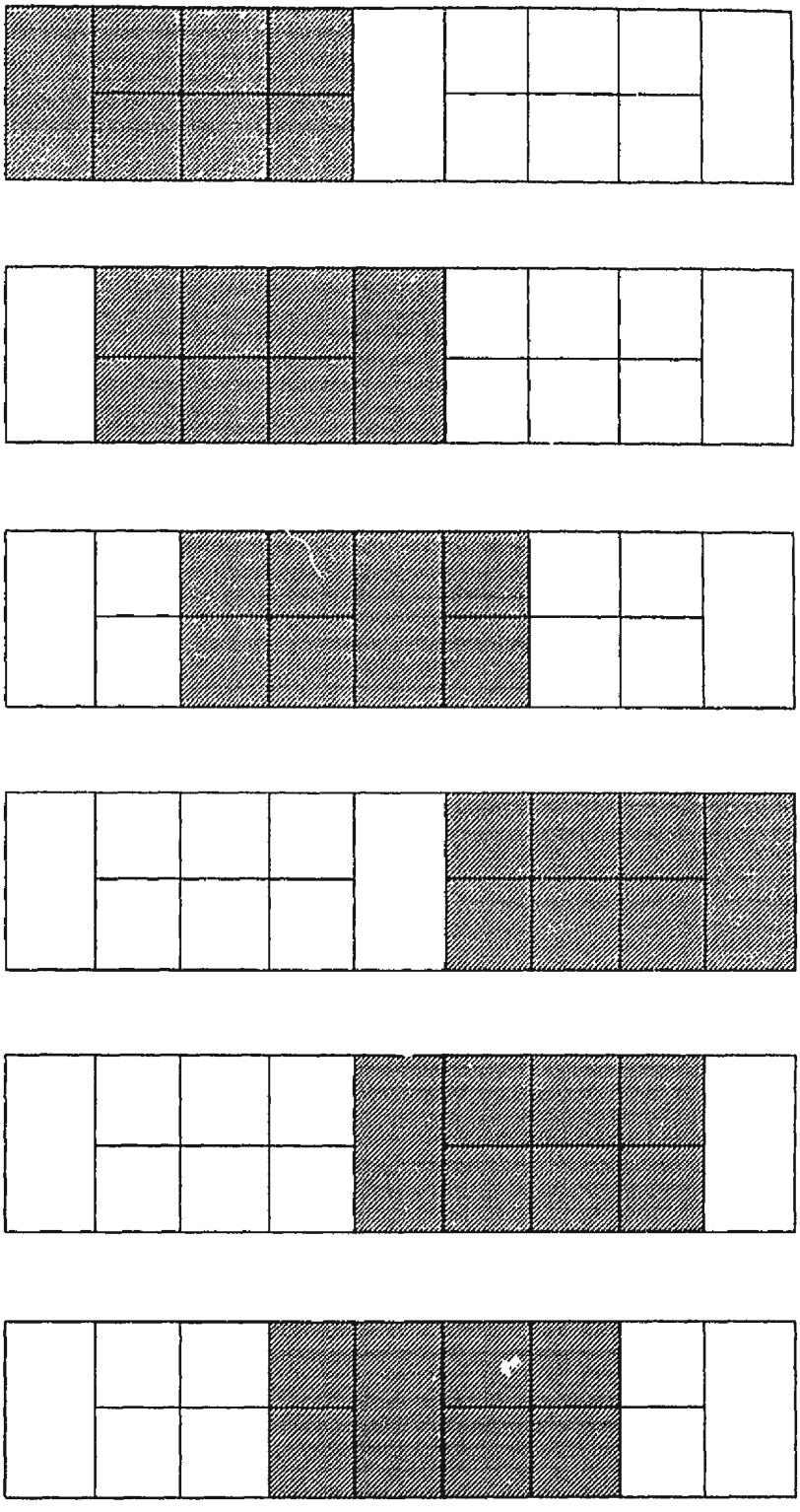

9 Subpanels:

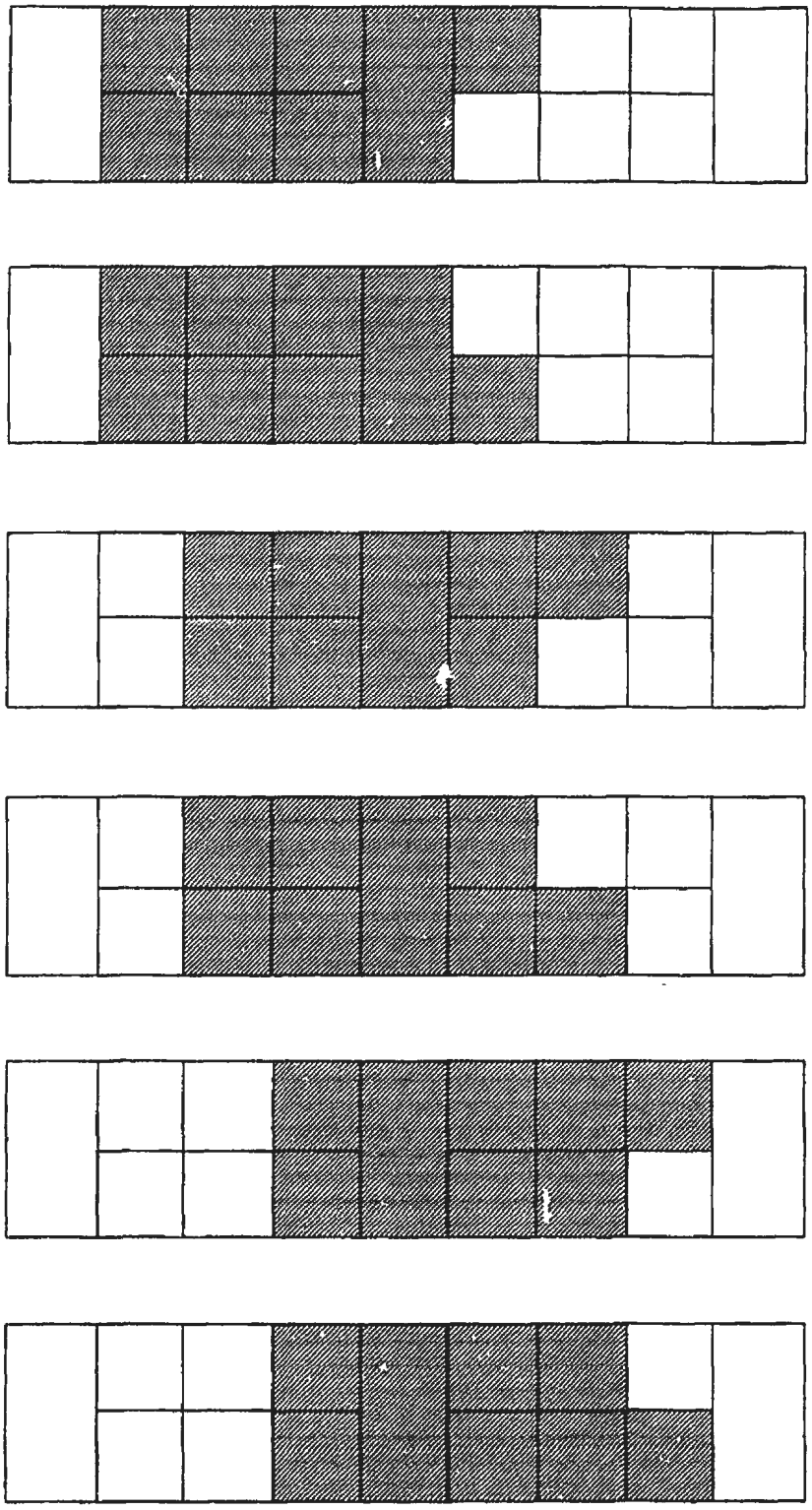

9 Subpanels (cont'd):

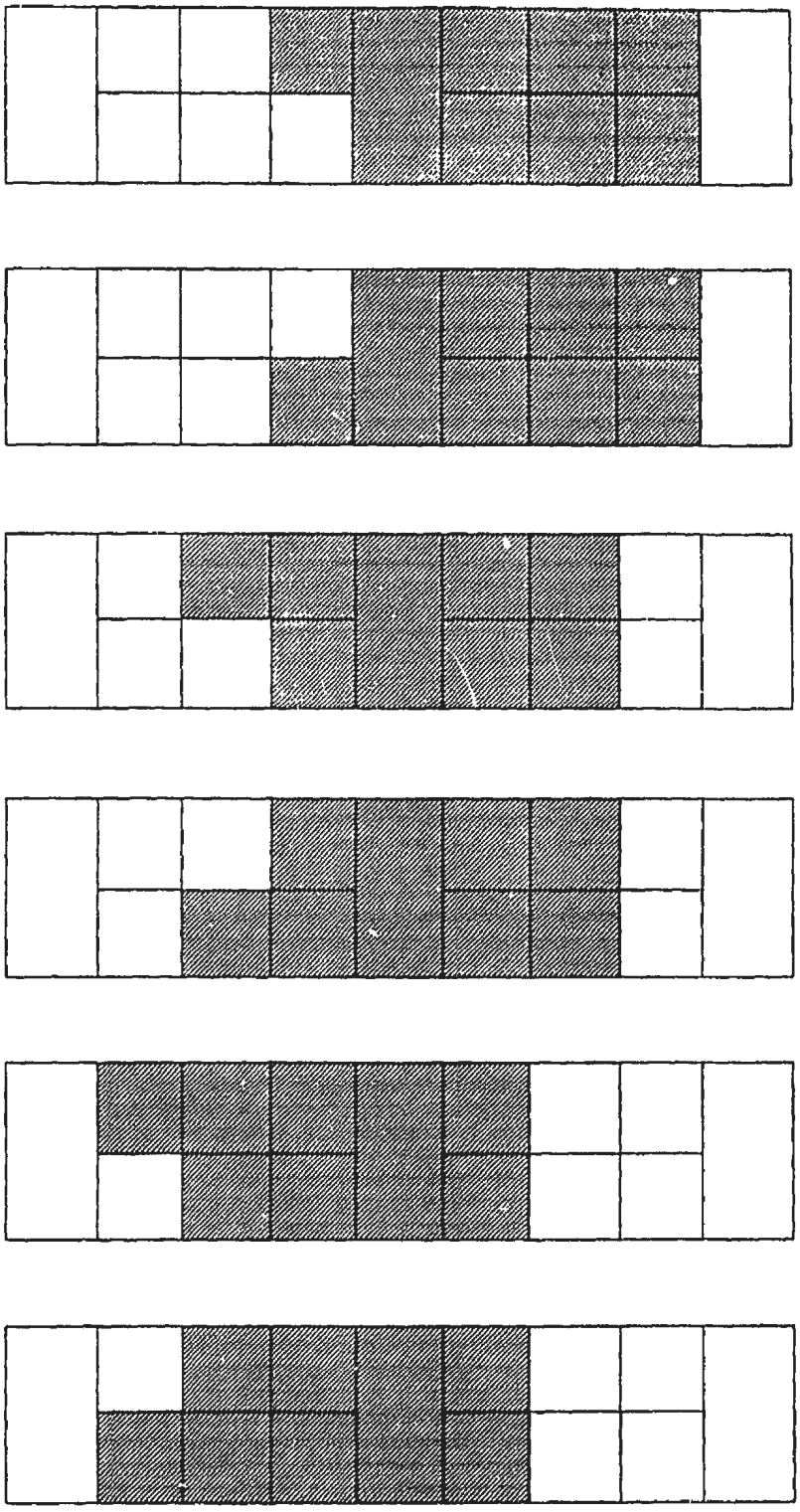

10 Subpanels:

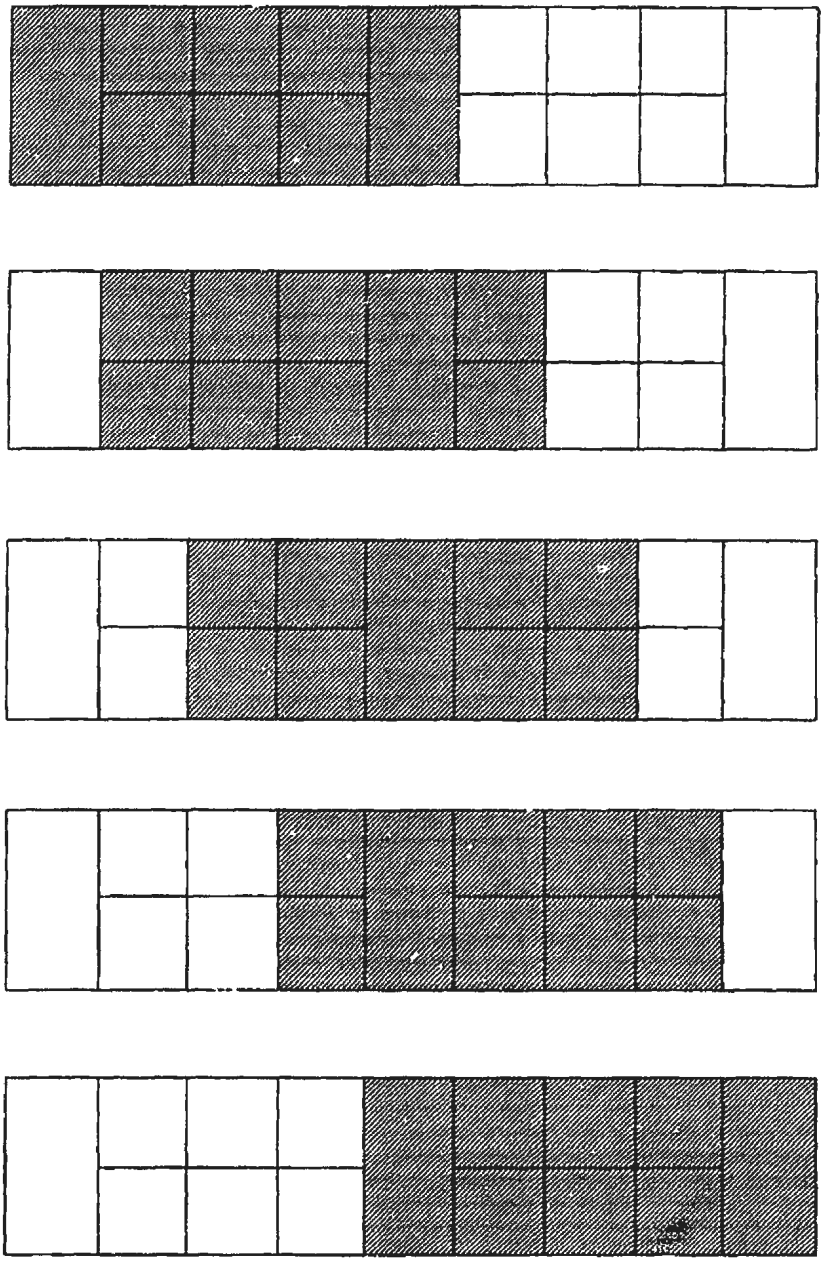

11 Subpanels:

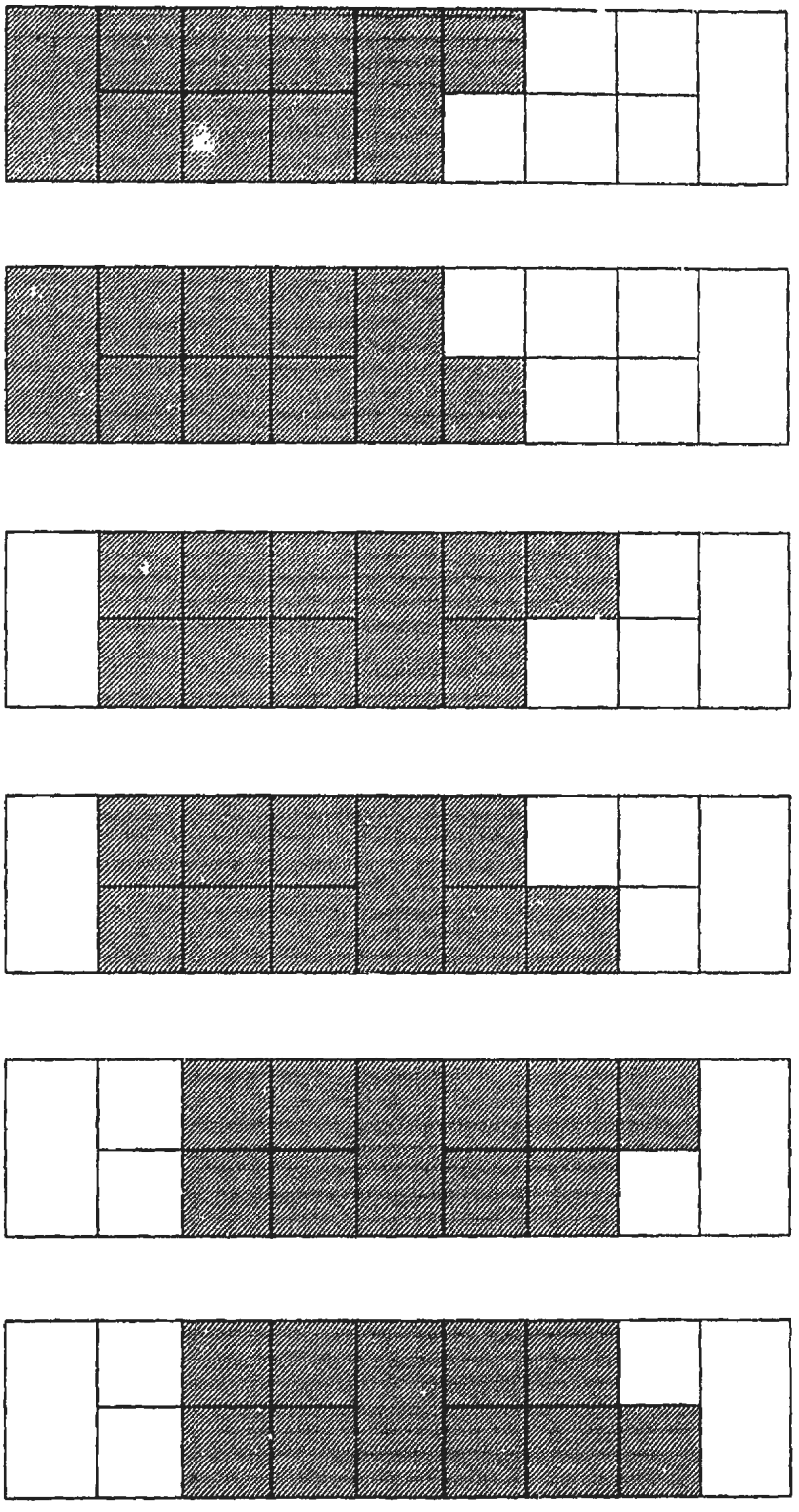

11 Subpanels (cont'd):

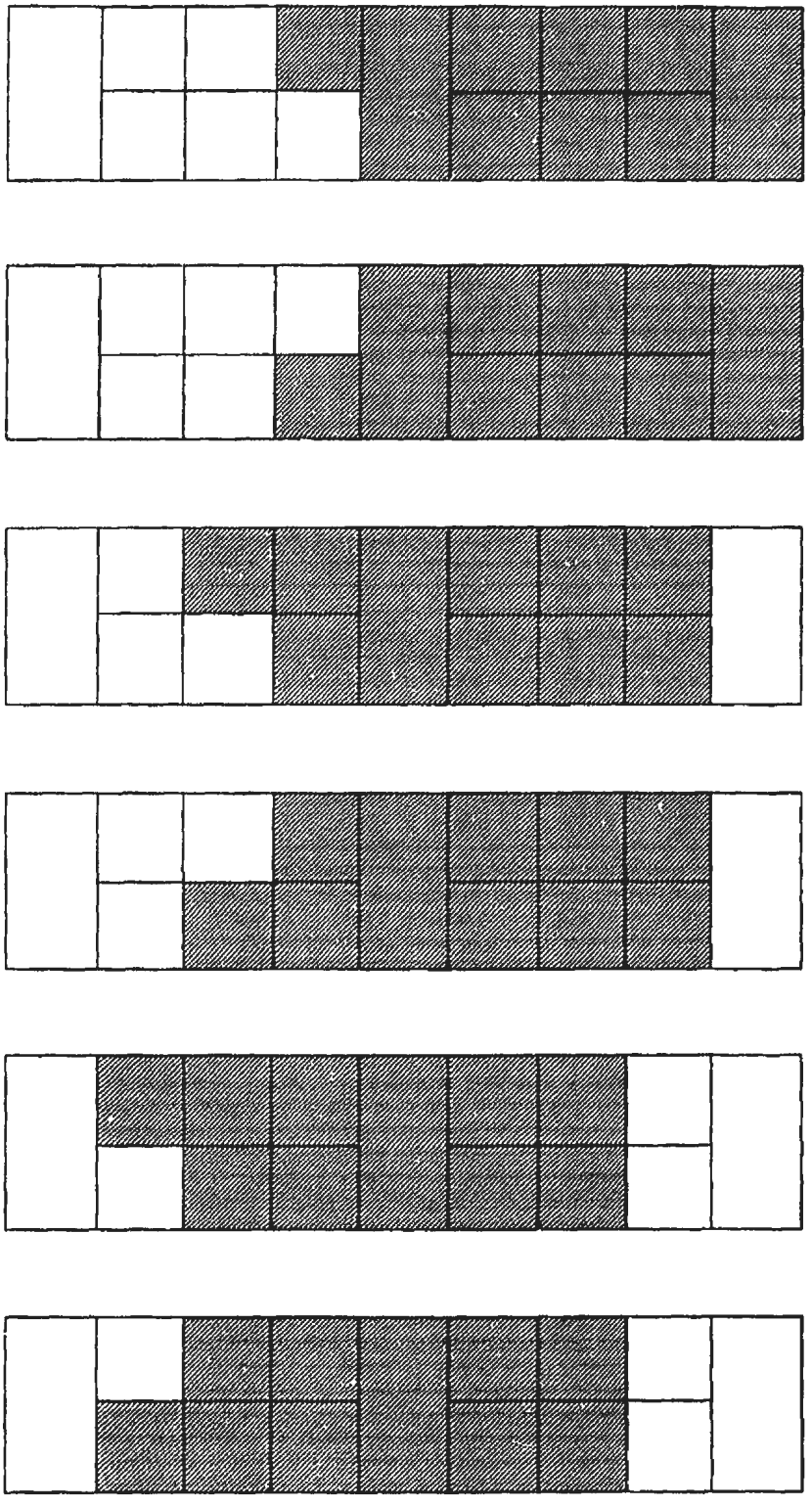

12 Subpanels:

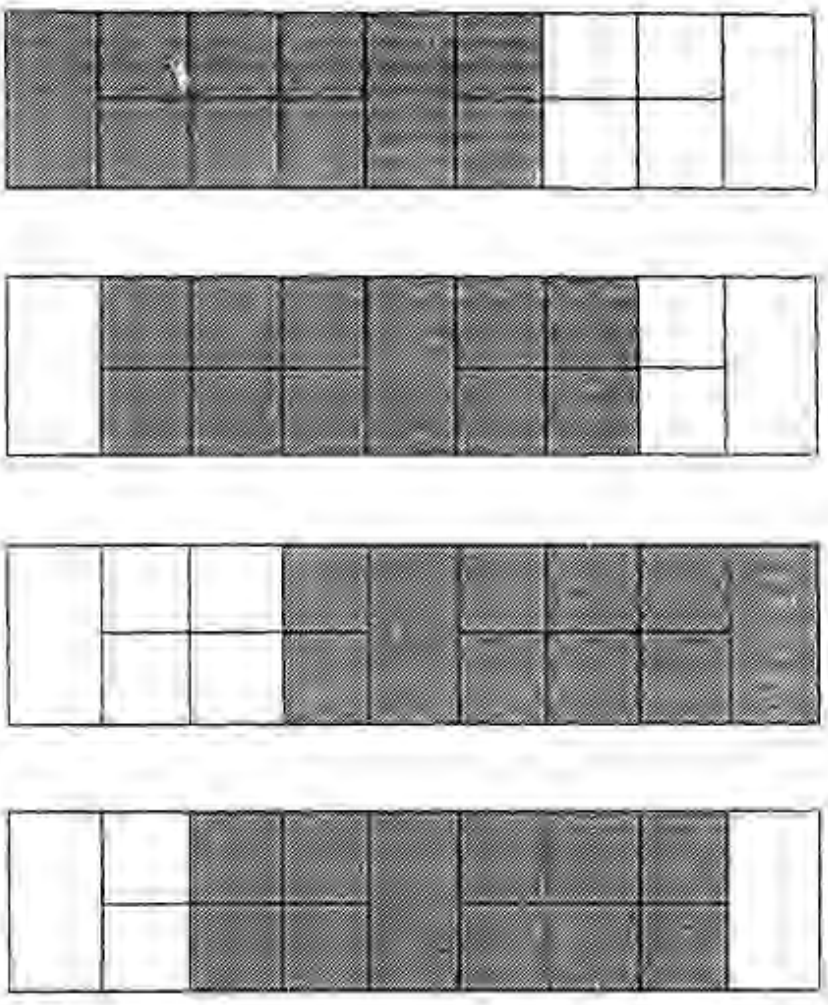

13 Subpanels:

13 Subpanels (cont'd):

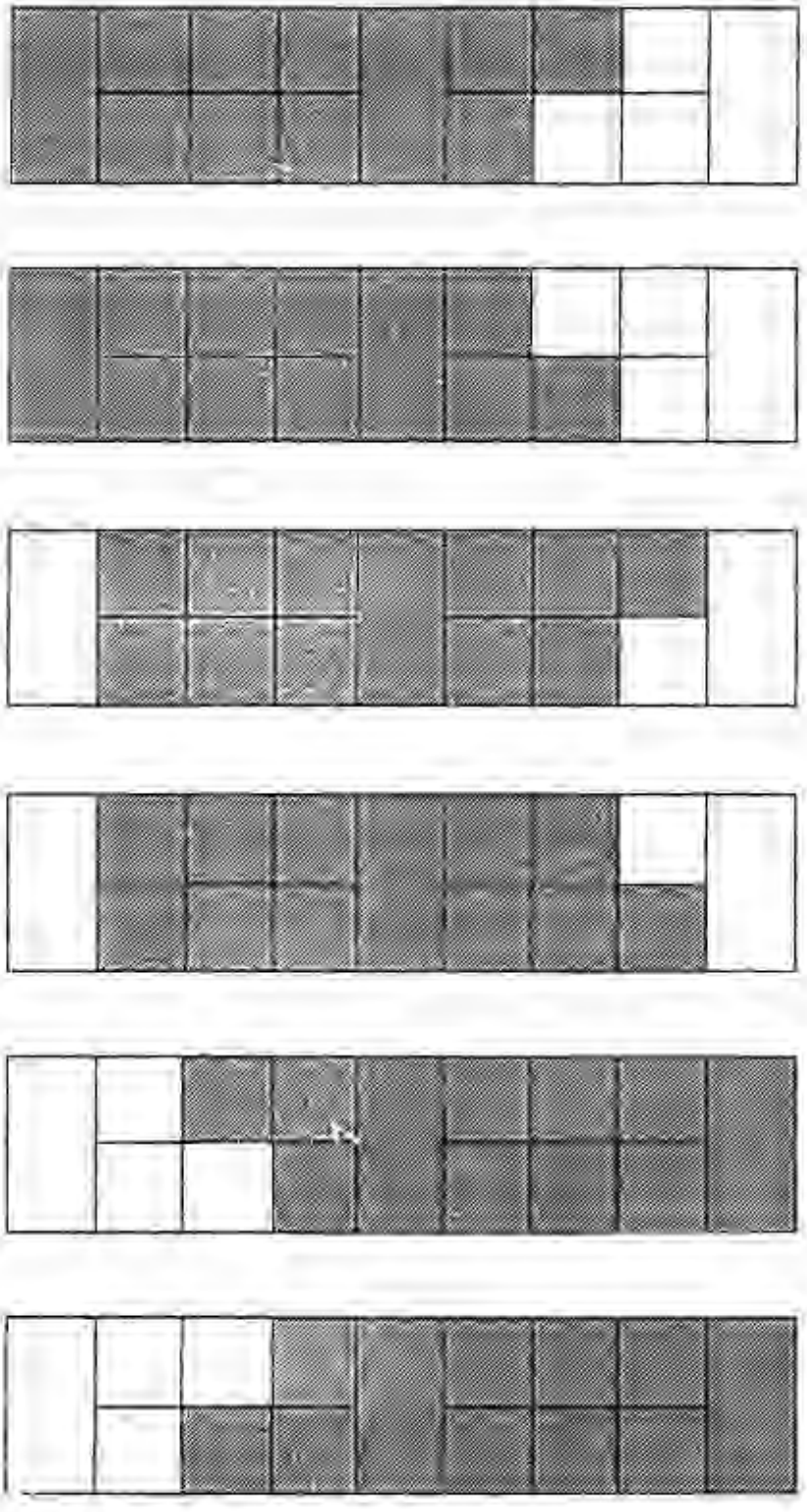

13 Subpanels (cont'd):

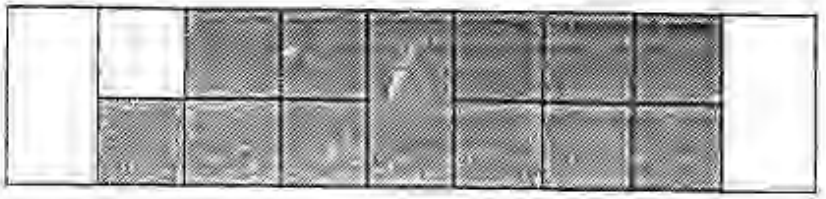

14 Subpanels:

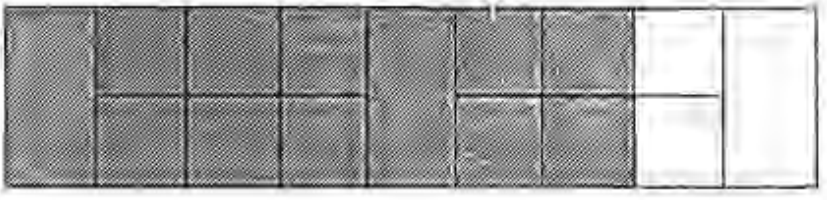

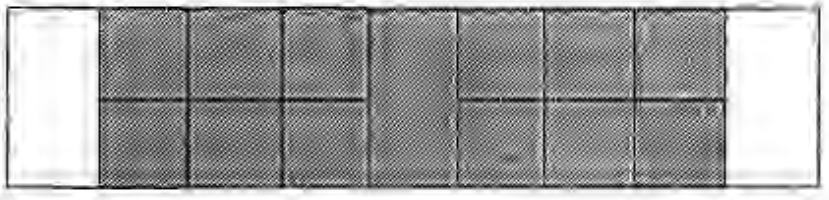

15 Subpanels:

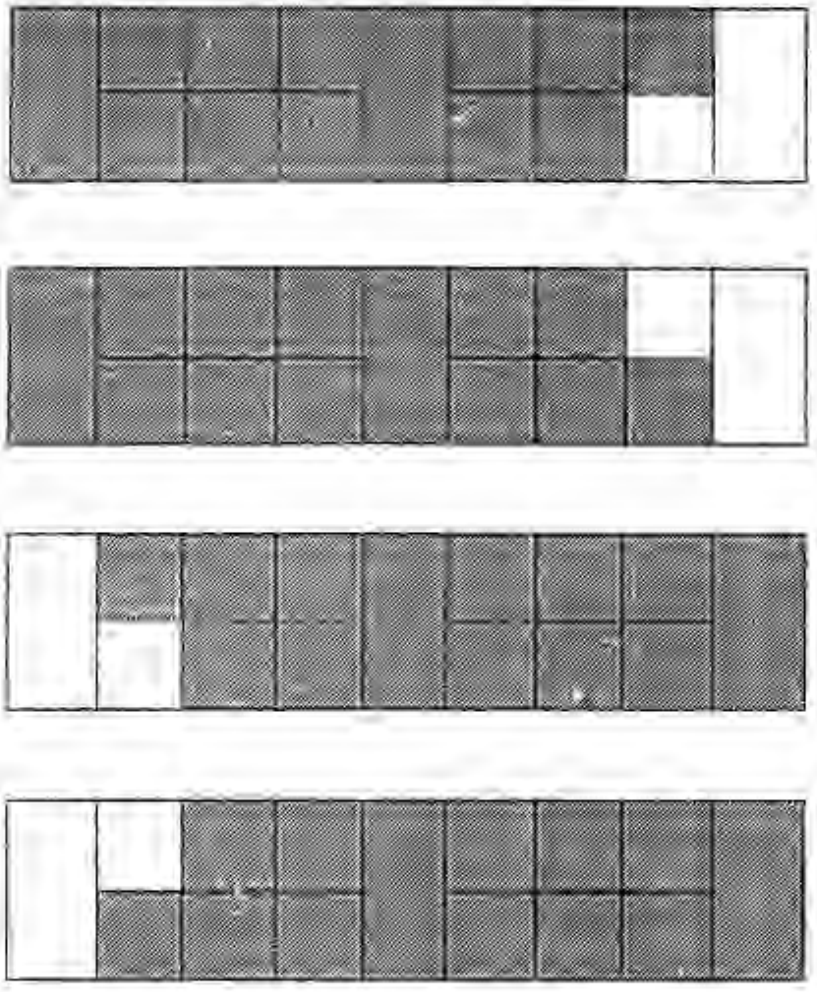

16 Subpanels:

16 Subpanels (cont'd):

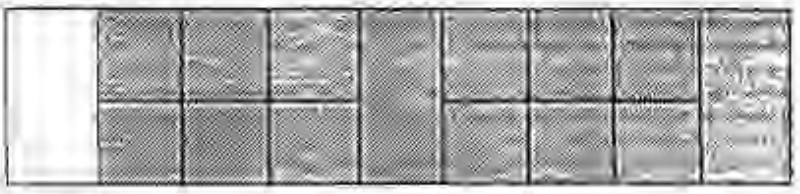

17 Subpanels:

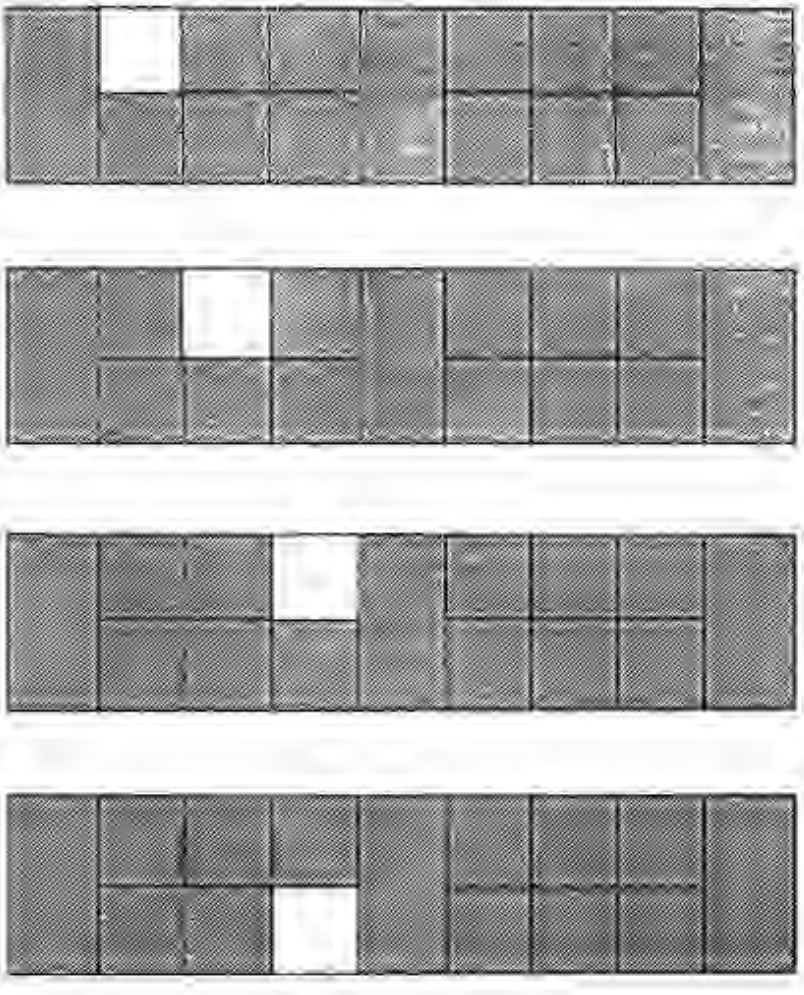

17 Subpanels (cont'd):

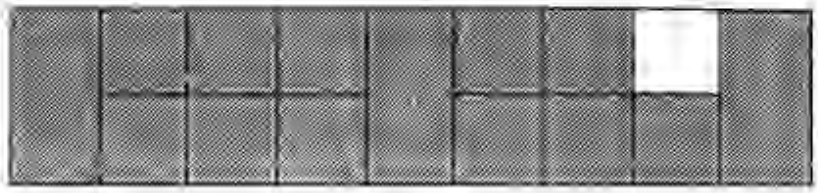

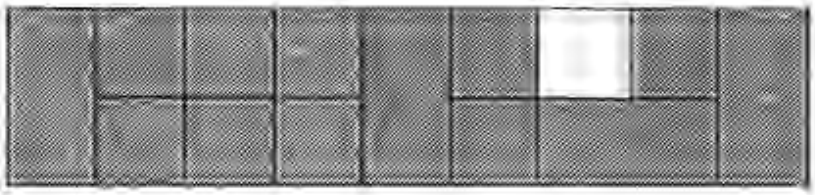

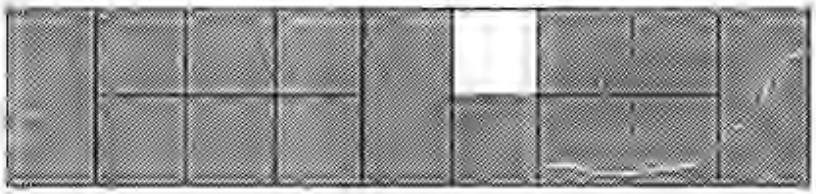

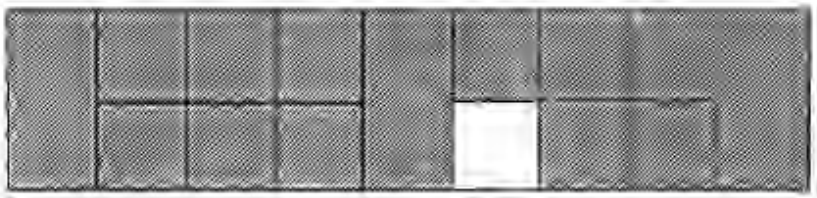

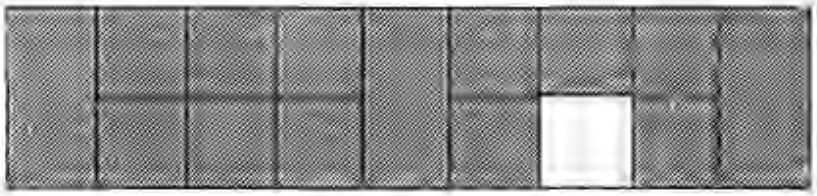

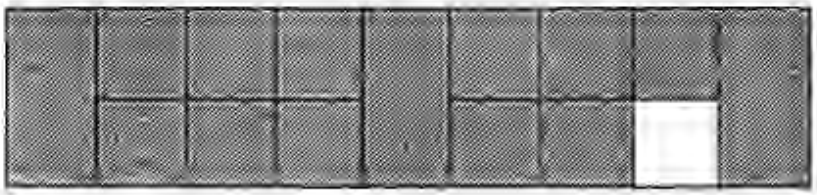

17 Subpanels (cont'd):

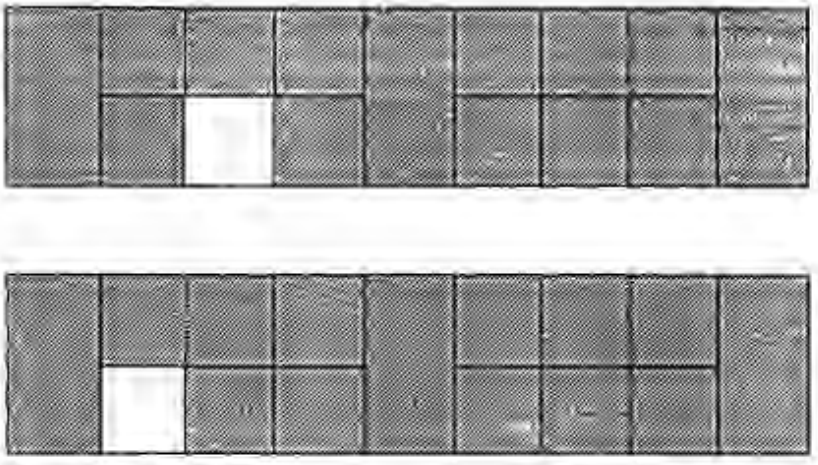

18 Subpanels:

Probability of Coverage for Given j and k, $p_c(j,k)$. Large Instrumented Panel, A2, on Canmar Kigoriak

j	c	k																	
		1	2	3	4	5	6	7	8	9	10	11	12	13	14	15	16	17	18
1	1	.083	.137	.250	.250	.317	.381	.458	.500	.583	.600	.667	.750	.833	.889	.917	1.00	.917	1.00
2	1	.137	.138	.176	.118	.147	.118	.176	.078	.196	.094	.176	.118	.147	.078	.118		.137	
	2		.059	.118	.176	.203	.193	.309	.431	.431	.529	.569	.588	.706	.804	.824	.941	.863	1.00
3	1	.250	.176		.500	.250	.143	.250	.167	.333	.200	.167	.250	.125					
	2		.118		.500	.200	.286	.313	.167	.333	.200	.333	.250	.250	.333	.250		.250	
	3			.250		.100	.143	.125	.333	.250	.400	.417	.500	.625	.667	.750	1.00	.750	1.00
4	1	.250	.118	.500		.125		.125		.125		.125		.125		.125			
	2		.176	.500	.219	.100	.214	.063	.208	.125	.200	.083	.188	.063	.167		.125		
	3					.075		.125		.125		.125		.125		.125		.250	
	4				.125	.125	.286	.250	.375	.375	.500	.542	.625	.625	.750	.750	.875	.750	1.00
5	1	.317	.147	.250	.125	.110	.114	.138	.100	.133	.080	.067	.100	.025	.067				
	2		.203	.200	.100	.130	.086	.125	.100	.133	.080	.067	.050	.100		.100			
	3			.100	.075	.120	.143	.100	.133	.133	.120	.133	.100	.100	.133		.100		
	4				.125	.150	.114	.200	.100	.167	.120	.150	.100	.050	.067	.150		.317	
	5					.050	.143	.175	.300	.317	.440	.483	.600	.700	.733	750	.900	.683	1.00

Probability of Coverage for Given j and k, $p_c(j,k)$. Large Instrumented Panel, A2, on Canmar Kigoriak

j	c	k																	
		1	2	3	4	5	6	7	8	9	10	11	12	13	14	15	16	17	18
6	1	.381	.118	.143		.114		.107		.095		.095		.071					
	2		.193	.286	.214	.086	.204	.107	.190	.095	.171	.048	.143		.095				
	3			.143		.143		.143		.143		.143		.143		.143			
	4				.286	.114	.245	.107	.238	.143	.229	.095	.214	.071	.190		.143		
	5					.143		.143		.143		.143		.143		.143		.381	
	6						.143	.143	.286	.286	.429	.429	.571	.571	.714	.714	.857	.619	1.00
7	1	.458	.176	.250	.125	.138	.107	.094	.089	.083	.050	.021	.063						
	2		.309	.313	.063	.125	.107	.094	.089	.042	.050	.042		.063					
	3			.125	.125	.100	.143	.125	.125	.083	.100	.083	.063		.083				
	4				.250	.200	.107	.156	.125	.125	.100	.083	.063	.063		.125			
	5					.175	.143	.125	.167	.167	.150	.083	.125	.125	.083		.125		
	6						.143	.125	.125	.229	.150	.229	.125	.125	.083	.063		.417	
	7							.063	.167	.271	.300	.438	.563	.625	.750	.813	.875	.583	1.00
8	1	.500	.078	167		.100		.083		.056		.056							
	2		.431	.167	.208	.100	.190	.083	.089	.056	.133		083						
	3			333		.133		.125		.111		111		.083					
	4				.375	.100	.238	.125	.222	.111	.200	056	.167		.111				
	5					.300		167		167		.167		.167		.167			

Probability of Coverage for Given j and k, $p_c(j,k)$. Large Instrumented Panel, A2, on Canmar Kigoriak

j	c	k																
		1	2	3	4	5	6	7	8	9	10	11	12	13	14	15	16	17	18
8	6						.286	.125	.278	.167	.267	.111	.250	.083	.222		.167		
	7							.167		.167		.167		.167		.167		.500	
	8								.167	.167	.333	.333	.500	.500	.667	.667	.833	.500	1.00
9	1	.583	.196	.333	.125	.133	.095	.083	.056										
	2		.431	.333	.125	.133	.095	.042	.056										
	3			.250	.125	.133	.143	.083	.111		.067								
	4				.375	.167	.143	.125	.111	.056	.067	.056							
	5					.317	.143	.167	.167	.111	.133	.056	.083						
	6						.286	.229	.167	.167	.133	.111	.083	.083					
	7							.271	.167	.222	.200	.167	.167	.083	.111				
	8								.167	.250	.200	.194	.167	.250	.111	.250		.583	
	9									.083	.200	.417	.500	.583	.778	.750	1.00	.417	1.00
10	1	.600	.094	.200		.080		.050											
	2		.529	.200	.200	.080	.171	.050	.133		.080								
	3			.400		.120		.100		.067		.067							
	4				.500	.120	.229	.100	.200	.067	.160		.100						
	5					440		.150		.133		.133		.100					
	6						.429	.150	.267	.133	.240	.067	.200		133				

Probability of Coverage for Given j and k, p_c (j,k) Large Instrumented Panel, A2, on Canmar Kigoriak																			
j	c	k																	
		1	2	3	4	5	6	7	8	9	10	11	12	13	14	15	16	17	18
10	7							.300		.200		.200		.200		.200			
	8								.333	.200	.320	.133	.300	.100	.267		.200		
	9									.200		.200		.200		.200		.600	
	10										.200	.200	.400	.400	.600	.600	.800	.400	1.00
11	1	.667	.176	.167	.125	.067	.095	.021	.056										
	2		.569	.333	.083	.067	.048	.042											
	3			.417	.125	.133	.143	.083	.111		.067								
	4				.542	.150	.095	.083	.056	.056		.056							
	5					.483	.143	.083	.167	.056	.133		.083						
	6						.429	.229	111	.111	.067	.111		.167					
	7							.438	.167	.167	.200	.111	.167		.111				
	8								.333	.194	.133	.139	.083	.167		.167			
	9									.417	.200	.194	.250	.167	.222		.167		
	10										.200	.222	.167	.167	.111	.250		694	
	11											.083	.250	.333	.556	.583	.833	.306	1.00

Probability of Coverage for Given j and k, $p_c(j,k)$. Large Instrumented Panel, A2, on Canmar Kigoriak

j	c	k																	
		1	2	3	4	5	6	7	8	9	10	11	12	13	14	15	16	17	18
12	1	.750	.118	.250		.100		.063											
	2		.588	.250	.188	.050	.143		.083										
	3			.500		.100		.063											
	4				.625	.100	.214	.063	.167		.100								
	5					.600		.125		.083		.083							
	6						.571	.125	.250	.083	.200		.125						
	7							.563		.167		.167		.125					
	8								.500	.167	.300	.083	.250		.167				
	9									.500		.250		.250		.250			
	10										.400	.167	.375	.125	.333		.250		
	11											.250		.250		.250		.750	
	12												.250	.250	.500	.500	.750	.250	1.00
13	1	.833	.147	.125	.125	.025	.071												
	2		.706	.250	.063	.100		.063											
	3			.625	.125	.100	.143		.083										
	4				.625	.050	.071	.063											
	5					.700	.143	.125	.167		.100								
	6						.571	.125	.083	.083		.167							

Probability of Coverage for Given j and k, p_c (j,k). Large Instrumented Panel, A2, on Canmar Kigoriak																		
j	c	k																
		1	2	3	4	5	6	7	8	9	10	11	12	13	14	15	16	17	18
13	7							.625	.167	.083	.200		.125						
	8								.500	.250	.100	.167		.125					
	9									.583	.200	.167	.250		.167				
	10										.400	.167	.125	.250		.250			
	11											.333	.250	.250	.333		.250		
	12												.250	.250	.167	.375		.833	
	13													.125	.333	.375	.750	.167	1.00
14	1	.889	.078			.067													
	2		.804	.333	.167		.095												
	3			.667		.133		.083											
	4				.750	.067	.190		.111										
	5					.733		.083											
	6						.714	.083	.222		.133								
	7							.750		.111		.111							
	8								.667	.111	.267		.167						
	9									.778		.222		.167					
	10										.600	.111	.333		.222				
	11											.556		333		333			

Probability of Coverage for Given j and k, $p_c(j,k)$. Large Instrumented Panel, A2, on Canmar Kigoriak

j	c	k																	
		1	2	3	4	5	6	7	8	9	10	11	12	13	14	15	16	17	18
14	12												.500	.167	.444		.333		
	13													.333		.333		.889	
	14														.333	.333	.667	.111	1.00
15	1	.917	.118		.125														
	2		.824	.250		.100													
	3			.750	.125		.143												
	4				.750	.150		.125											
	5					.750	.143		.167										
	6						.714	.063											
	7							.813	.167		.200		.						
	8								.667	.250		.167							
	9									.750	.200		.250						
	10										.600	.250		.250					
	11											.583	.250		.333				
	12												.500	.375		.500			
	13													.375	.333		.500		
	14														.333	.250		.917	
	15															.250	.500	.083	1.00

Probability of Coverage for Given j and k, $p_c(j,k)$. Large Instrumented Panel, A2, on Canmar Kigoriak

j	c	k																
		1	2	3	4	5	6	7	8	9	10	11	12	13	14	15	16	17	18
16	1	1.00																	
	2		.941		.125														
	3			1.00		.100													
	4				.875		.143												
	5					.900		.125											
	6						.857		.167										
	7							.875											
	8								.833		.200								
	9									1.00		.167							
	10										.800		.250						
	11											.833		.250					
	12												.750		.333				
	13													.750		.500			
	14														.667		.500		
	15															.500		1.00	
	16																.500		1.00

Probability of Coverage for Given j and k, $p_c(j,k)$. Large Instrumented Panel, A2, on Canmar Kigoriak

j	c	k																	
		1	2	3	4	5	6	7	8	9	10	11	12	13	14	15	16	17	18
17	1	.917	.137																
	2		.863	.250															
	3			.750	.250														
	4				.750	.317													
	5					.683	.381												
	6						.619	.417											
	7							.583	.500										
	8								.500	.583									
	9									.417	.600								
	10										.400	.694	.						
	11											.306	.750						
	12												.250	.833					
	13													.167	.889				
	14														.111	917			
	15															.083	1.00		
	16																	.917	
	17																	.083	1.00

Probability of Coverage for Given j and k, $p_c(j,k)$. Large Instrumented Panel, A2, on Canmar Kigoriak

j	c	k																	
		1	2	3	4	5	6	7	8	9	10	11	12	13	14	15	16	17	18
18	1	1.00																	
	2		1.00																
	3			1.00															
	4				1.00														
	5					1.00													
	6						1.00												
	7							1.00											
	8								1.00										
	9									1.00									
	10										1.00								
	11											1.00							
	12												1.00						
	13													1.00					
	14														1.00				
	15															1.00			
	16																1.00		
	17																	1.00	
	18																		1.00

Appendix 2 OBJECTIVE FUNCTION RESULTS

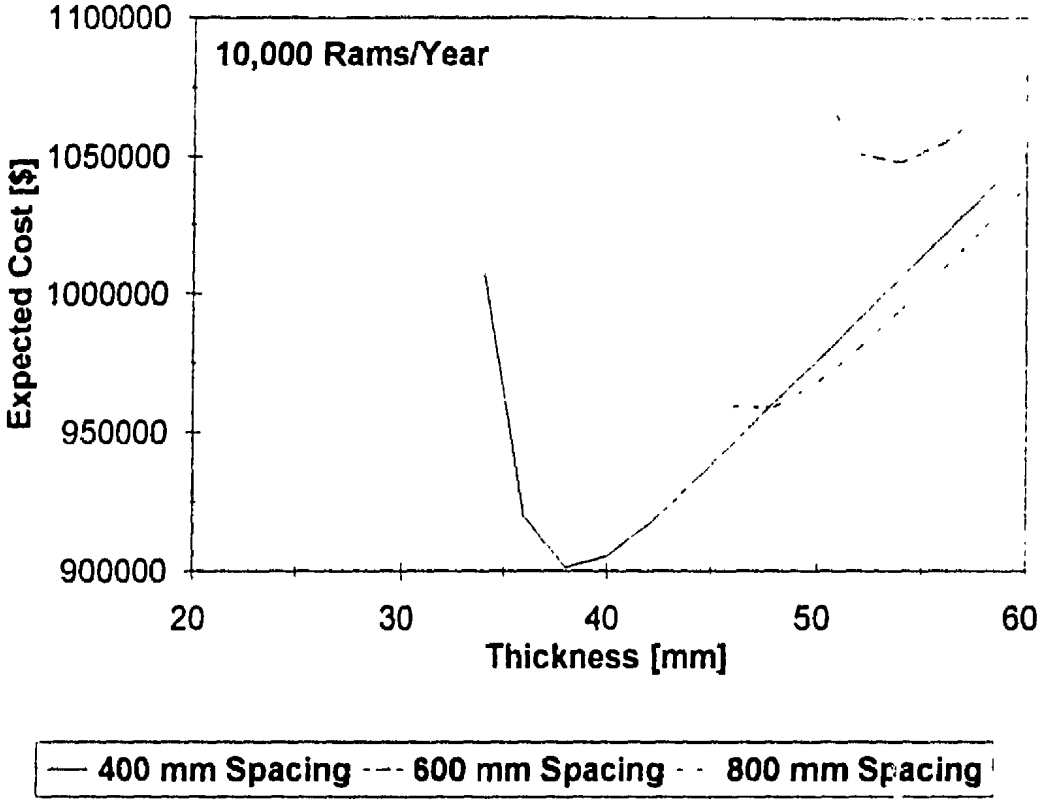

Figure A: Expected Cost of the Bow Structure for a Ship Designed for v = 10,000.

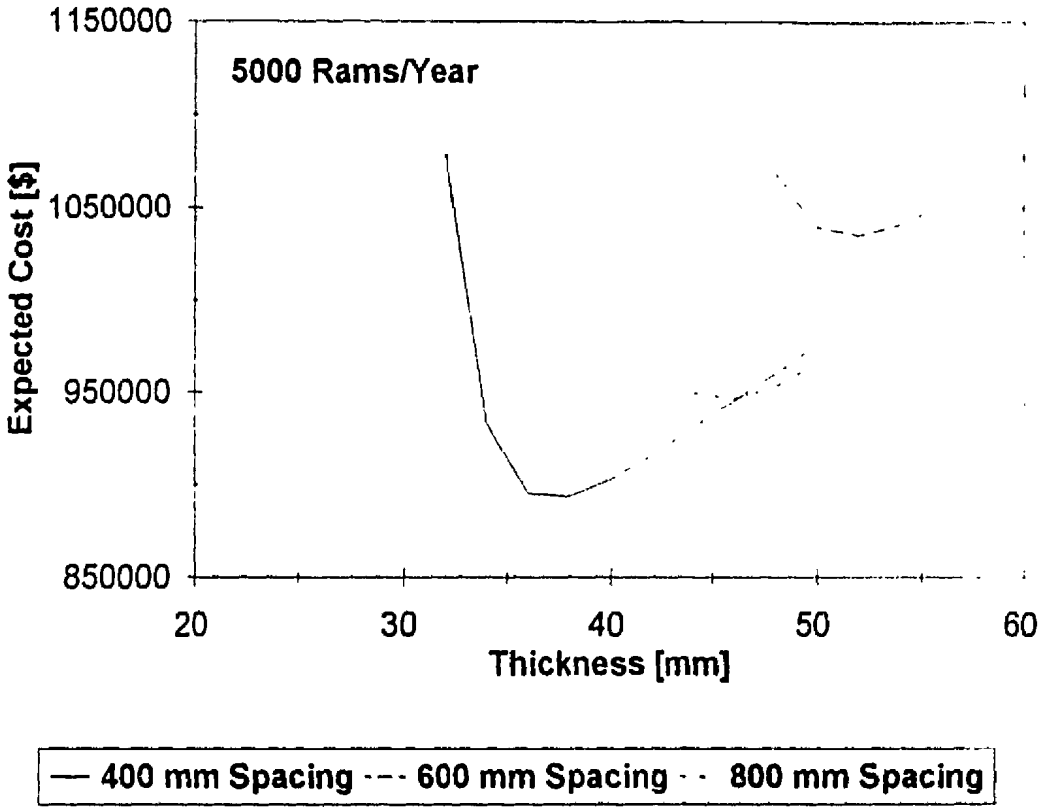

Figure B: Expected Cost of the Bow Structure for a Ship Designed for v = 5000.

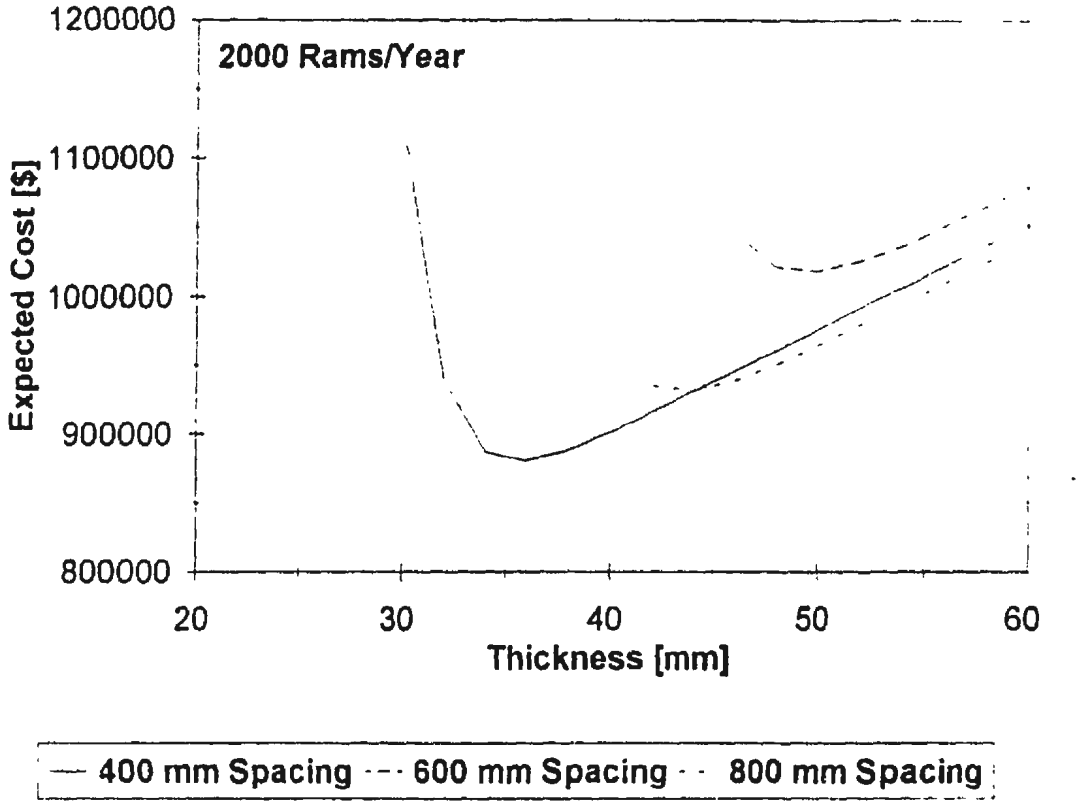

Figure C: Expected Cost of the Bow Structure for a Ship Designed for $\nu = 2000$.

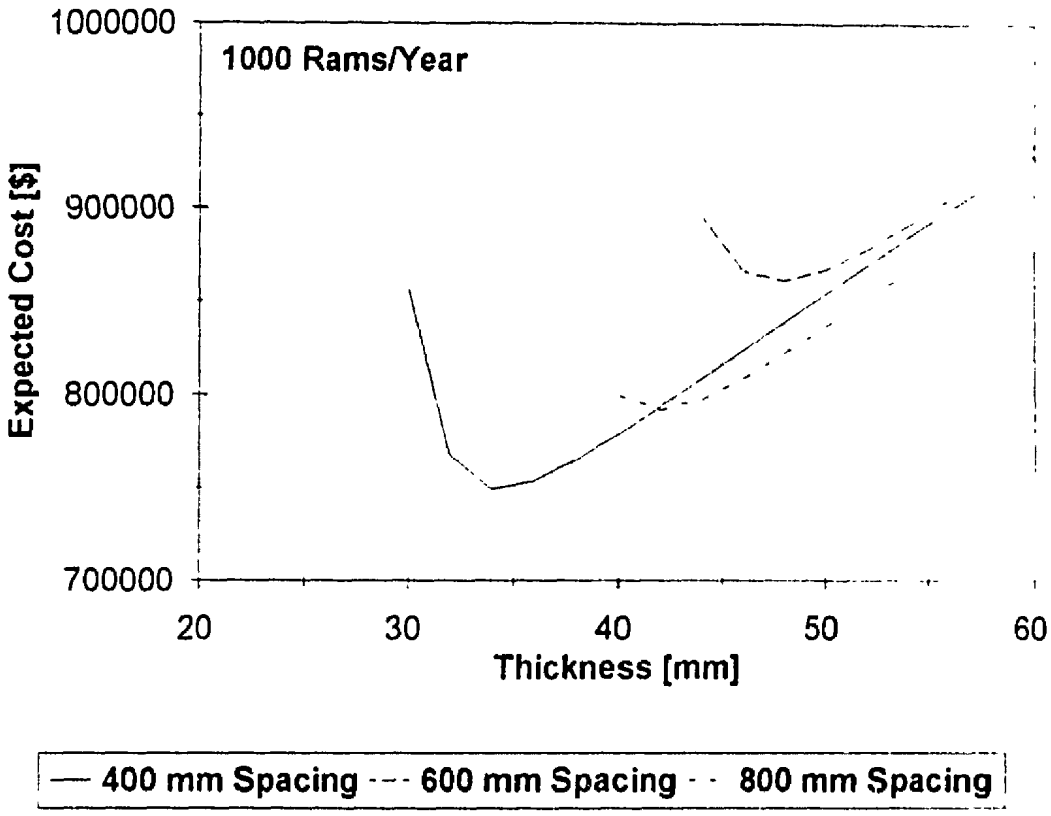

Figure D: Expected Cost of the Bow Structure for a Ship Designed for v = 1000.

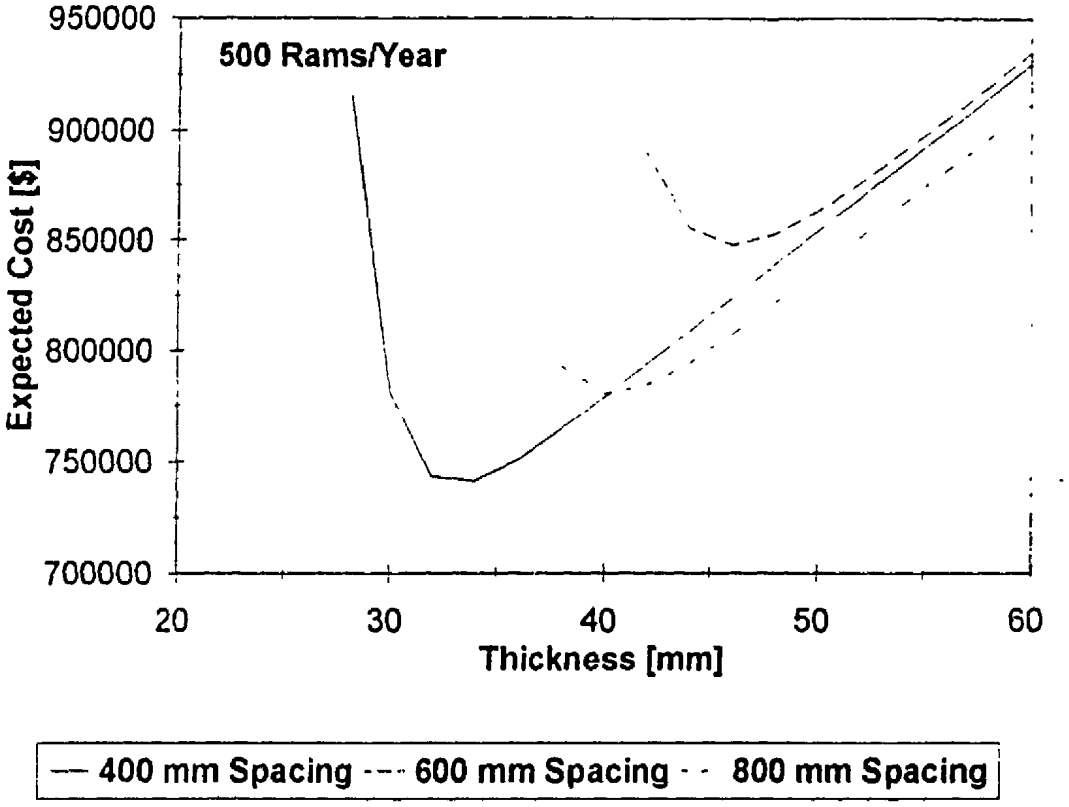

Figure E: Expected Cost of the Bow Structure for a Ship Designed for ν = 500.

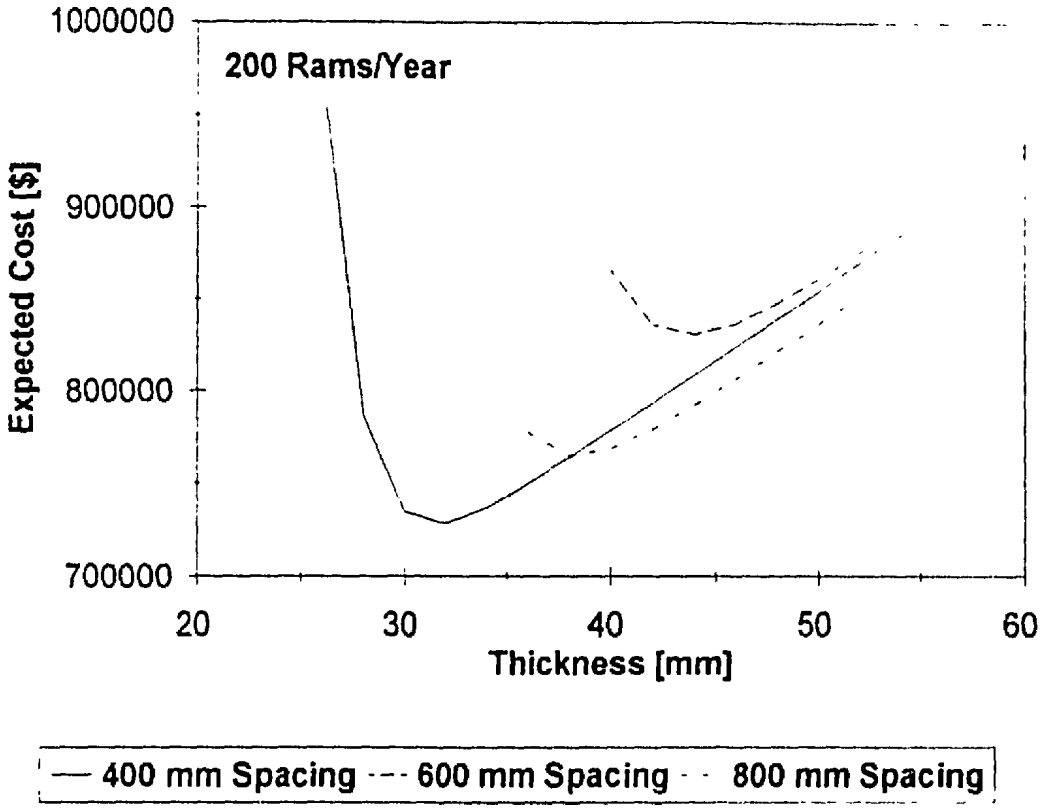

Figure F: Expected Cost of the Bow Structure for a Ship Designed for $\nu = 200$.

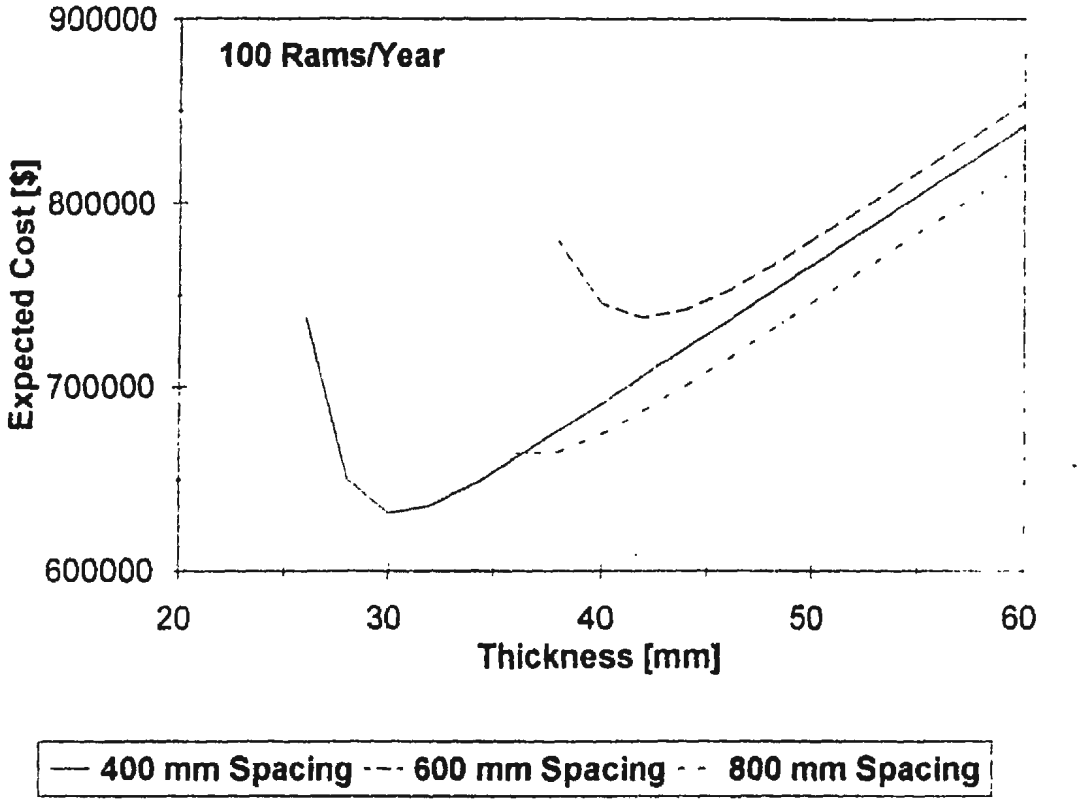

Figure G: Expected Cost of the Bow Structure for a Ship Designed for $\nu = 100$.

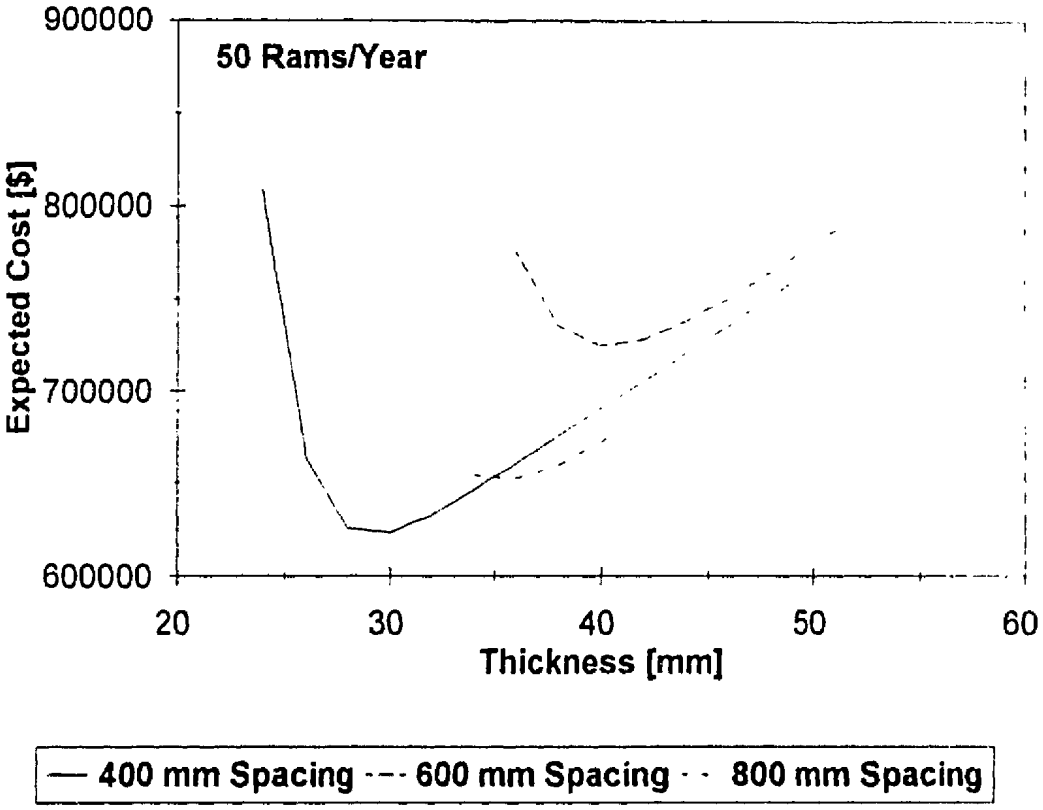

Figure H: Expected Cost of the Bow Structure for a Ship Designed for v = 50.

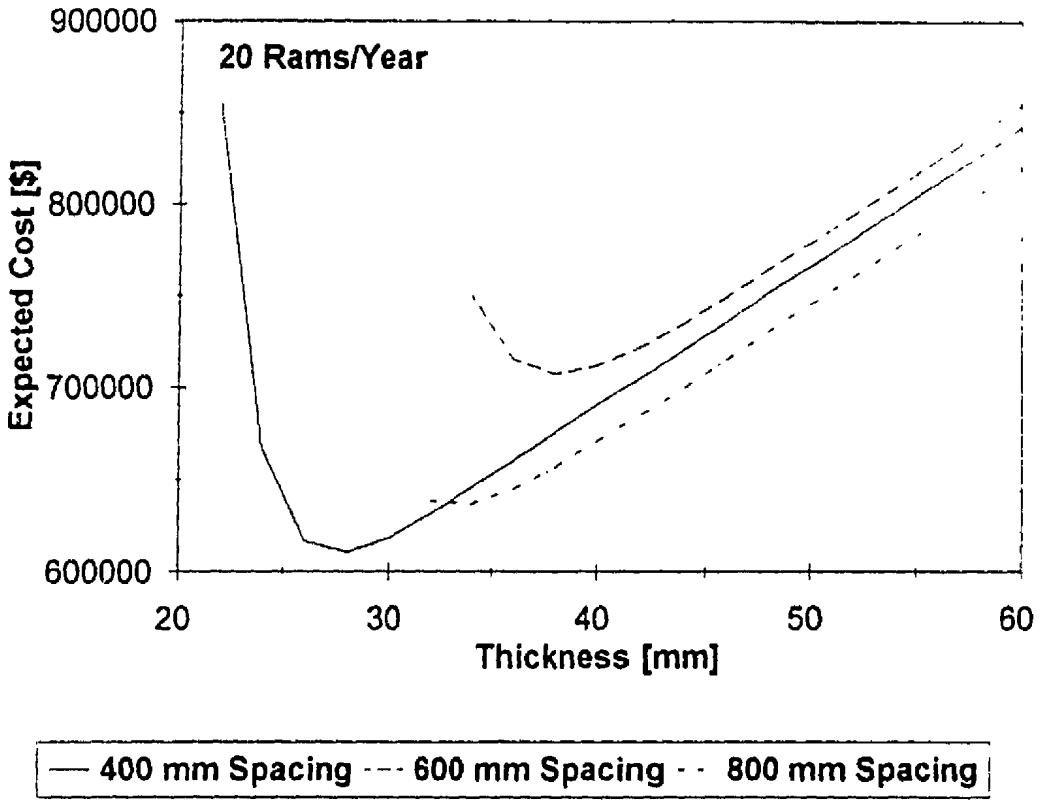

Figure I: Expected Cost of the Bow Structure for a Ship Designed for $\nu = 20$.

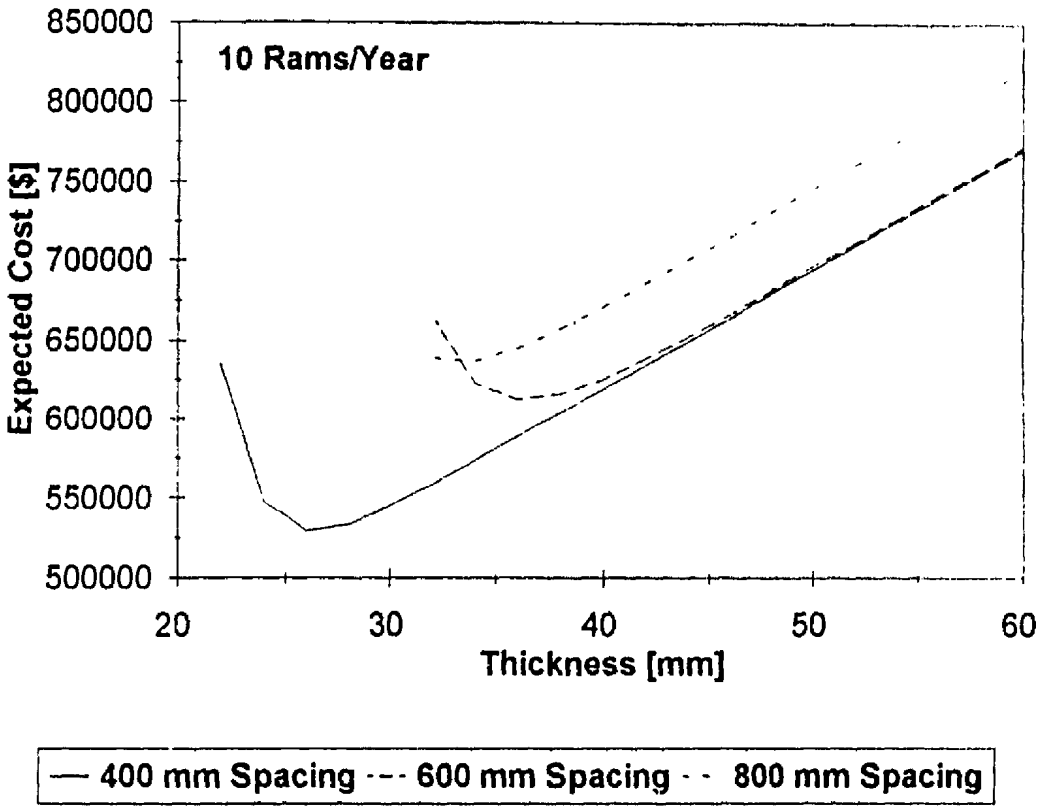

Figure J: Expected Cost of the Bow Structure for a Ship Designed for v = 10.

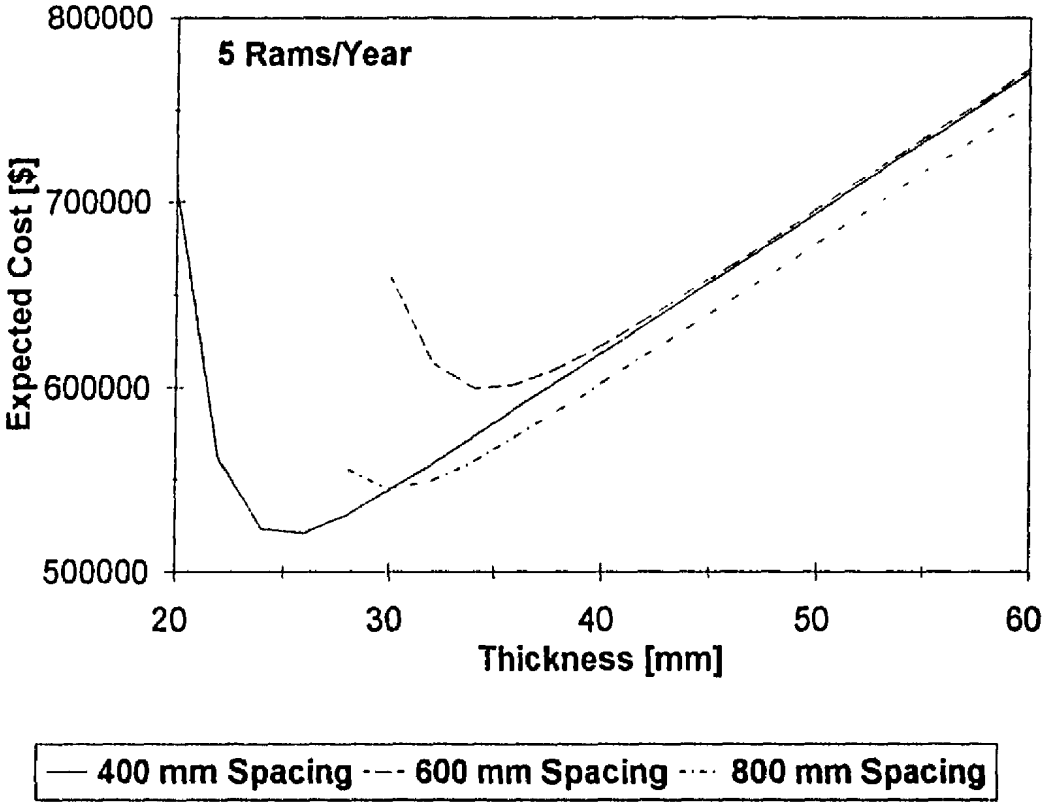

Figure K: Expected Cost of the Bow Structure for a Ship Designed for $v = 5$.